Three-Dimensional Electron Temperature Gradient Turbulence in the Tokamak Pedestal

PPPL Theory Seminar

January 6 2022

Jason Parisi

Princeton Plasma Physics Laboratory

Thanks to my collaborators on this project:

Felix Parra, Colin Roach, Michael Hardman, Michael Barnes, Denis St-Onge, Justin Ball, David Hatch, Bill Dorland, Ian Abel, David Dickinson, Carine Giroud, Ben Chapman, Samuli Saarelma, Jon Hillesheim, Juan Ruiz Ruiz, Nobuyuki Aiba, JET Contributors.

PPPL

PRINCETON PLASMA PHYSICS LABORATORY

The pedestal

- Region at plasma edge with significantly increased equilibrium temperature and density gradients. Appears once external heating crosses threshold [Wagner, PRL, 1982].

a) Typical tokamak pressure profiles.

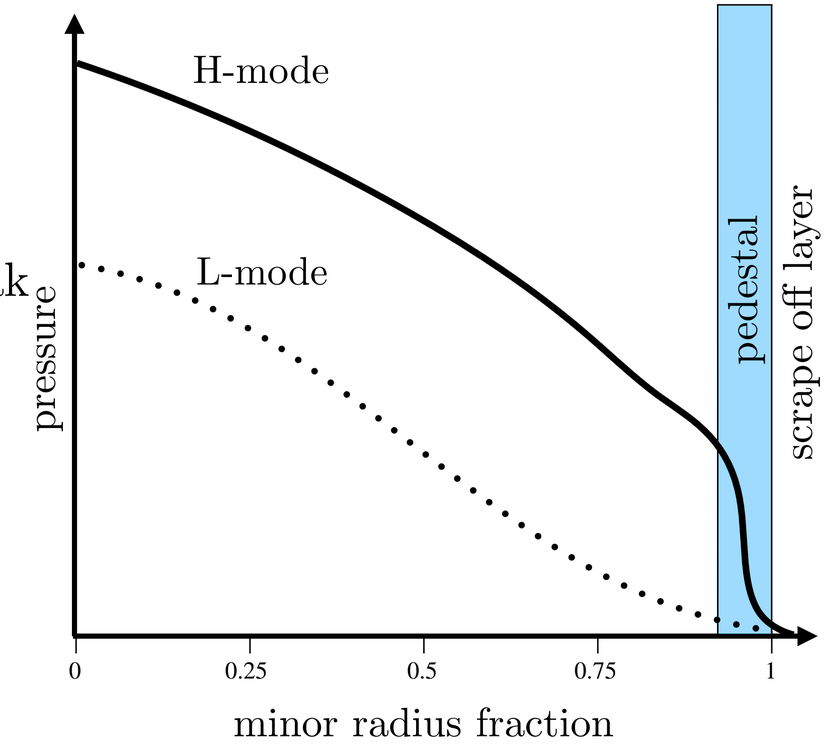

b) Pedestal highlighted by colored contours representing final 10% of poloidal flux.

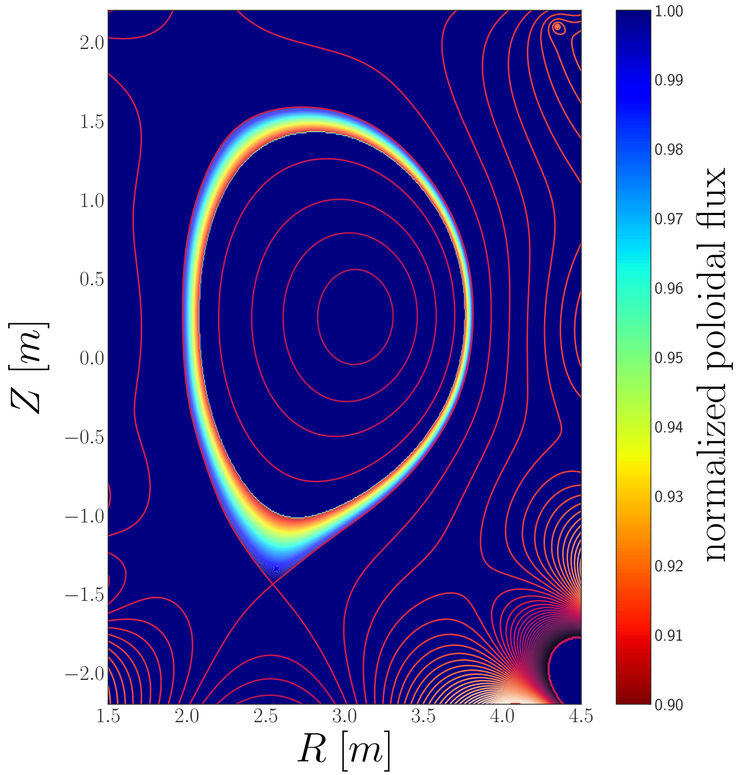

- For geometry in this work, we use Miller equilibrium in steep gradient region of JET-ILW discharge # 92174. Here, $R/L_{Te} \simeq 130$, where R is major radius and $L_{Te} = |\nabla \ln T_e|^{-1}$.

Nomenclature

- Use $\{x, y, \theta\}$ real space coordinates: x radial, y field line label, θ poloidal angle.
- Frequencies, $\omega_{Me} = \mathbf{k}_\perp \cdot \mathbf{v}_{Me}$, $\omega_{*e}^T = i \nabla T_e \cdot \mathbf{v}_E^{tb} / e\phi^{tb} = k_y v_{te} \rho_e / L_{Te}$, where the electrostatic magnetic drift is $\mathbf{v}_{Me} = (\hat{\mathbf{b}} \times \nabla \ln B)(v_\parallel^2 + v_\perp^2/2)/\Omega_e$, ϕ^{tb} is the turbulent electrostatic potential, and $\hat{\mathbf{b}} = \mathbf{B}/B$.

a) Coordinate system.

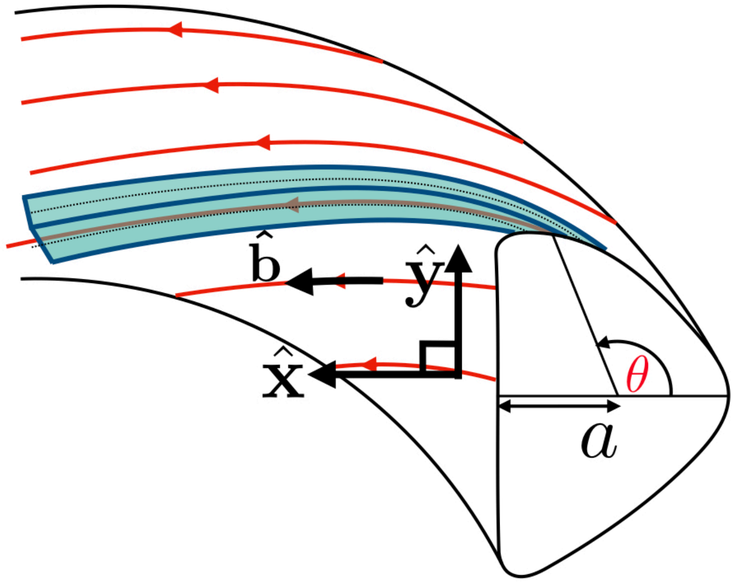

b) Magnetic shear $\hat{s}$ acting on a perturbation.

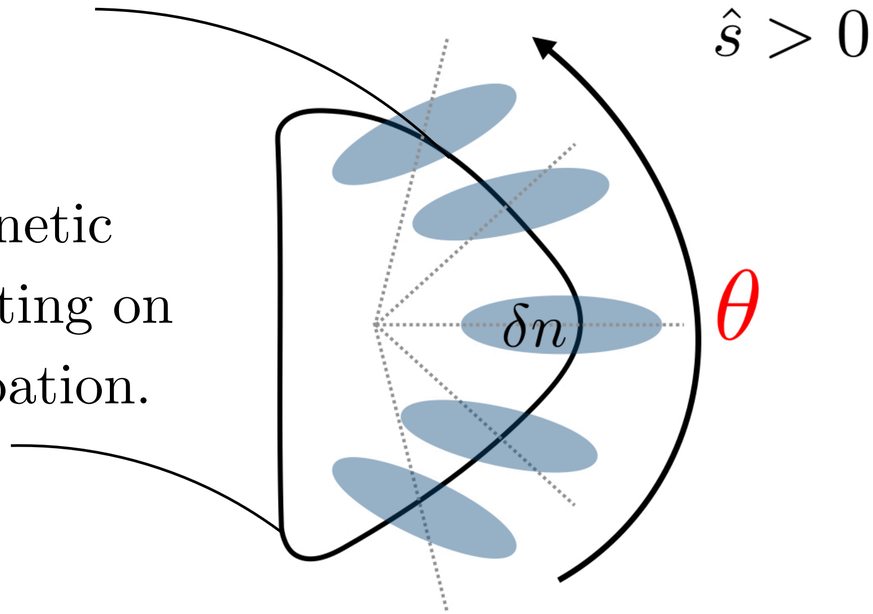

Pedestal microstability

- Zoo of pedestal microinstabilities: KBM, ITG, MTM, ETG: [Dickinson, 2013], [Hatch, 2016], [Kotschenreuther, 2019], [Pueschel, 2019], [Parisi, 2020], [Guttenfelder, 2021].

Pedestal microstability

- Zoo of pedestal microinstabilities: KBM, ITG, MTM, ETG: [Dickinson, 2013], [Hatch, 2016], [Kotschenreuther, 2019], [Pueschel, 2019], [Parisi, 2020], [Guttenfelder, 2021].

- We focus on ETG instability, which is important linearly and nonlinearly in JET-ILW pedestal discharges we have investigated. *Note: these pedestal ETG modes are very different to core ETG modes* [Drake, 1988], [Cowley, 1991], [Dorland, 2000], [Jenko, 2000].

Pedestal microstability

- Zoo of pedestal microinstabilities: KBM, ITG, MTM, ETG: [Dickinson, 2013], [Hatch, 2016], [Kotschenreuther, 2019], [Pueschel, 2019], [Parisi, 2020], [Guttenfelder, 2021].

- We focus on ETG instability, which is important linearly and nonlinearly in JET-ILW pedestal discharges we have investigated. *Note: these pedestal ETG modes are very different to core ETG modes* [Drake, 1988], [Cowley, 1991], [Dorland, 2000], [Jenko, 2000].

- We care about pedestal ETG modes because they are important for fluctuations and transport in simulations we have performed (and because they are interesting!).

Outer scale pedestal ETG turbulence at ion-scales

- Balance parallel streaming term $\omega_{\parallel}$ with drive term at outer scale,

$$\omega_{\parallel} \sim \frac{v_{te}}{l_{\parallel}} \sim \omega_{*e}^{T} \sim \frac{k_y \rho_e v_{te}}{L_{Te}}, \qquad \text{[Barnes, PRL, 2011]}$$

  where $l_{\parallel} \sim qR$ is the parallel correlation length, q safety factor.

Outer scale pedestal ETG turbulence at ion-scales

- Balance parallel streaming term $\omega_{\parallel}$ with drive term at outer scale,

$$\omega_{\parallel} \sim \frac{v_{te}}{l_{\parallel}} \sim \omega_{*e}^{T} \sim \frac{k_y \rho_e v_{te}}{L_{Te}}, \qquad \text{[Barnes, PRL, 2011]}$$

  where $l_{\parallel} \sim qR$ is the parallel correlation length, q safety factor. Get scaling

$$\text{—>} \quad k_y \rho_e \sim \frac{1}{q} \frac{L_{Te}}{R}.$$

Outer scale pedestal ETG turbulence at ion-scales

- Balance parallel streaming term $\omega_\parallel$ with drive term at outer scale,

$$\omega_\parallel \sim \frac{v_{te}}{l_\parallel} \sim \omega_{*e}^T \sim \frac{k_y \rho_e v_{te}}{L_{Te}}, \qquad \text{[Barnes, PRL, 2011]}$$

  where $l_\parallel \sim qR$ is the parallel correlation length, q safety factor. Get scaling

$$\text{—>} \quad k_y \rho_e \sim \frac{1}{q} \frac{L_{Te}}{R}.$$

- In pedestal, $qR/L_{Te} \gtrsim \rho_i/\rho_e \gg 1$, turbulence outer scale satisfies

$$\text{—>} \quad k_y \rho_i \sim 1.$$

Outer scale pedestal ETG turbulence at ion-scales

- Balance parallel streaming term $\omega_\parallel$ with drive term at outer scale,

$$\omega_\parallel \sim \frac{v_{te}}{l_\parallel} \sim \omega_{*e}^T \sim \frac{k_y \rho_e v_{te}}{L_{Te}}, \qquad \text{[Barnes, PRL, 2011]}$$

  where $l_\parallel \sim qR$ is the parallel correlation length, q safety factor. Get scaling

$$\text{—>} \quad k_y \rho_e \sim \frac{1}{q}\frac{L_{Te}}{R}.$$

- In pedestal, $qR/L_{Te} \gtrsim \rho_i/\rho_e \gg 1$, turbulence outer scale satisfies

$$\text{—>} \quad k_y \rho_i \sim 1.$$

- ETG instability important linearly for $k_y \rho_i \sim 1$ in pedestal [Parisi, NF, 2020].

Outer scale pedestal ETG turbulence at ion-scales

- Balance parallel streaming term $\omega_\parallel$ with drive term at outer scale,

$$\omega_\parallel \sim \frac{v_{te}}{l_\parallel} \sim \omega_{*e}^T \sim \frac{k_y \rho_e v_{te}}{L_{Te}}, \qquad \text{[Barnes, PRL, 2011]}$$

  where $l_\parallel \sim qR$ is the parallel correlation length, q safety factor. Get scaling

$$\text{—>} \quad k_y \rho_e \sim \frac{1}{q}\frac{L_{Te}}{R}.$$

- In pedestal, $qR/L_{Te} \gtrsim \rho_i/\rho_e \gg 1$, turbulence outer scale satisfies

$$\text{—>} \quad k_y \rho_i \sim 1.$$

- ETG instability important linearly for $k_y \rho_i \sim 1$ in pedestal [Parisi, NF, 2020].
- In this talk: **ETG $k_y \rho_e \ll 1$ turbulence has complex parallel distribution, regulates $k_y \rho_e \sim 1$ ETG transport.**

Physical picture for core toroidal ETG mode

- To better understand $k_y \rho_i \sim 1$ ETG turbulence, begin with linear toroidal ETG physics in tokamak core [Rudakov, 1961], [Coppi, 1967], [Cowley, 1991].

Physical picture for core toroidal ETG mode

- Toroidal instability usually has strongest linear drive at outboard midplane.

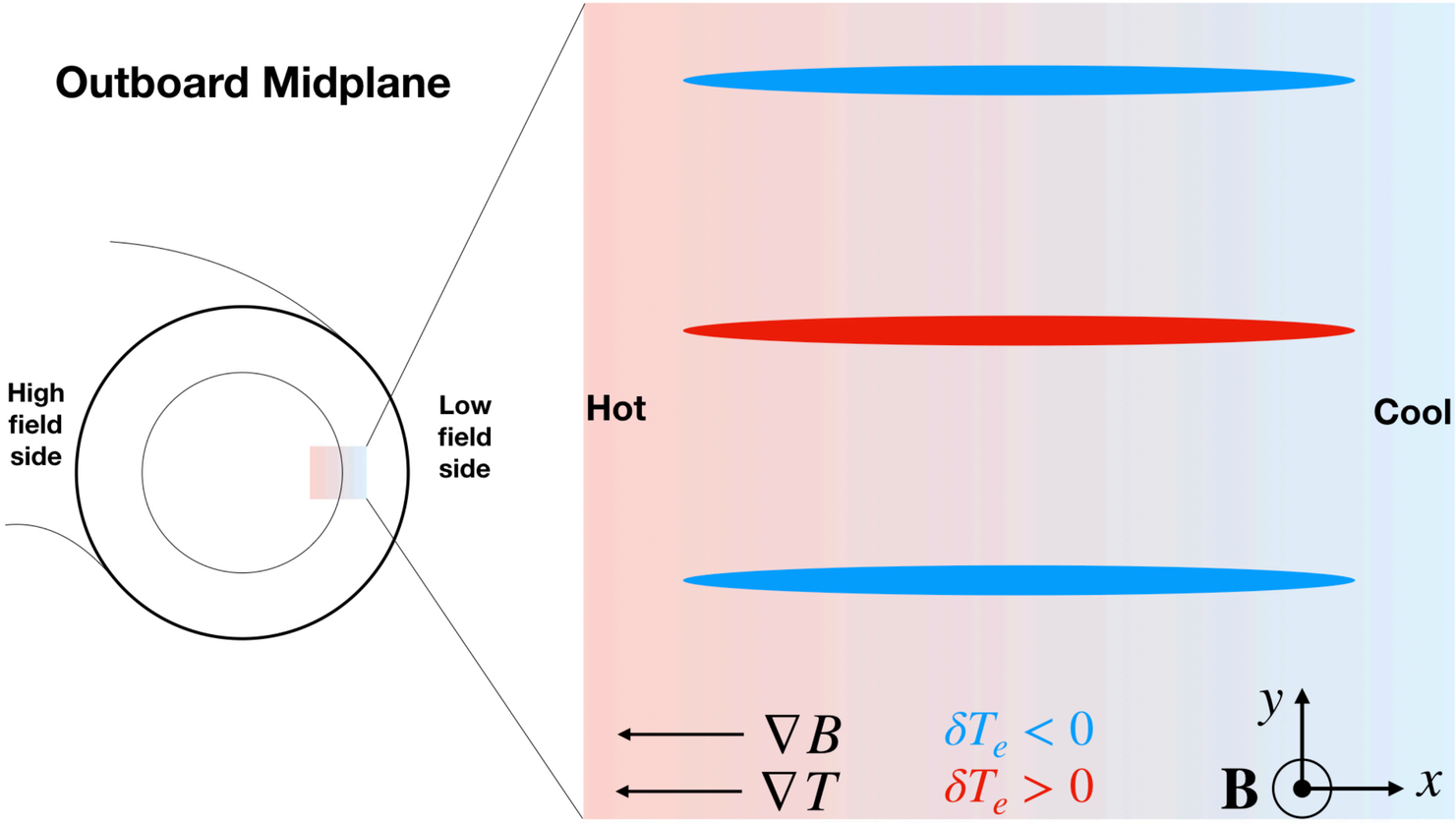

Physical picture for core toroidal ETG mode

- Toroidal instability usually has strongest linear drive at outboard midplane.
- Recall standard mechanism for core ETG (or ITG) mode.

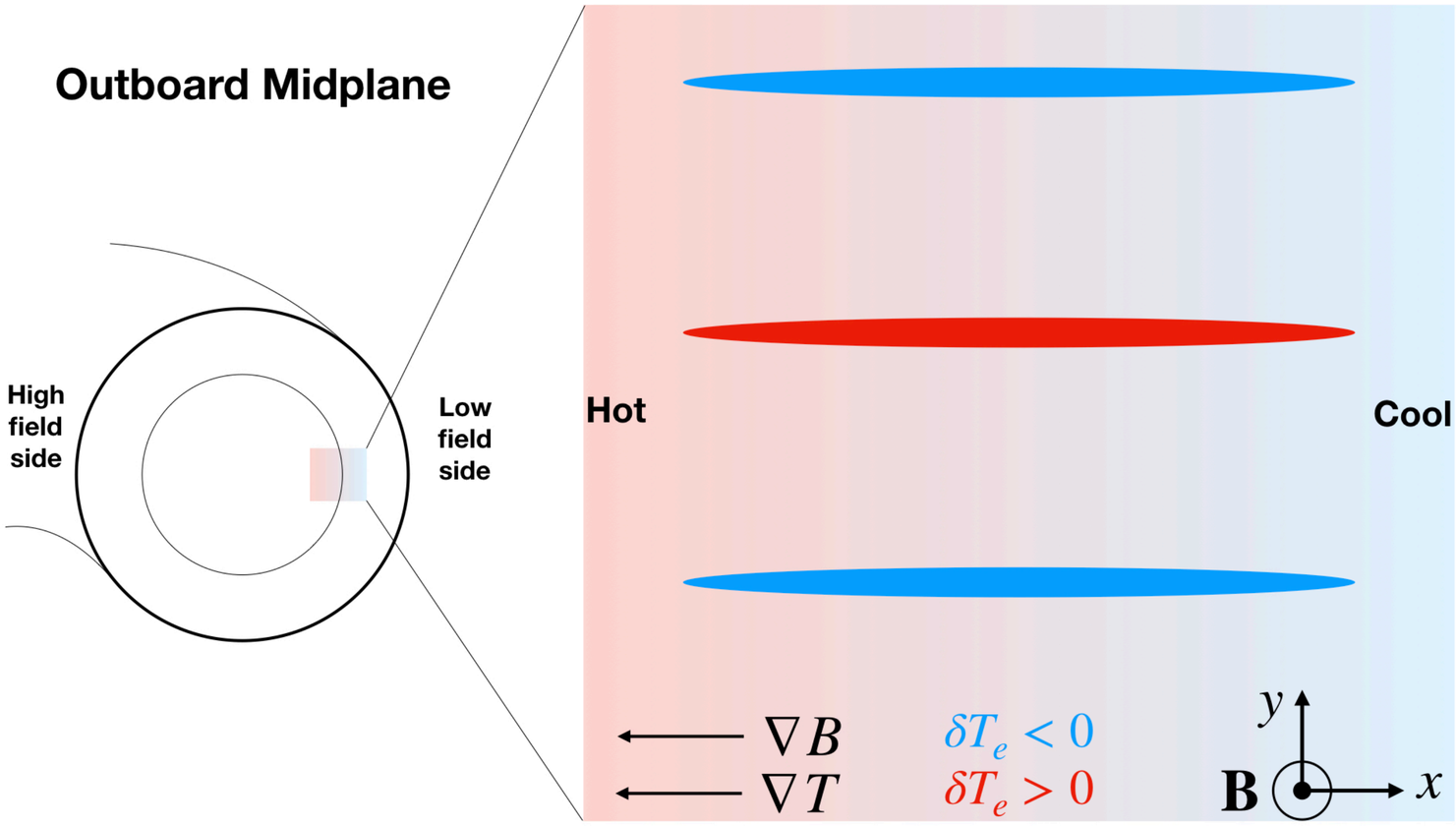

Physical picture for core toroidal ETG mode

- Toroidal instability usually has strongest linear drive at outboard midplane.
- Recall standard mechanism for core ETG (or ITG) mode.

Consider a temperature perturbation δT_e on a background, with some binormal wavenumber.

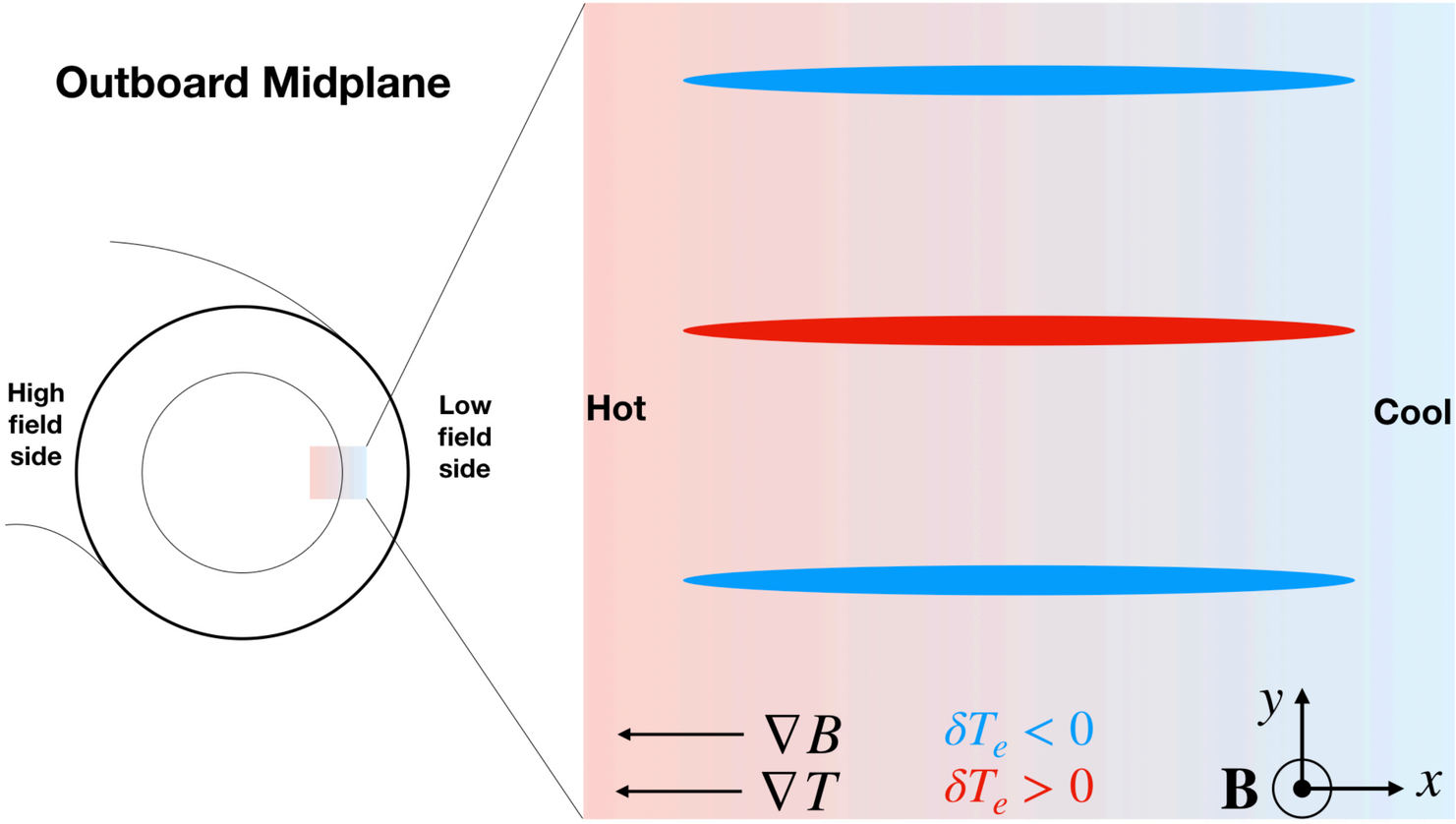

Physical picture for core toroidal ETG mode

- Toroidal instability usually has strongest linear drive at outboard midplane.
- Recall standard mechanism for core ETG (or ITG) mode.

Consider a temperature perturbation δT_e on a background, with some binormal wavenumber.

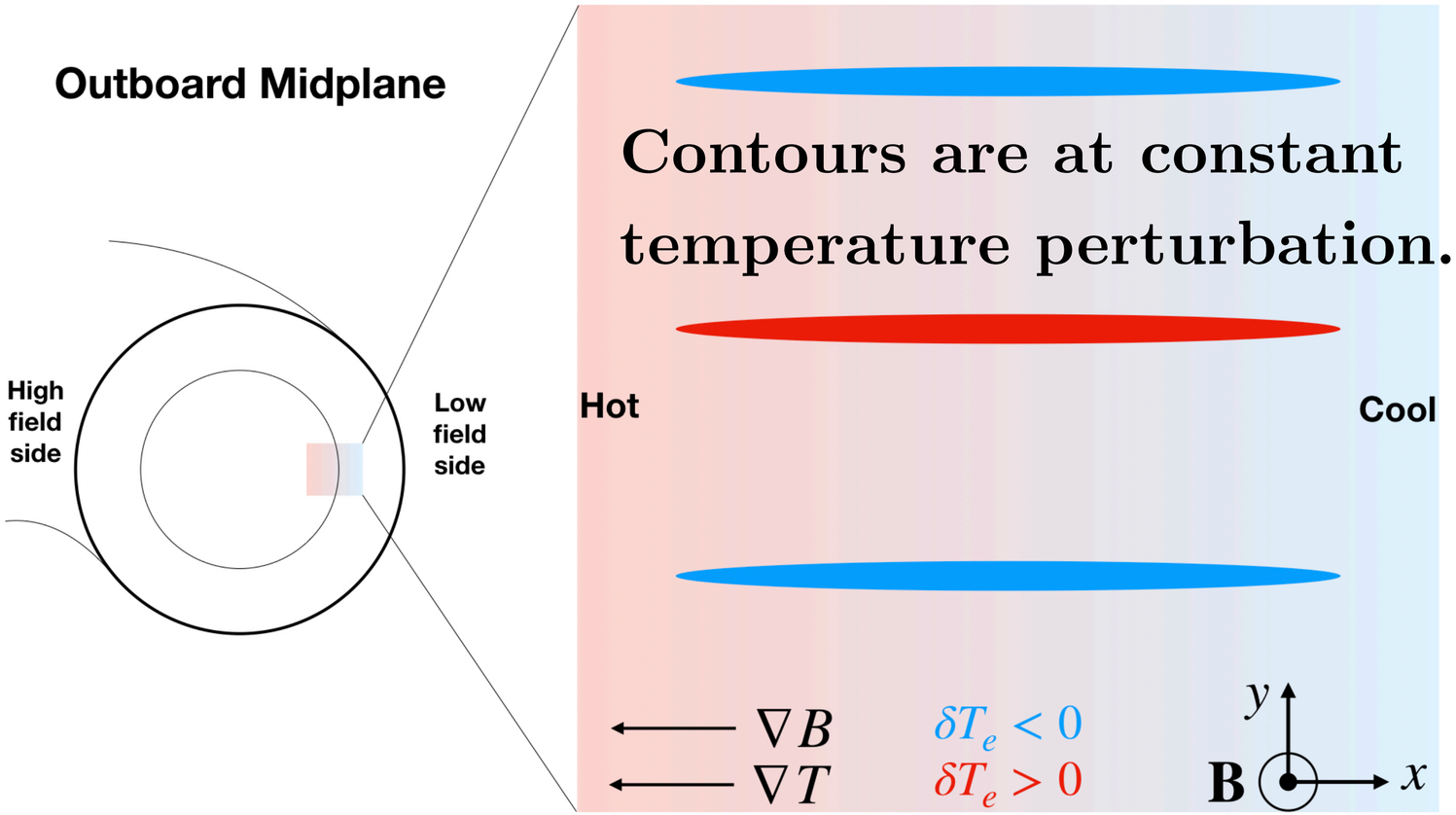

Physical picture for core toroidal ETG mode

- Toroidal instability usually has strongest linear drive at outboard midplane.
- Recall standard mechanism for core ETG (or ITG) mode.

Perturbed electron magnetic drifts $\delta \mathbf{v}_{Me}$ are upwards.

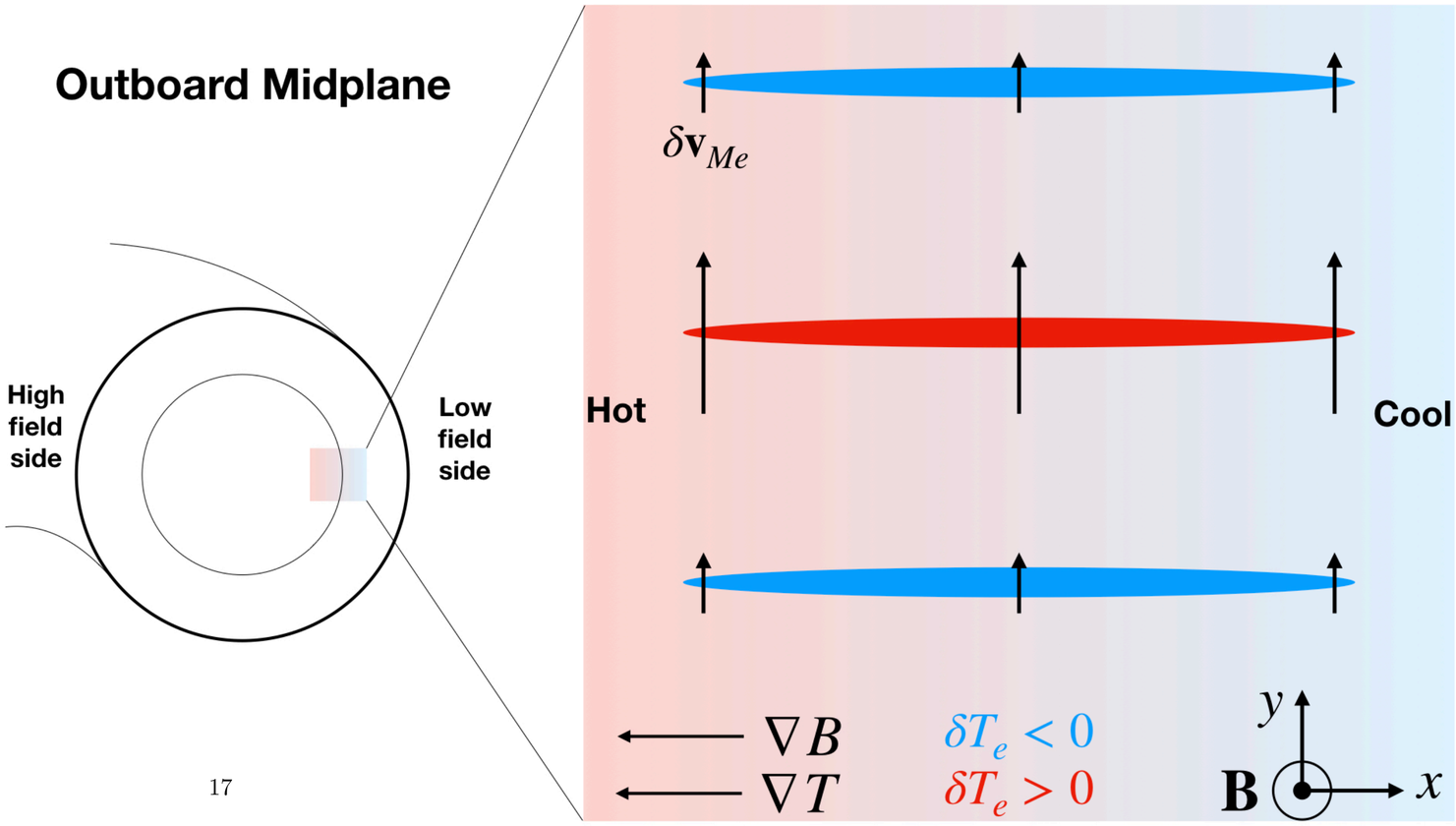

Physical picture for core toroidal ETG mode

- Toroidal instability usually has strongest linear drive at outboard midplane.

- Recall standard mechanism for core ETG (or ITG) mode.

$\rightarrow$ **compression and rarefaction**

$\rightarrow$ **charge accumulation**

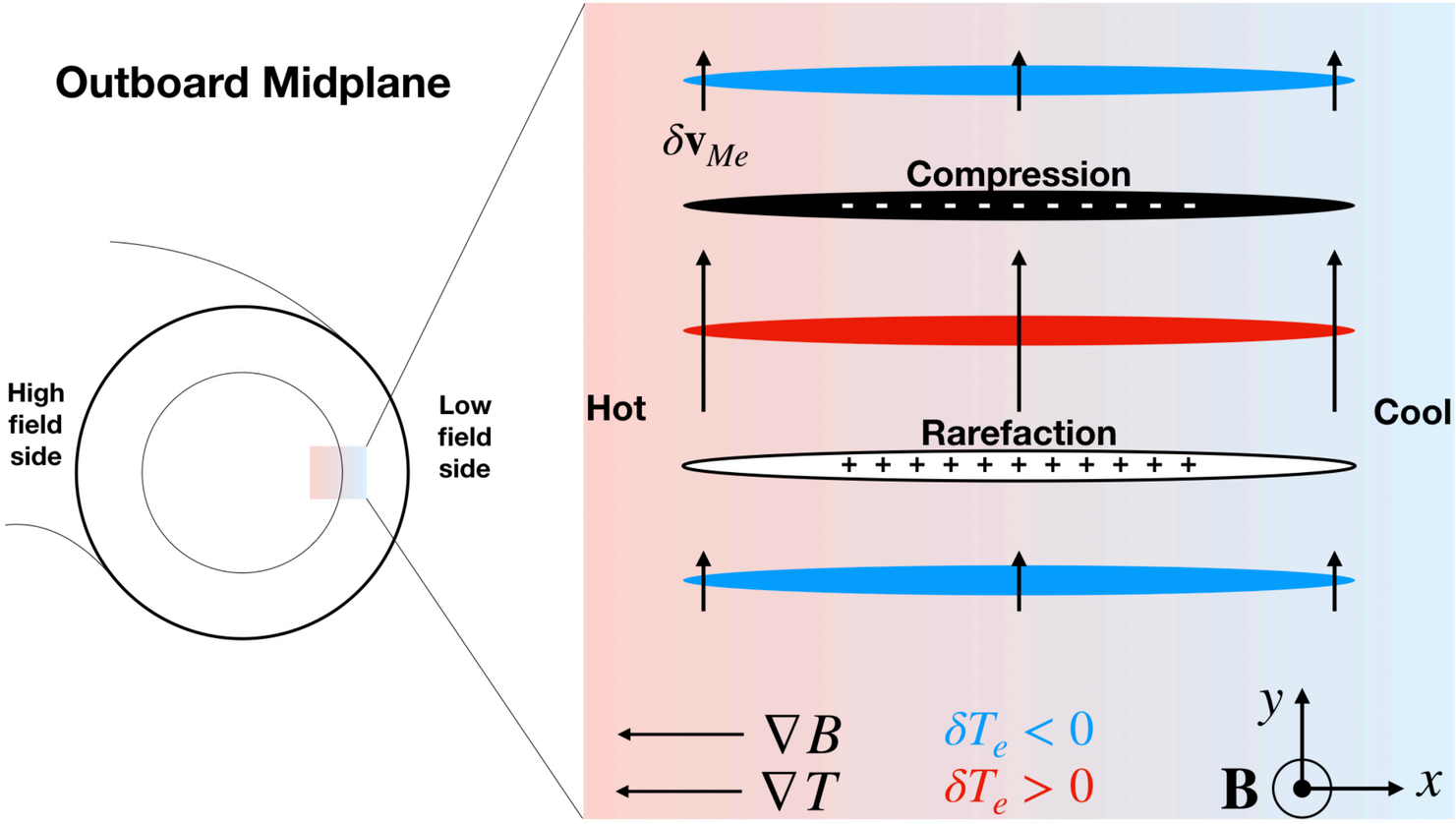

Physical picture for core toroidal ETG mode

- Toroidal instability usually has strongest linear drive at outboard midplane.

- Recall standard mechanism for core ETG (or ITG) mode.

$\rightarrow$ **induce δE.**

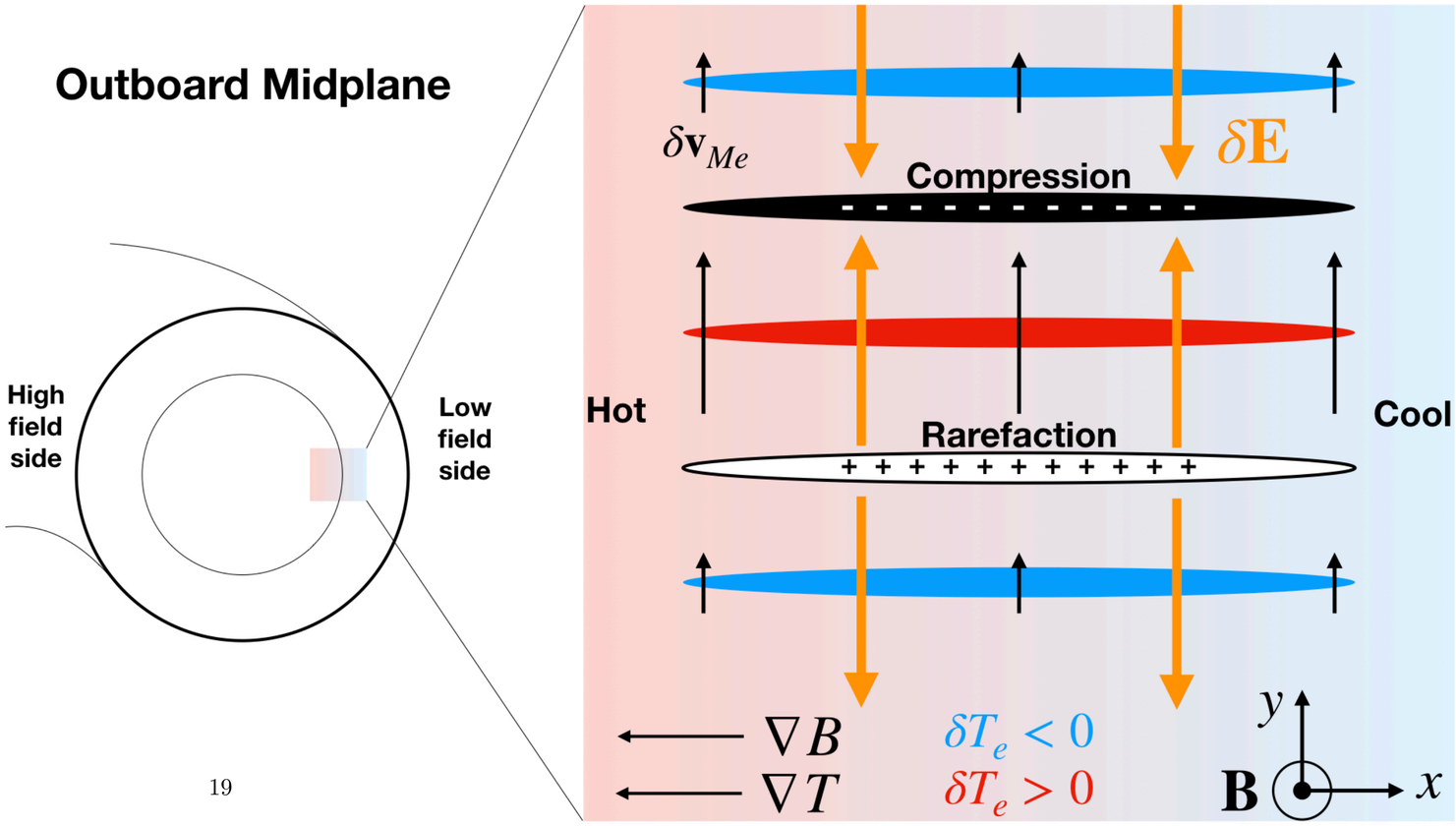

Physical picture for core toroidal ETG mode

- Toroidal instability usually has strongest linear drive at outboard midplane.

- Recall standard mechanism for core ETG (or ITG) mode.

$\rightarrow$ **cause** $\delta \mathbf{v}_{\boldsymbol{E}}$**.**

$\delta \mathbf{v_E}$ **sucks hot plasma into** $\delta \boldsymbol{T_e} > \mathbf{0}$**,**

cold plasma into $\delta \boldsymbol{T_e} < \mathbf{0}$**,**

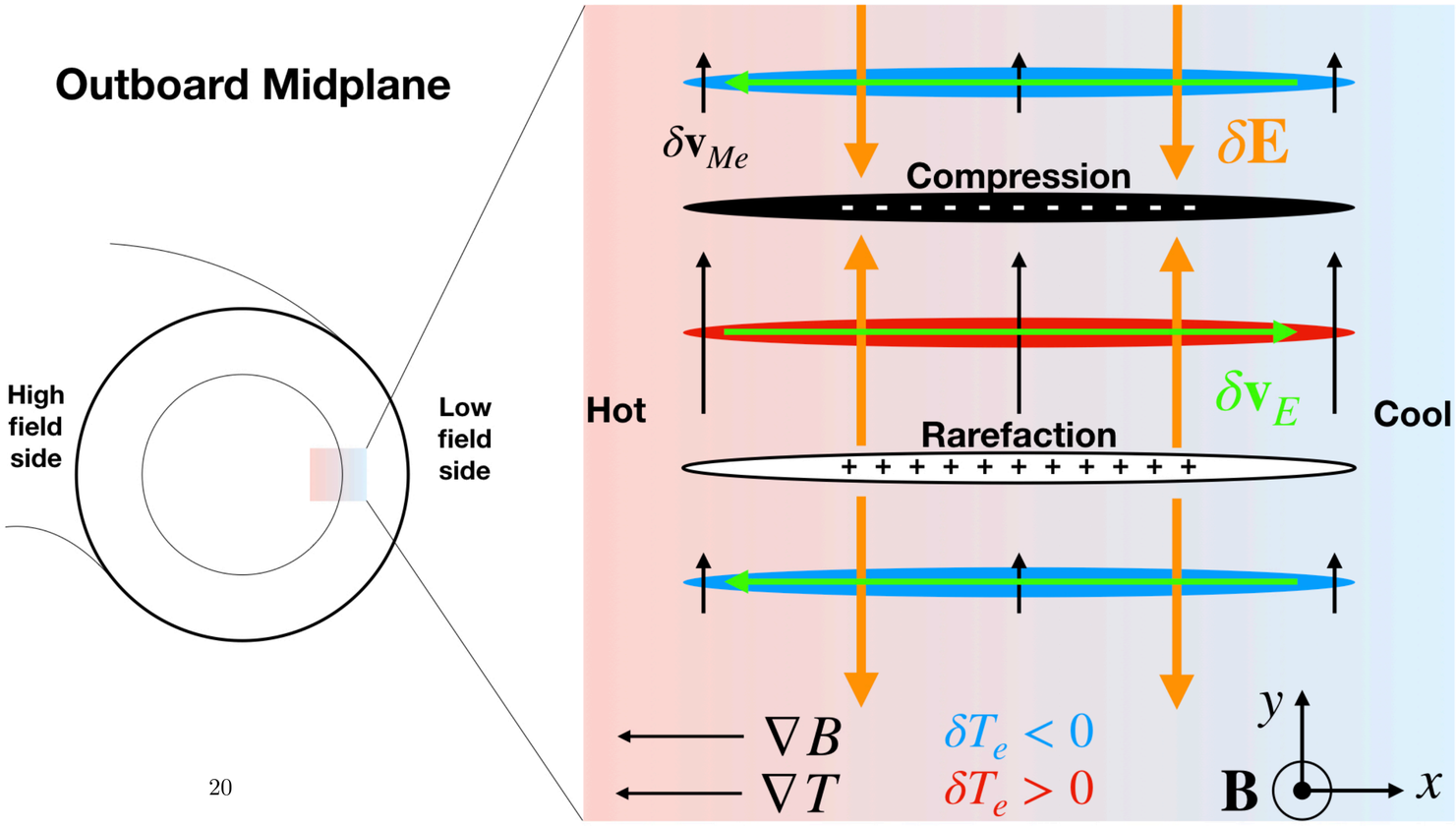

Physical picture for core toroidal ETG mode

- Toroidal instability usually has strongest linear drive at outboard midplane.
- Recall standard mechanism for core ETG (or ITG) mode.

Reinforces temperature perturbation, causes positive feedback loop, → **instability**!

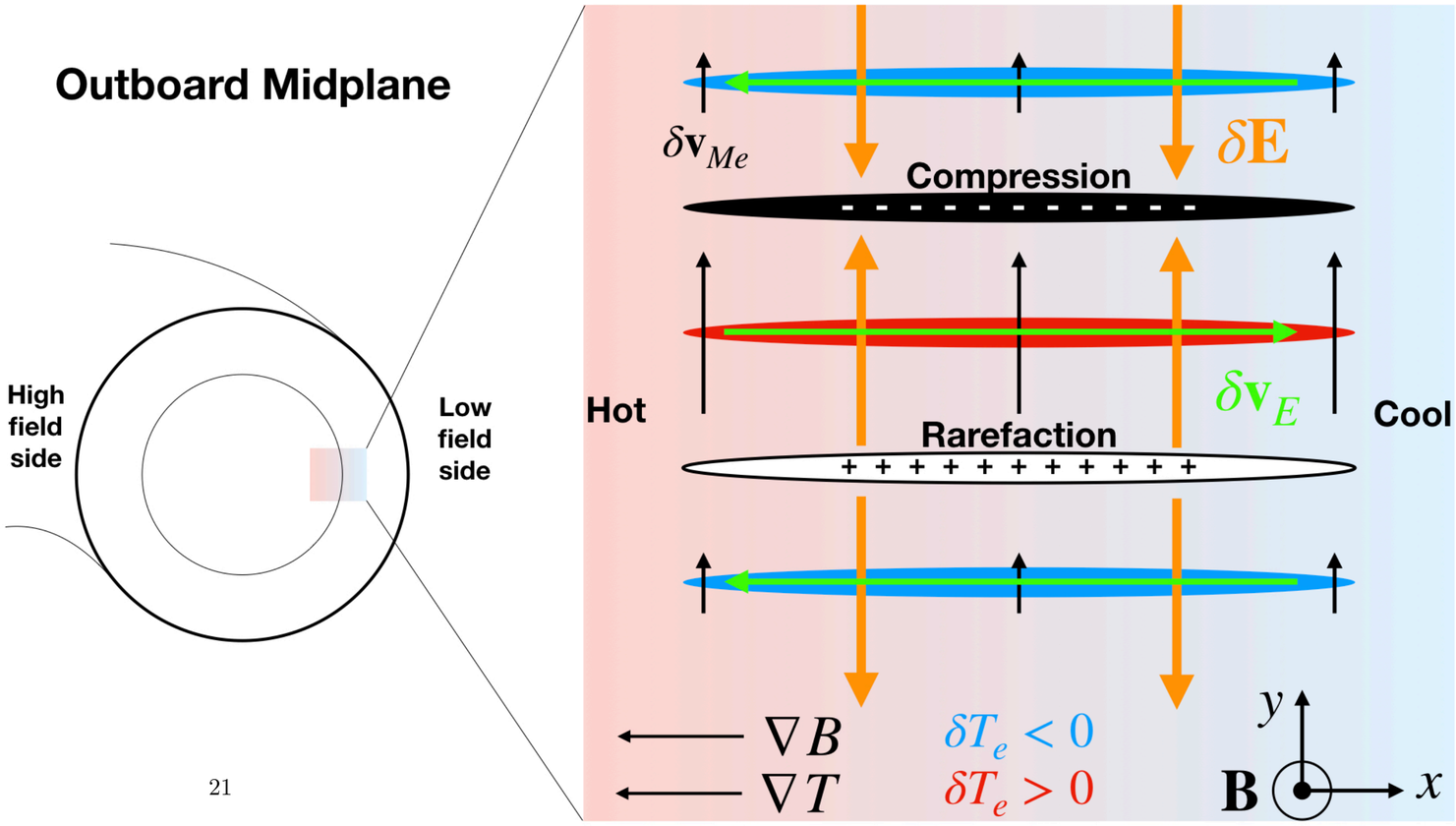

Physical picture for core toroidal ETG mode

Instability far away from outboard midplane with nonzero k_{radial}

At plasma top, need radial wavenumber to generate compression.

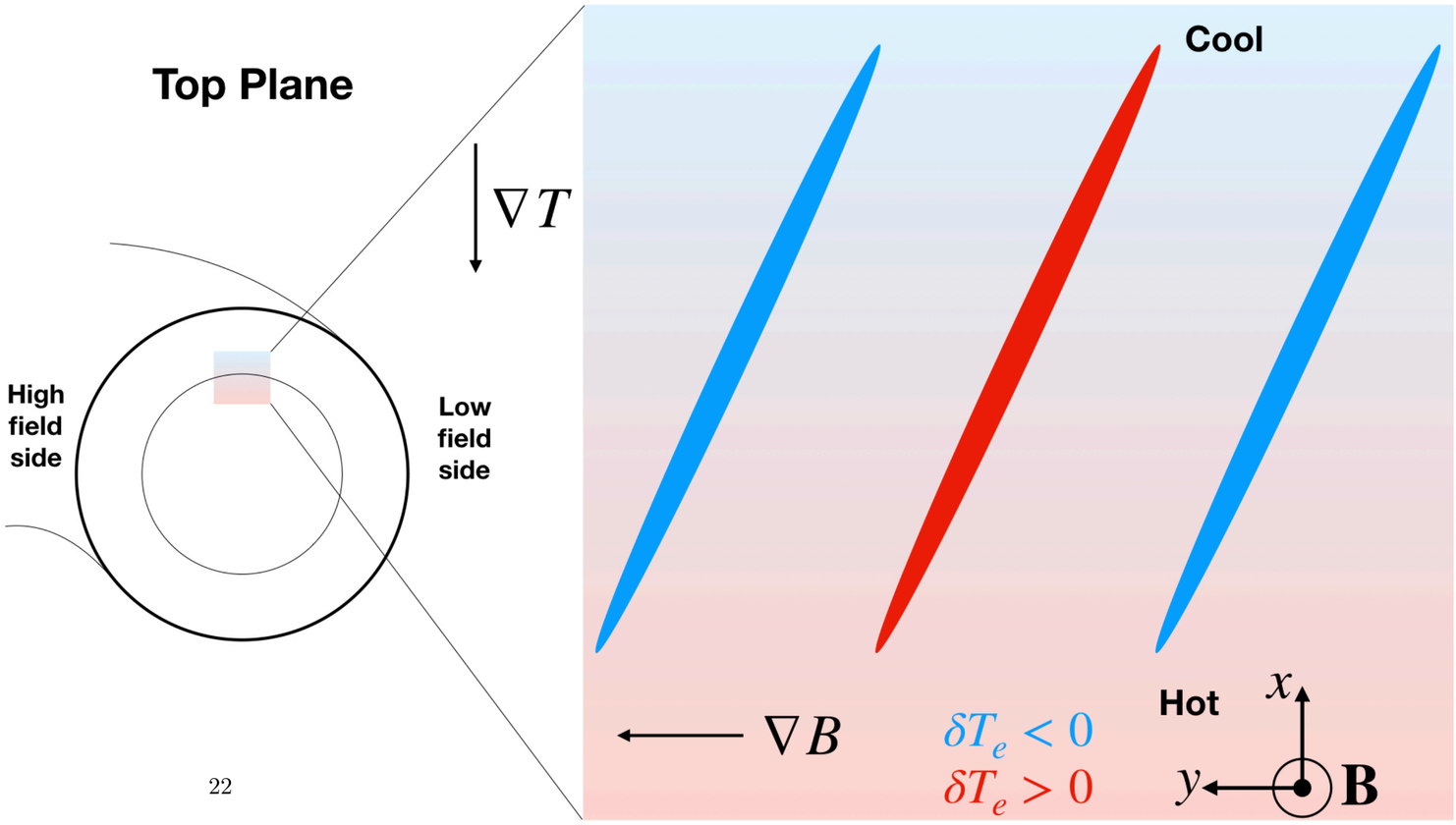

Physical picture for core toroidal ETG mode

Instability far away from outboard midplane with nonzero k_{radial}

Magnetic drifts now have component parallel to $\mathbf{k}_\perp$.

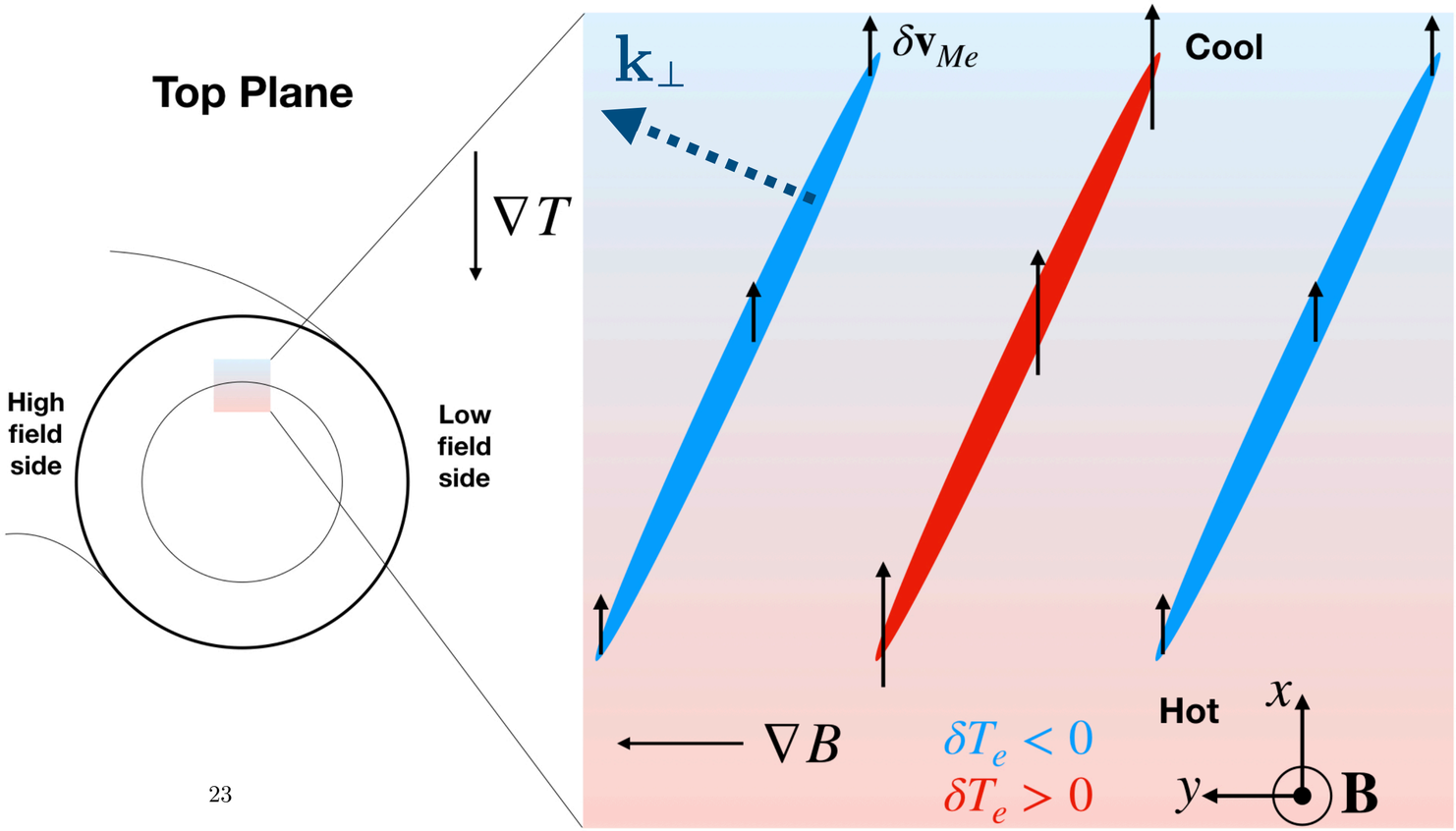

Physical picture for core toroidal ETG mode

Instability far away from outboard midplane with nonzero k_{radial}

Magnetic drifts cause compression and rarefaction.

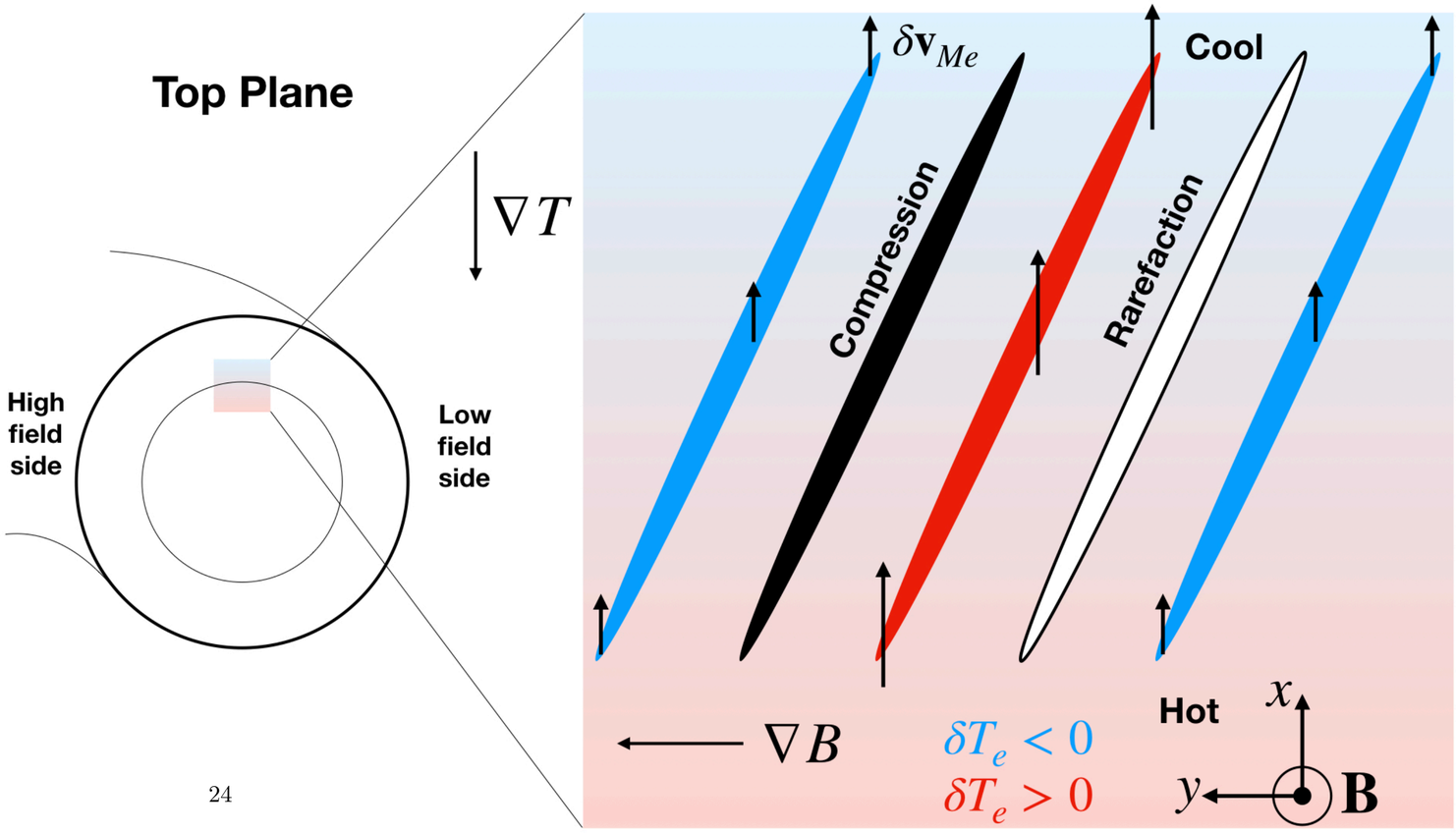

Physical picture for core toroidal ETG mode

Instability far away from outboard midplane with nonzero $\mathbf{k}_{\mathrm{radial}}$

Note: if $\mathbf{k}_{\mathrm{radial}} = 0$, no compression/rarefaction

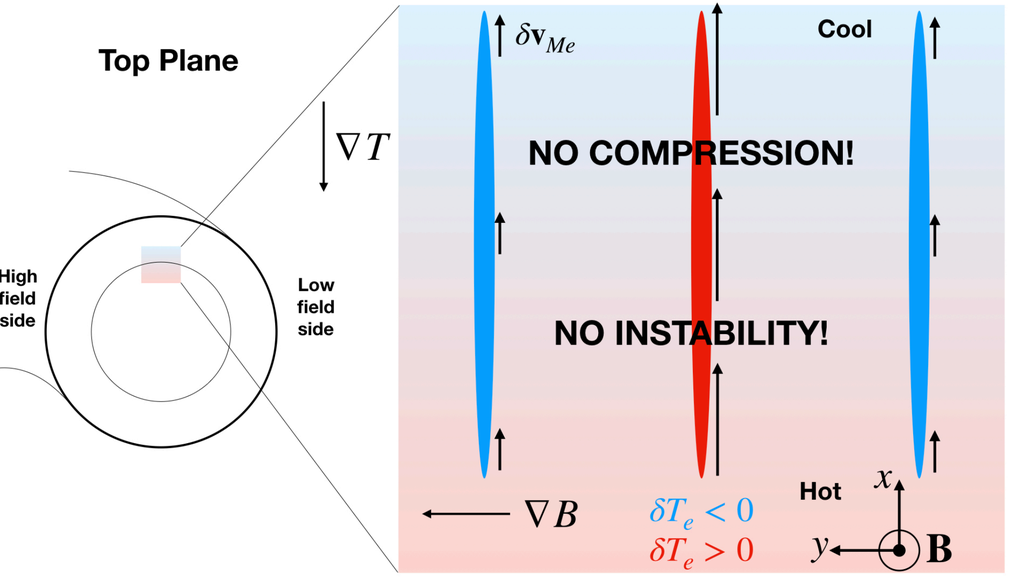

Magnetic drifts cause compression and rarefaction.

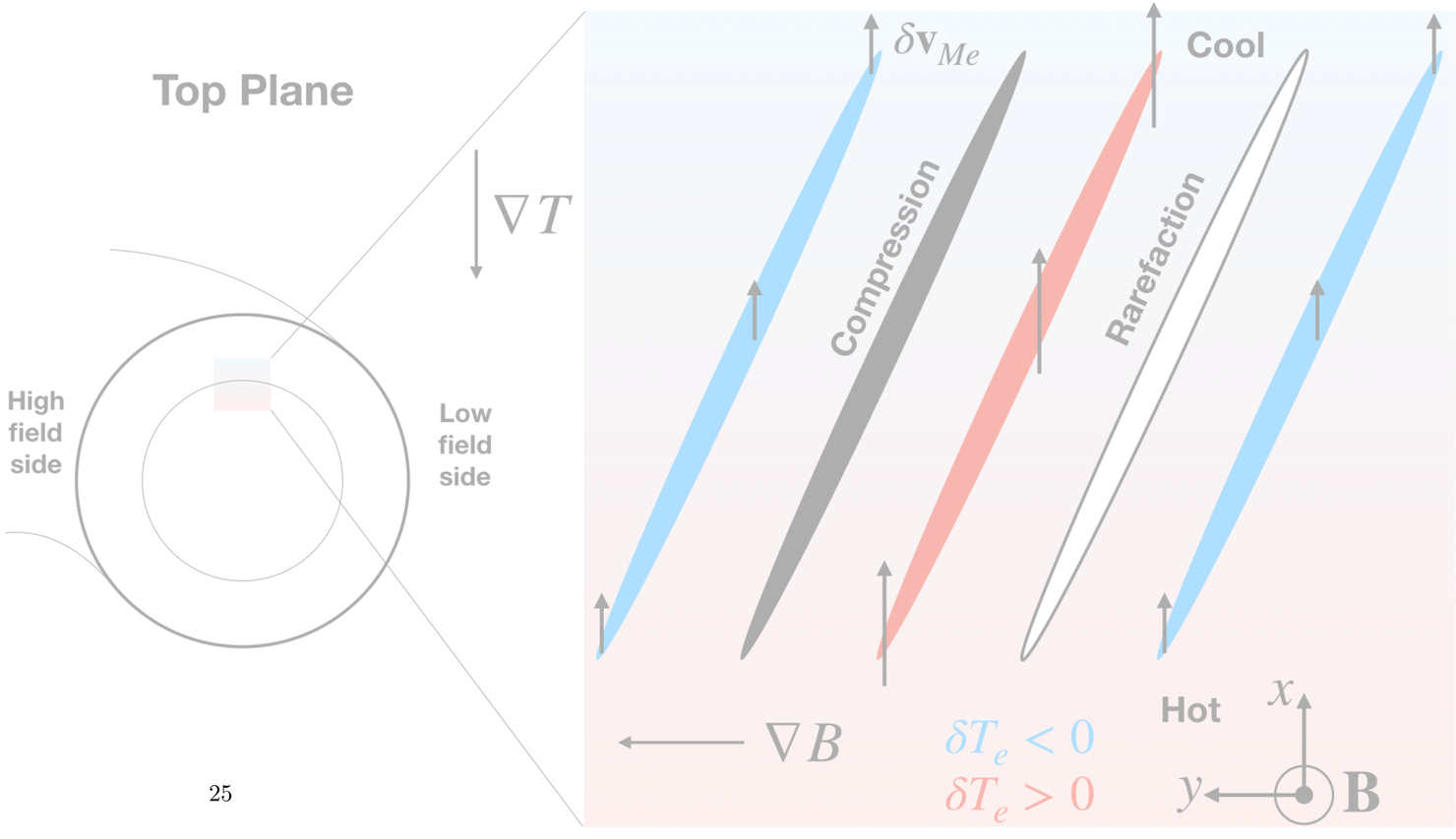

For instability, need $\mathbf{k}_{\perp} \cdot \mathbf{v}_{Me} \neq 0$.

Physical picture for core toroidal ETG mode

Instability far away from outboard midplane with nonzero k_{radial}

$\rightarrow$ induce δE.

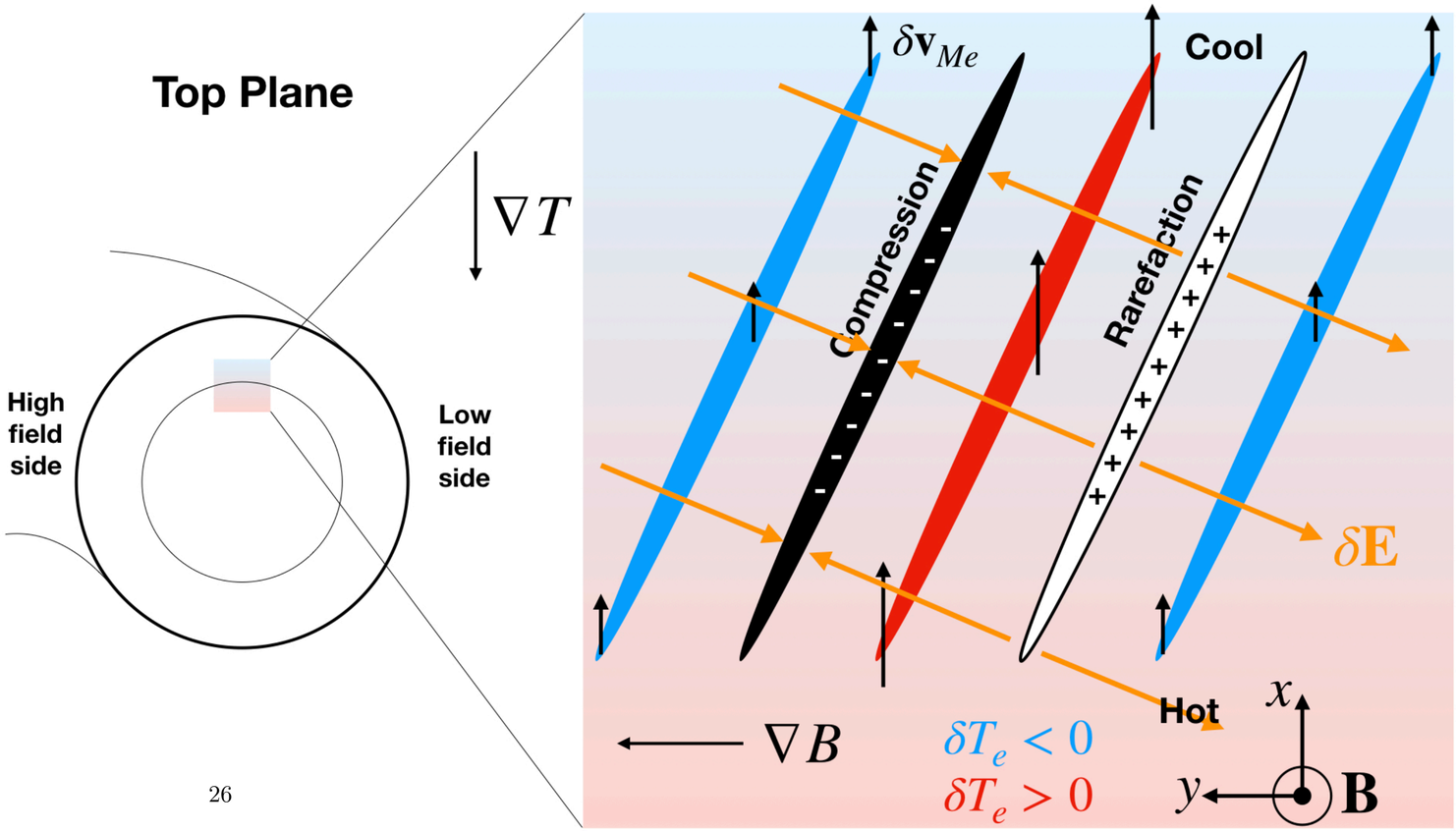

Physical picture for core toroidal ETG mode

Instability far away from outboard midplane with nonzero k_{radial}

$\rightarrow \delta \mathbf{v}_E$.

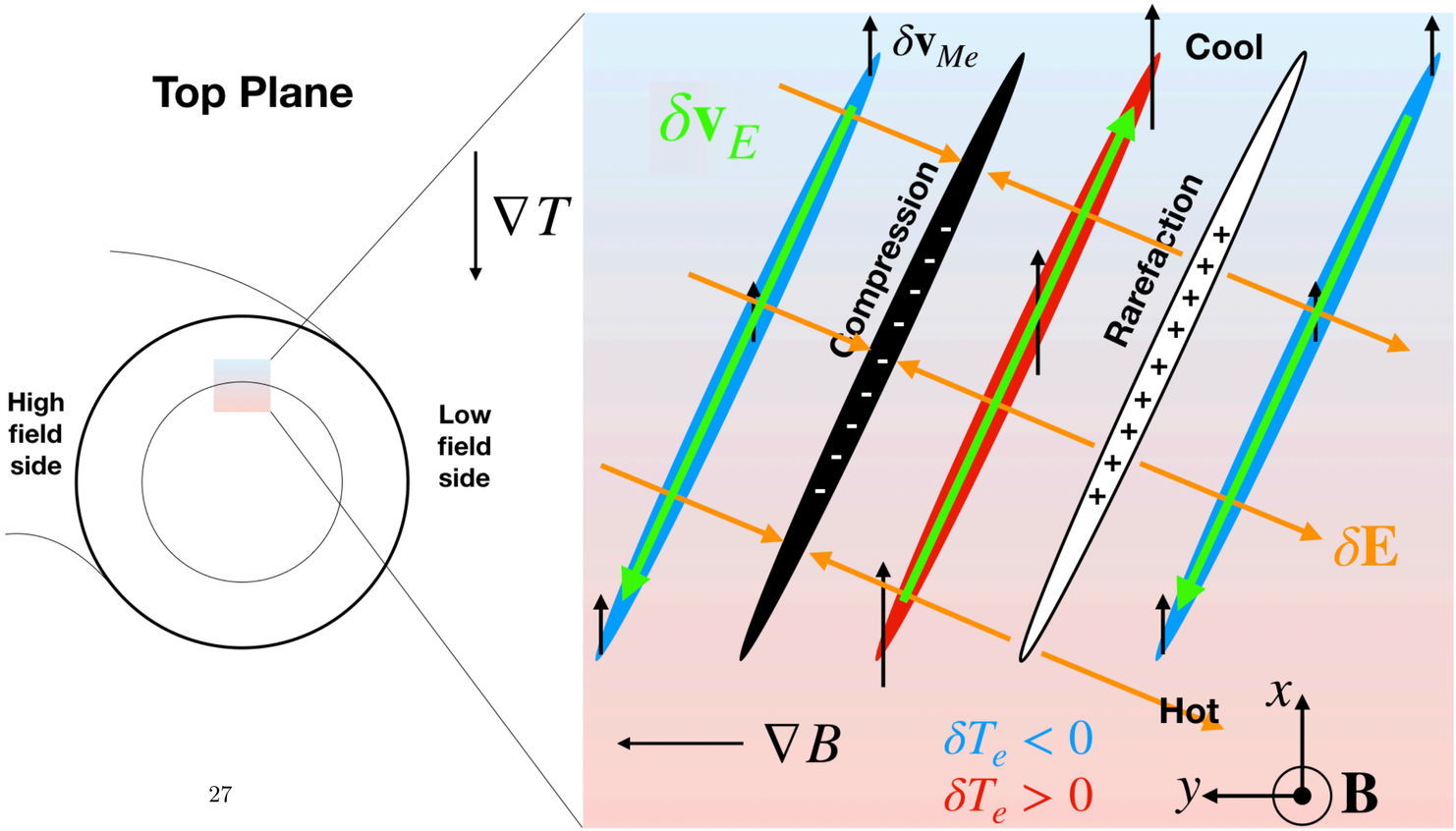

Physical picture for core toroidal ETG mode

Instability far away from outboard midplane with nonzero k_{radial}

Instability!

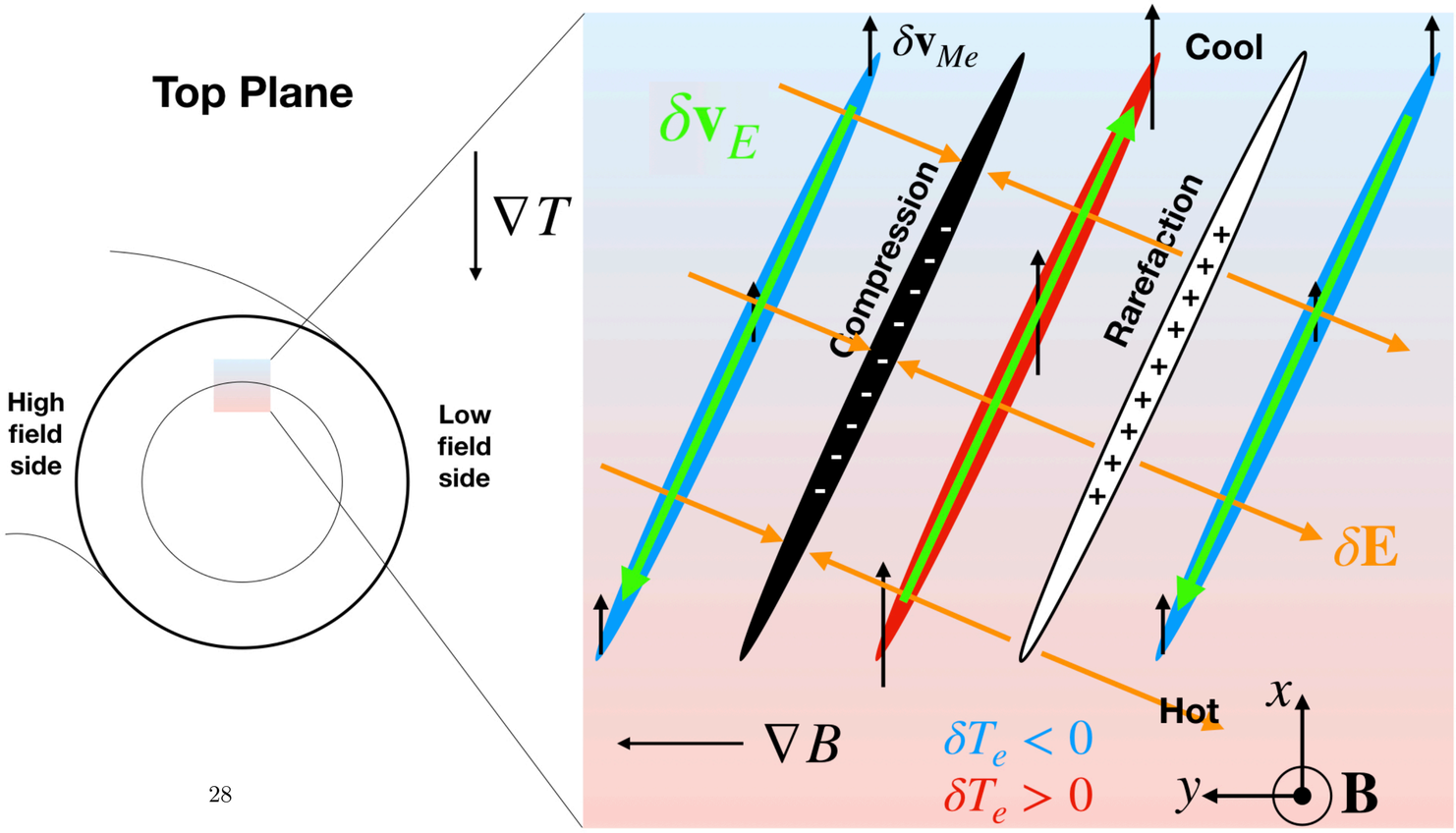

Why don't we see significant ITG/ETG core turbulence away from outboard midplane?

Why don't we see significant ITG/ETG core turbulence away from outboard midplane?

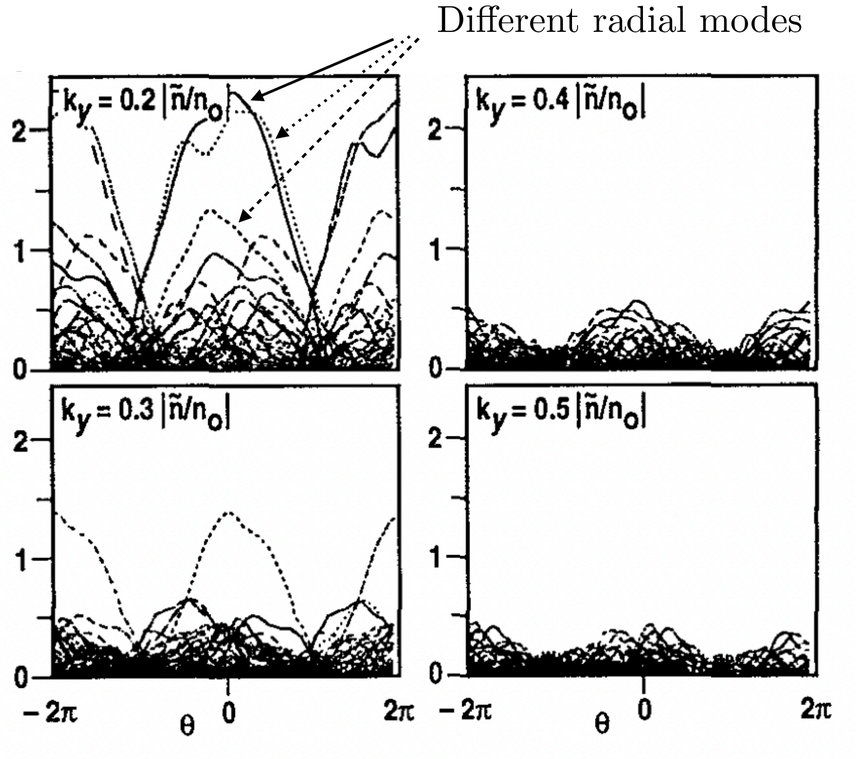

Waltz et al. PoP, **1**, 2229 (1994):
Electron density perturbations versus extended poloidal angle for nonlinear gyrofluid ITG simulation, core TFTR geometry.

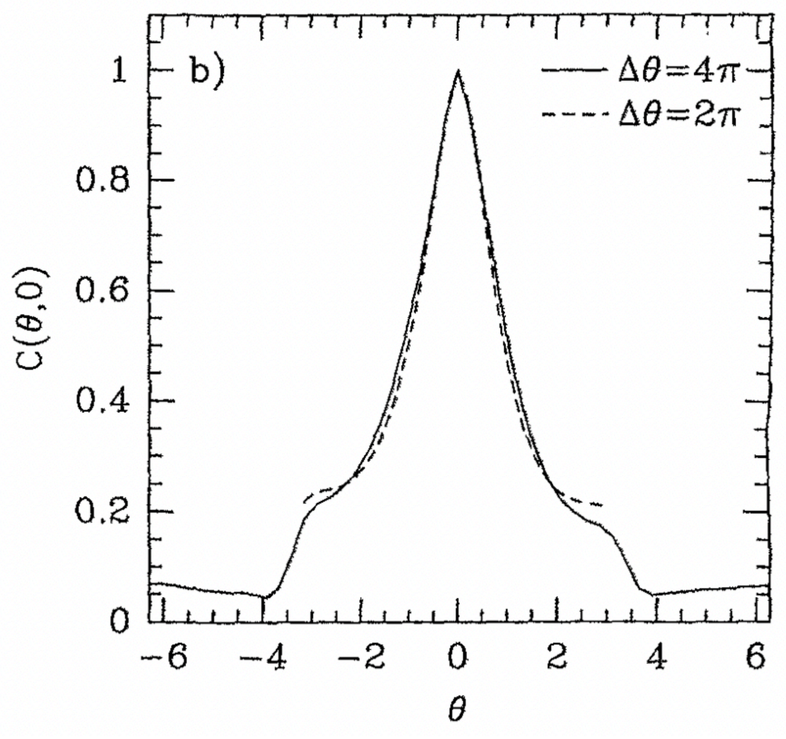

Beer et al. PoP, **2**, 2687 (1995):
Parallel correlation function for electrostatic potential in nonlinear gyrofluid ITG simulation, core TFTR geometry.

Why don't we see significant ITG/ETG core turbulence away from outboard midplane?

Answer: recall outer scale relation

$$k_y \rho_e \sim \frac{1}{q} \frac{L_{Te}}{R}.$$

—> in core, $k_y \rho_i \gg 1$ for ETG outer scale.

- At $k_y \rho_e \sim 1$, finite Larmor radius (FLR) damping constrains strongly-driven modes to outboard midplane region.

Why don't we see significant ITG/ETG core turbulence away from outboard midplane?

Answer: recall outer scale relation

$$k_y \rho_e \sim \frac{1}{q} \frac{L_{Te}}{R}.$$

—> in core, $k_y \rho_i \gg 1$ for ETG outer scale.

- At $k_y \rho_e \sim 1$, finite Larmor radius (FLR) damping constrains strongly-driven modes to outboard midplane region.
- **In pedestal, we are freed of this FLR constraint because outer scale at longer wavelengths $k_y \rho_i \sim 1$.**

Why don't we see significant ITG/ETG core turbulence away from outboard midplane?

For any toroidal ETG instability we require

$$\frac{\omega_{*e}^{T}}{\omega_{Me}} \sim \frac{k_y}{k_\perp}\frac{R_0}{L_{Te}} \gtrsim 1$$

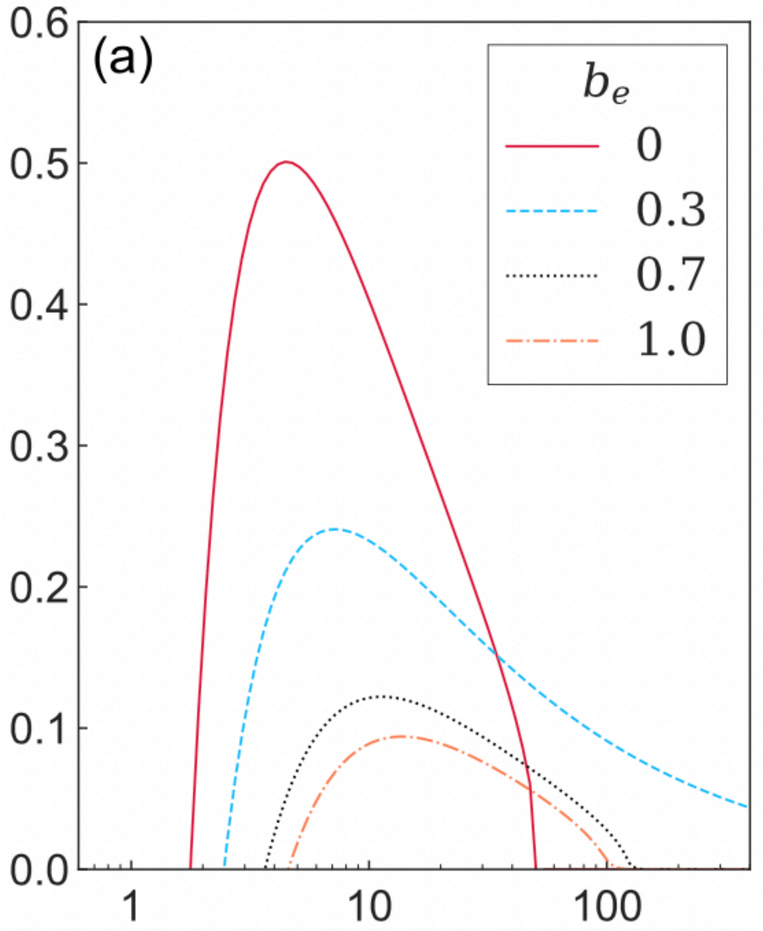

Linear growth rate (γ) versus $\omega_{*e}^{T}/\omega_{Me}$ at different b_e values [Parisi, 2020].

$b_e = (k_\perp \rho_e)^2/2.$

Why don't we see significant ITG/ETG core turbulence away from outboard midplane?

For any toroidal ETG instability we require

$$\frac{\omega_{*e}^{T}}{\omega_{Me}} \sim \frac{k_y}{k_\perp}\frac{R_0}{L_{Te}} \gtrsim 1$$

Important: $\omega_{*e}^{T}/\omega_{Me}$ constraint independent of k_y.

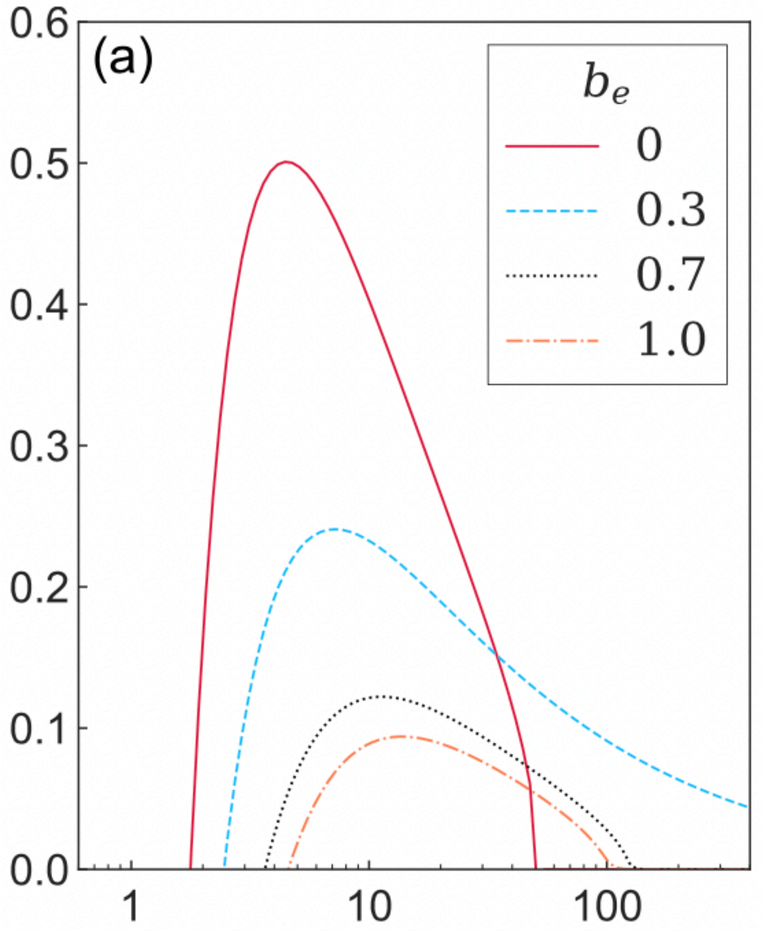

Linear growth rate (γ) versus $\omega_{*e}^{T}/\omega_{Me}$ at different b_e values [Parisi, 2020].

$b_e = (k_\perp \rho_e)^2/2.$

Why don't we see significant ITG/ETG core turbulence away from outboard midplane?

For any toroidal ETG instability we require

$$\frac{\omega_{*e}^{T}}{\omega_{Me}} \sim \frac{k_y}{k_\perp}\frac{R_0}{L_{Te}} \gtrsim 1$$

Important: $\omega_{*e}^{T}/\omega_{Me}$ constraint independent of k_y.

Highest growth rate for $3 \lesssim \omega_{*e}^{T}/\omega_{Me} \lesssim 30$.

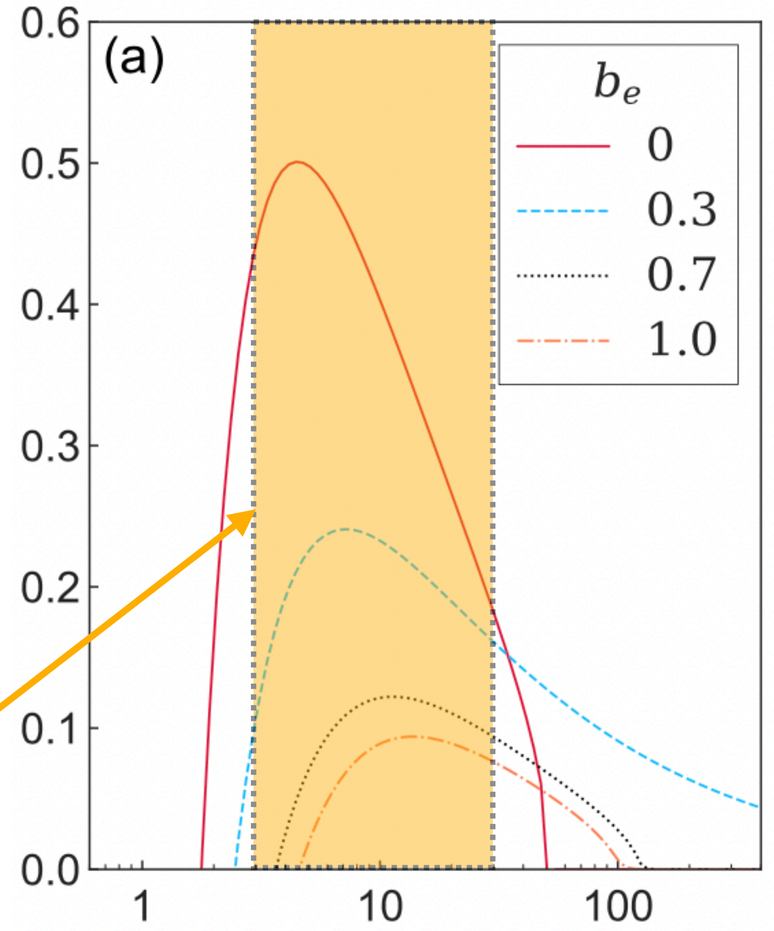

Linear growth rate (γ) versus $\omega_{*e}^{T}/\omega_{Me}$ at different b_e values [Parisi, 2020].

$b_e = (k_\perp \rho_e)^2/2$.

Linear core toroidal ETG physics

Magnetic drifts in CBC

- Take cyclone base case (CBC) core-like geometry and plot $\omega_{*e}^{T}/\omega_{Me}$ versus θ and θ_0.

Linear core toroidal ETG physics

Magnetic drifts in CBC

- Take cyclone base case (CBC) core-like geometry and plot $\omega_{*e}^{T}/\omega_{Me}$ versus θ and θ_0.
- Quantity $\theta_0 = k_x/\hat{s}k_y$ is the θ angle at which a mode has $k_{\text{radial}} = 0$ in a concentric-circle, large aspect ratio, low β tokamak [Beer, PoP, 1995], where you can write $k_{\text{radial}} = k_y\hat{s}(\theta_0 - \theta)$.
- In highly shaped pedestal geometry, θ_0 has less obvious physical meaning.

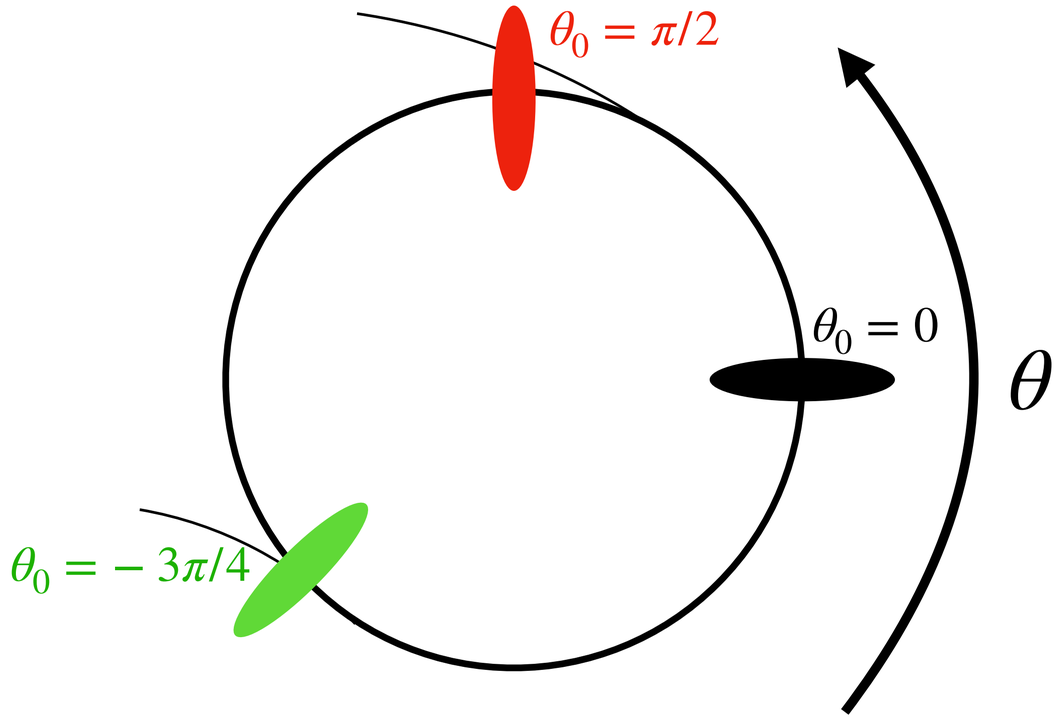

Different θ_0 values on a flux surface.

Linear core toroidal ETG physics

Magnetic drifts in CBC

We can identify where linear toroidal ETG is driven in (θ, θ_0) space.

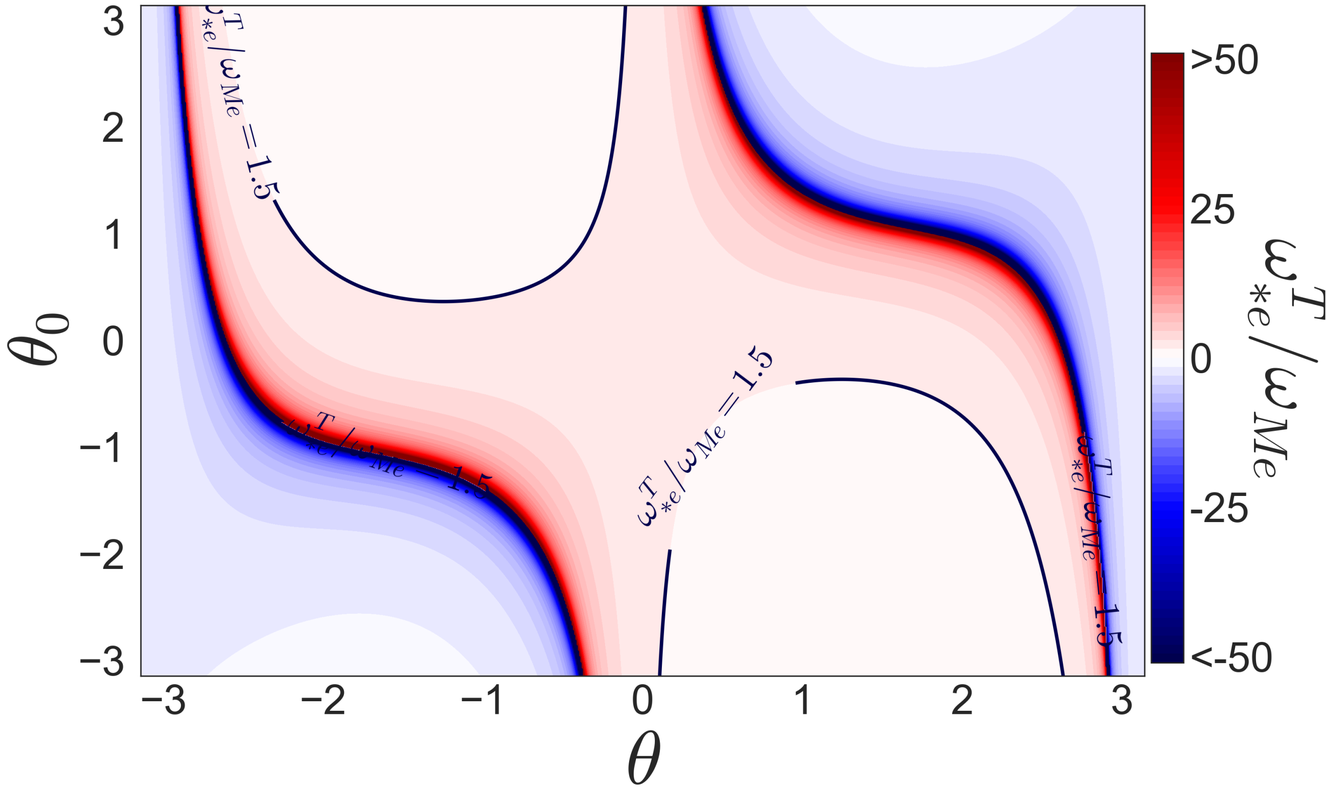

Linear core toroidal ETG physics

Magnetic drifts in CBC

$\omega^T_{*e}/\omega_{Me} < 0$ <—> **stable good curvature regions**

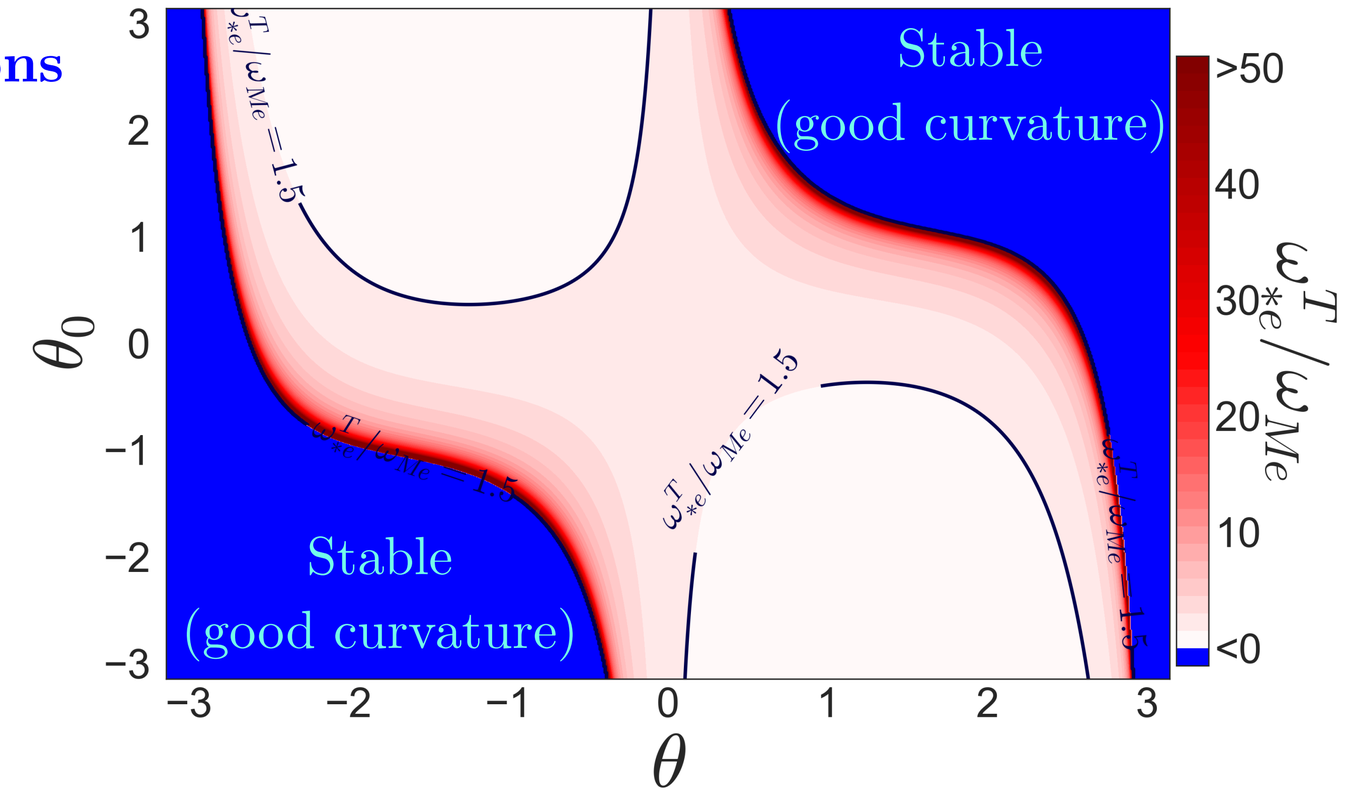

Linear core toroidal ETG physics

Magnetic drifts in CBC

stable

$\omega^T_{*e}/\omega_{Me} < 0$ <—> good curvature regions

stable

$0 < \omega^T_{*e}/\omega_{Me} \lesssim 1.5$ <—> bad curvature regions

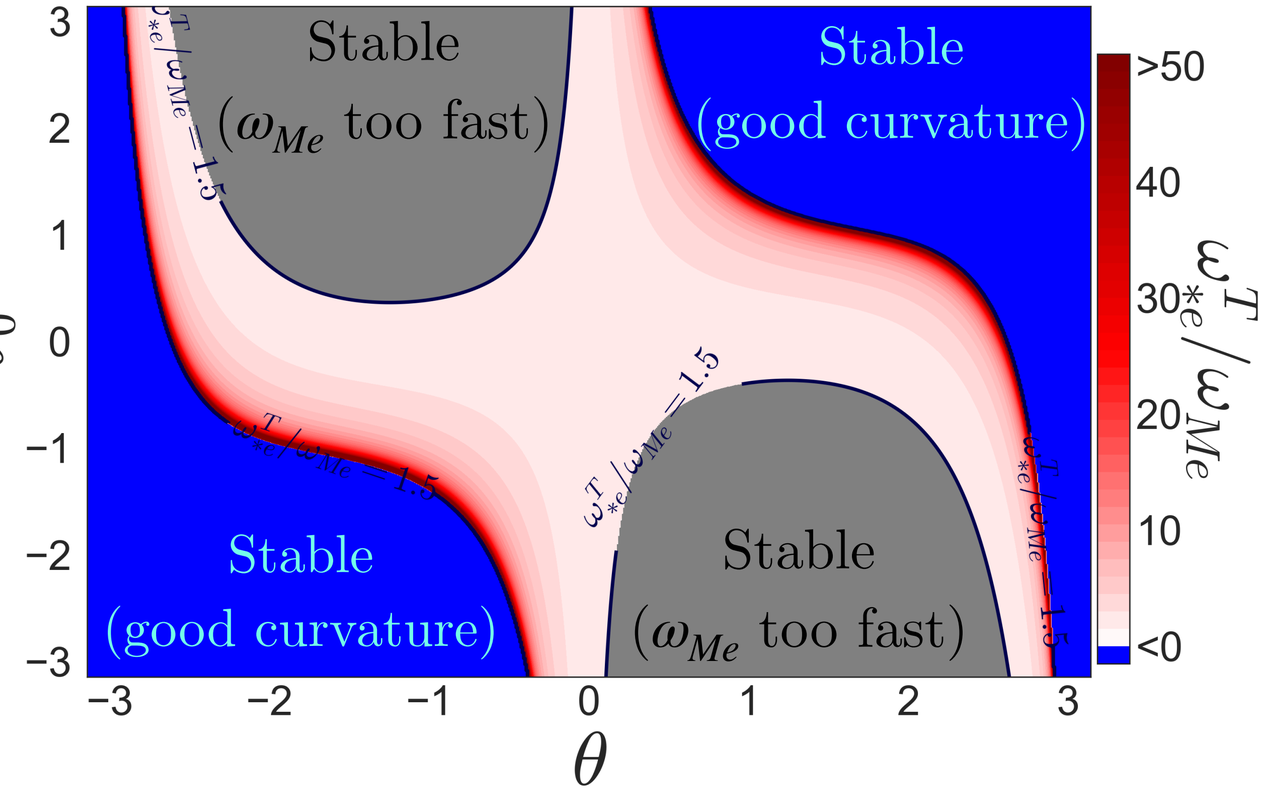

Linear core toroidal ETG physics

Magnetic drifts in CBC

stable

$\omega^T_{*e}/\omega_{Me} < 0$ <—> **good curvature regions**

stable

$0 < \omega^T_{*e}/\omega_{Me} \lesssim 1.5$ <—> **bad curvature regions**

highly unstable

$3 < \omega^T_{*e}/\omega_{Me} \lesssim 30$ <—> **bad curvature regions**

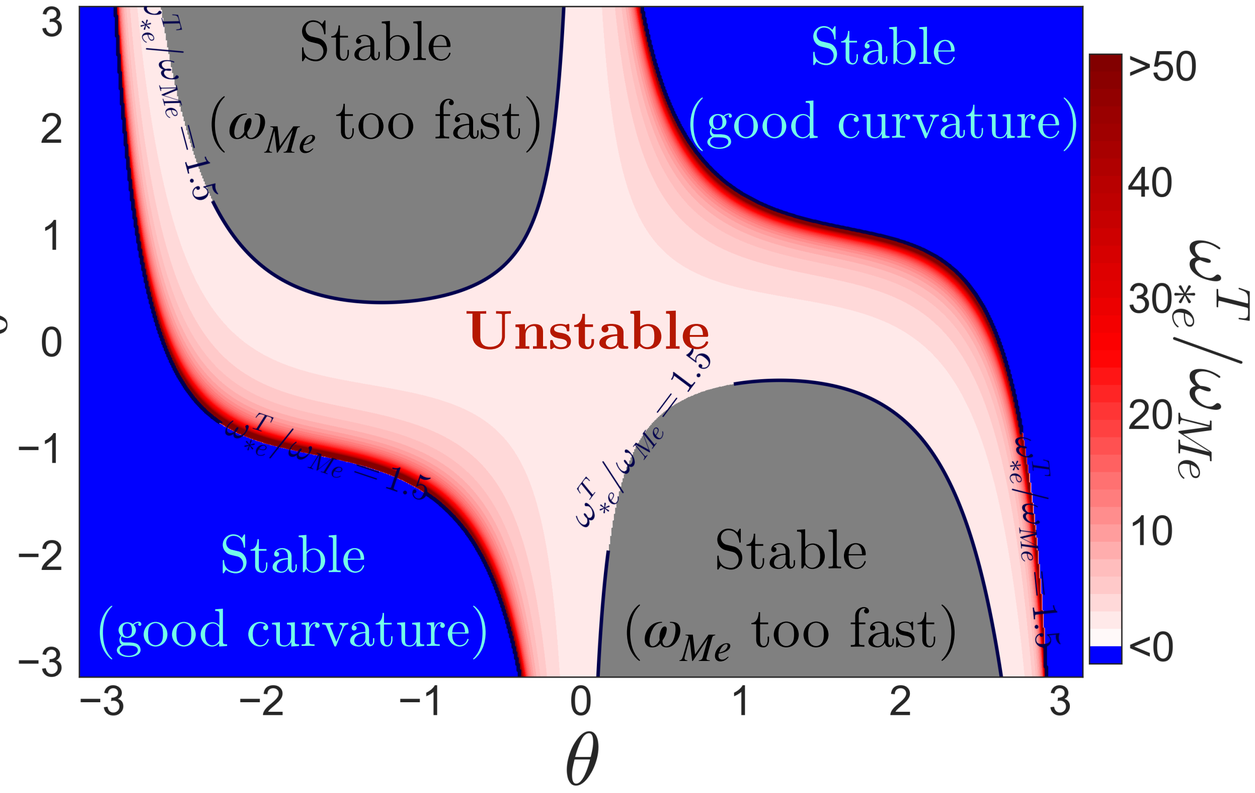

Linear core toroidal ETG physics

Magnetic drifts in CBC

stable

$\omega_{*e}^T/\omega_{Me} < 0$ <—> **good curvature regions**

stable

$0 < \omega_{*e}^T/\omega_{Me} \lesssim 1.5$ <—> bad curvature regions

highly unstable

$3 < \omega_{*e}^T/\omega_{Me} \lesssim 30$ <—> **bad curvature regions**

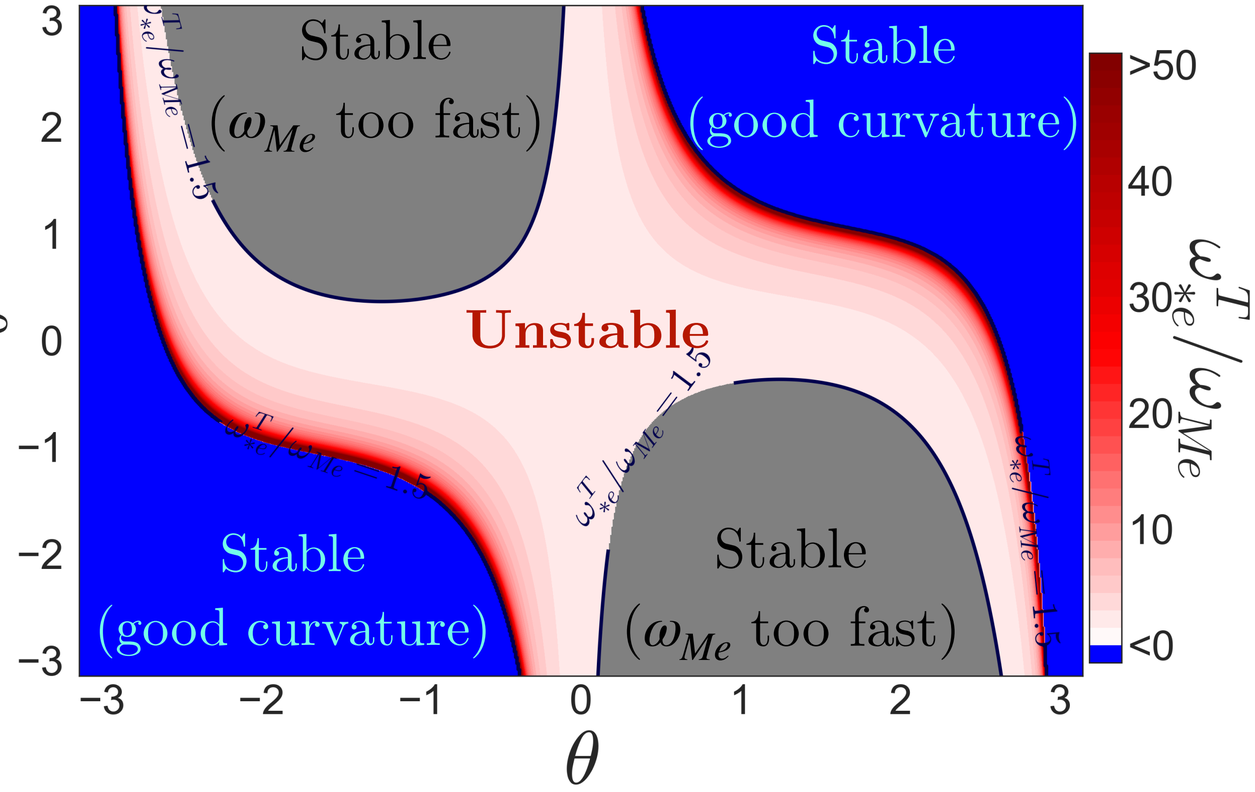

note: $|\theta_0| > \pi$ relatively unimportant nonlinearly, so ignore for now.

Linear core toroidal ETG physics

Finite Larmor radius (FLR) damping

- FLR damping competes with magnetic drifts to determine parallel distribution of turbulence.

Linear core toroidal ETG physics

Finite Larmor radius (FLR) damping

- FLR damping competes with magnetic drifts to determine parallel distribution of turbulence.

- We use quantity $\Gamma_0(b_e) = I_0(b_e)\exp(-b_e)$ to measure strength of FLR damping. Appears in toroidal ETG dispersion relation.

Linear core toroidal ETG physics

Finite Larmor radius (FLR) damping

- FLR damping competes with magnetic drifts to determine parallel distribution of turbulence.
- We use quantity $\Gamma_0(b_e) = I_0(b_e)\exp(-b_e)$ to measure strength of FLR damping. Appears in toroidal ETG dispersion relation.
- When $\Gamma_0 \lesssim 0.5$, linear growth rate decreases significantly.

Linear core toroidal ETG physics

Finite Larmor radius (FLR) damping

- FLR damping competes with magnetic drifts to determine parallel distribution of turbulence.
- We use quantity $\Gamma_0(b_e) = I_0(b_e)\exp(-b_e)$ to measure strength of FLR damping. Appears in toroidal ETG dispersion relation.
- When $\Gamma_0 \lesssim 0.5$, linear growth rate decreases significantly.

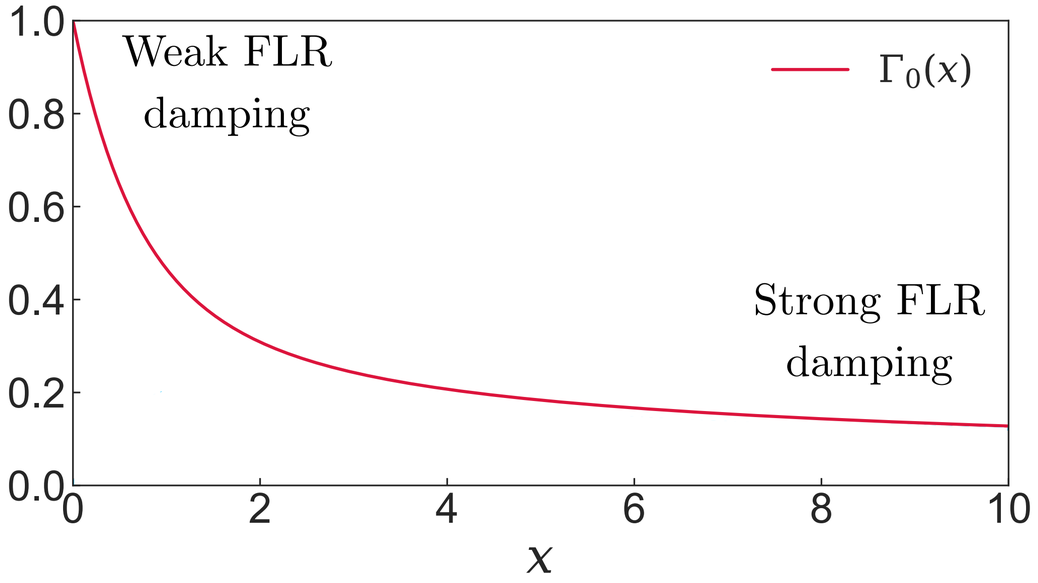

Linear core toroidal ETG physics

Finite Larmor radius damping in CBC for $k_y\rho_e = 1.0$.

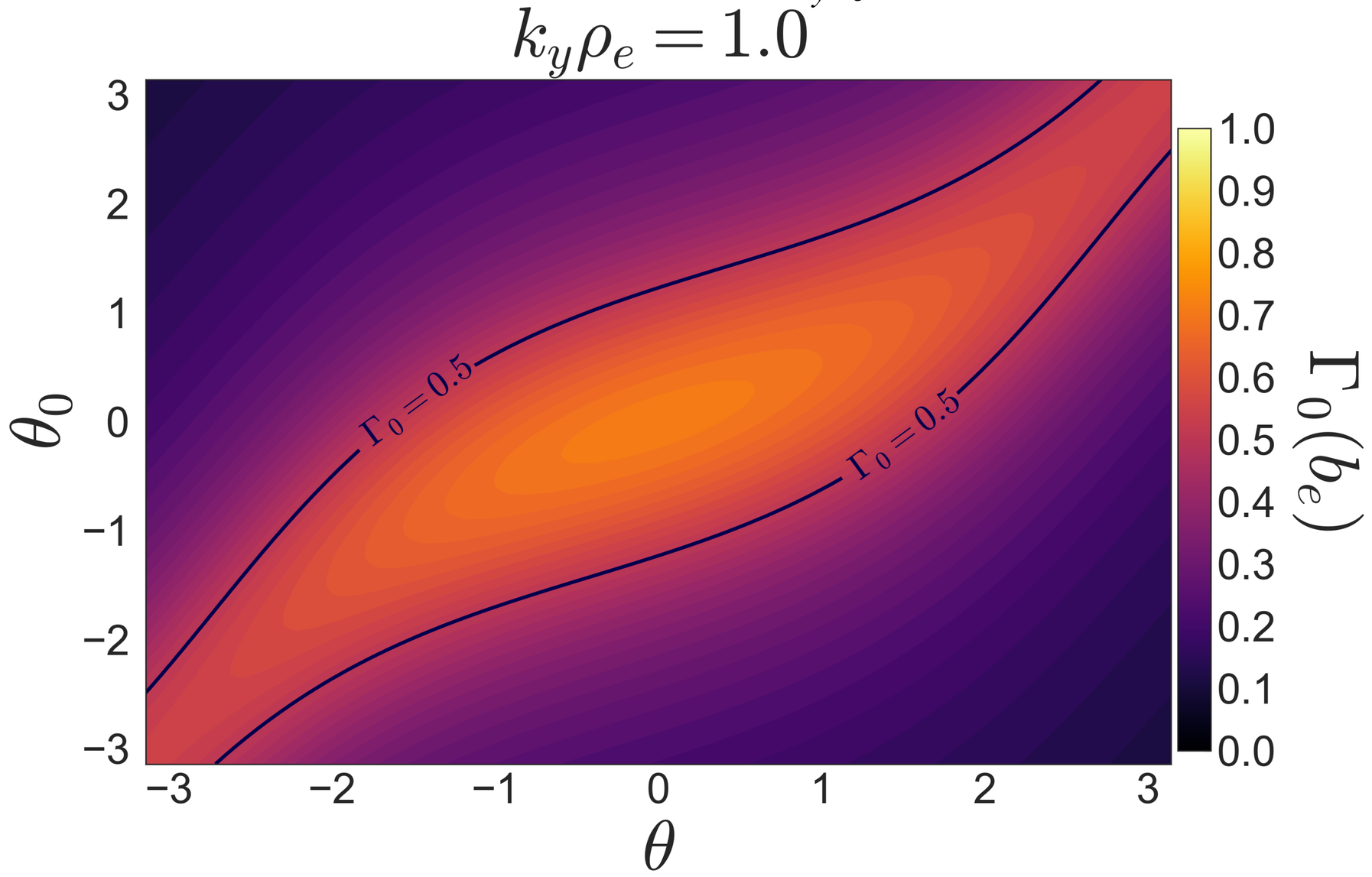

Linear core toroidal ETG physics

Finite Larmor radius damping in CBC for $k_y\rho_e = 1.0$.

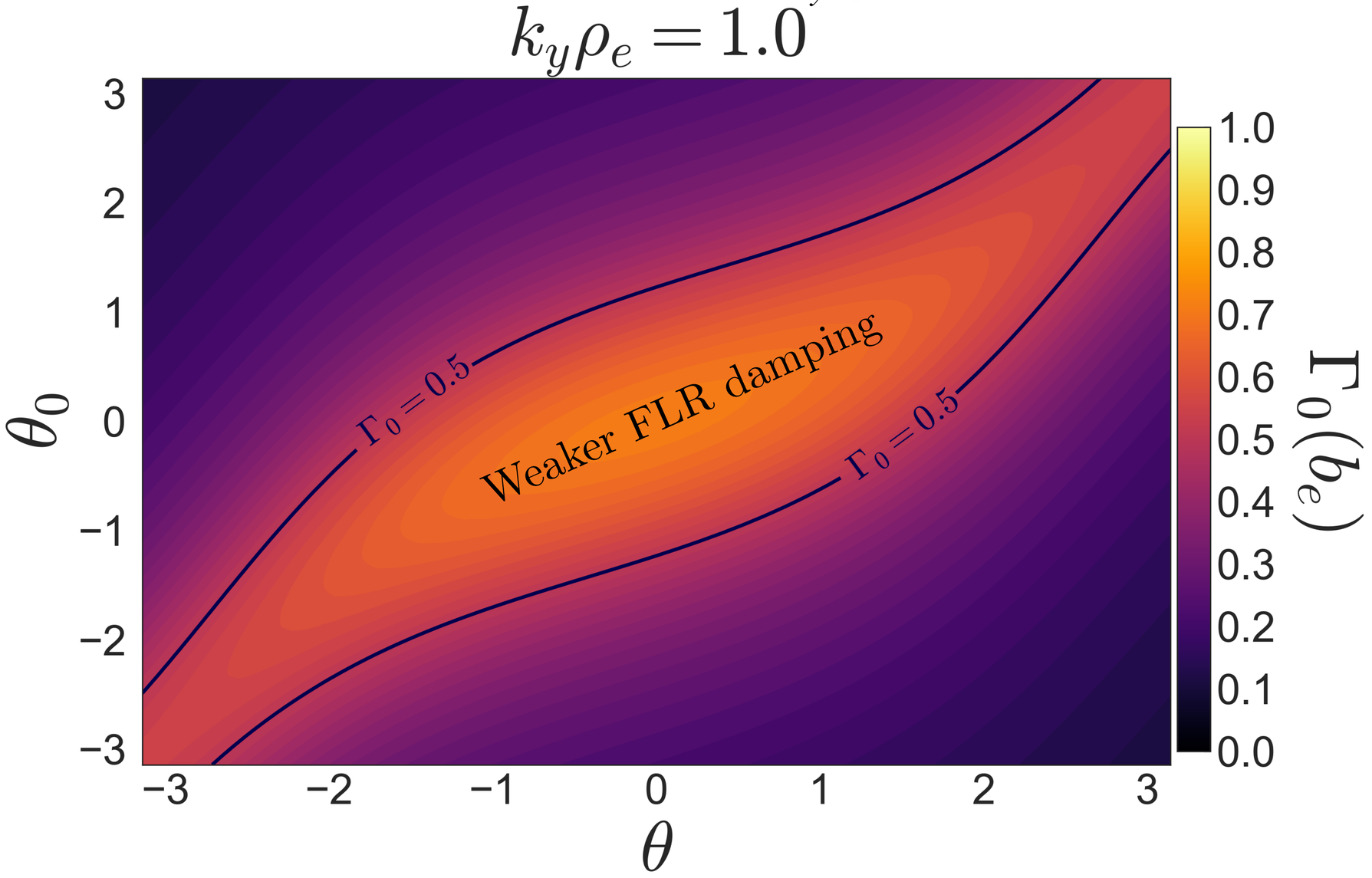

Linear core toroidal ETG physics

Finite Larmor radius damping in CBC for $k_y\rho_e = 1.0$.

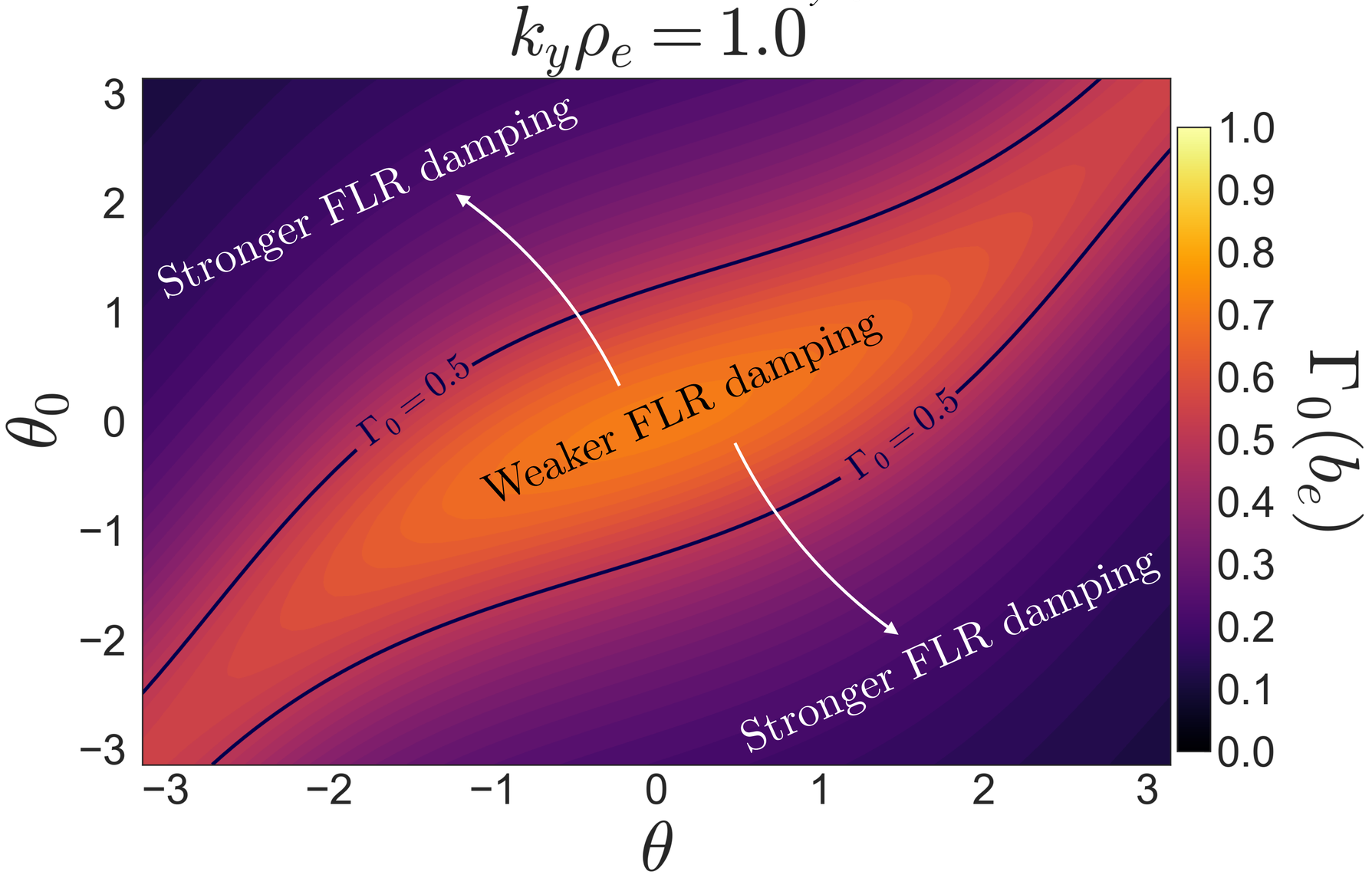

Linear core toroidal ETG physics

Combine constraints:

Magnetic drift constraint:

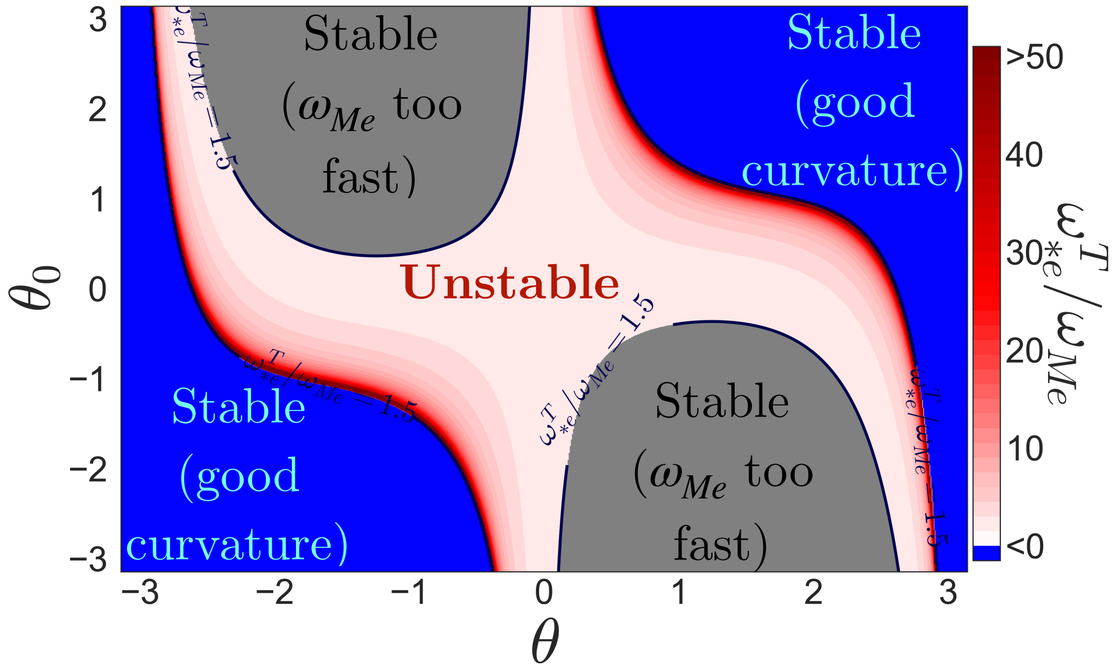

+

FLR damping constraint:

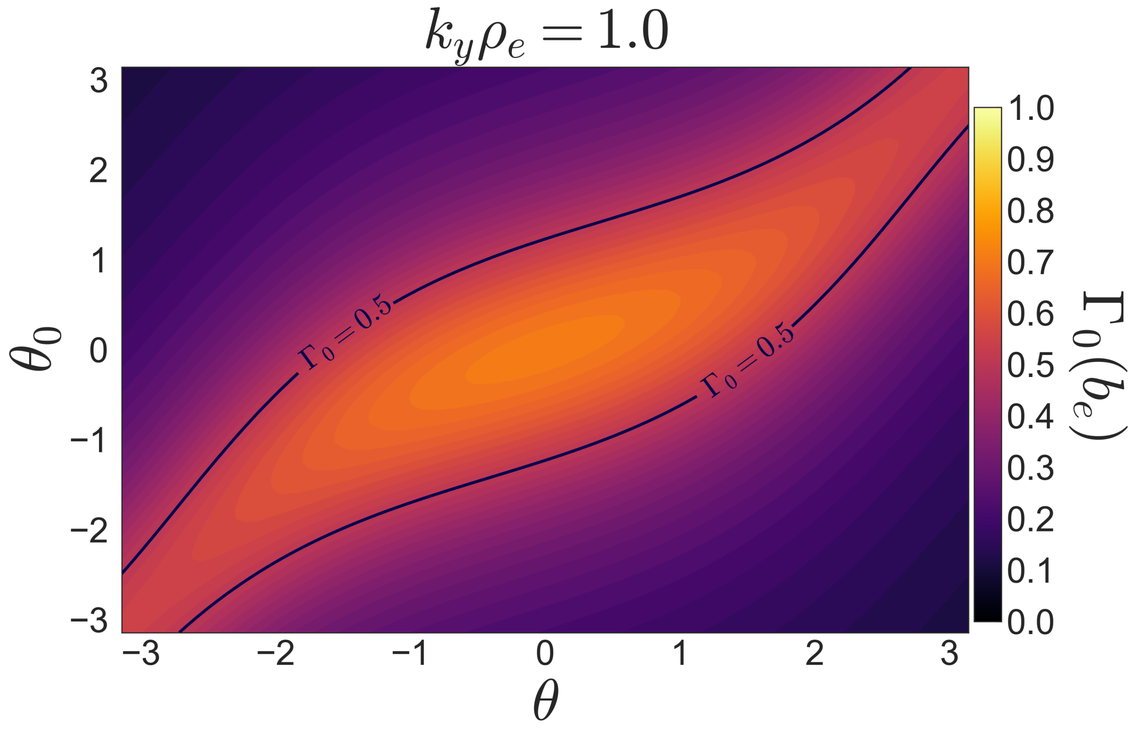

Linear core toroidal ETG physics

Combining magnetic drift and FLR constraints at $k_y\rho_e = 1$

FLR damping constraint: select only unstable regions with $\Gamma_0 \geq 0.5$

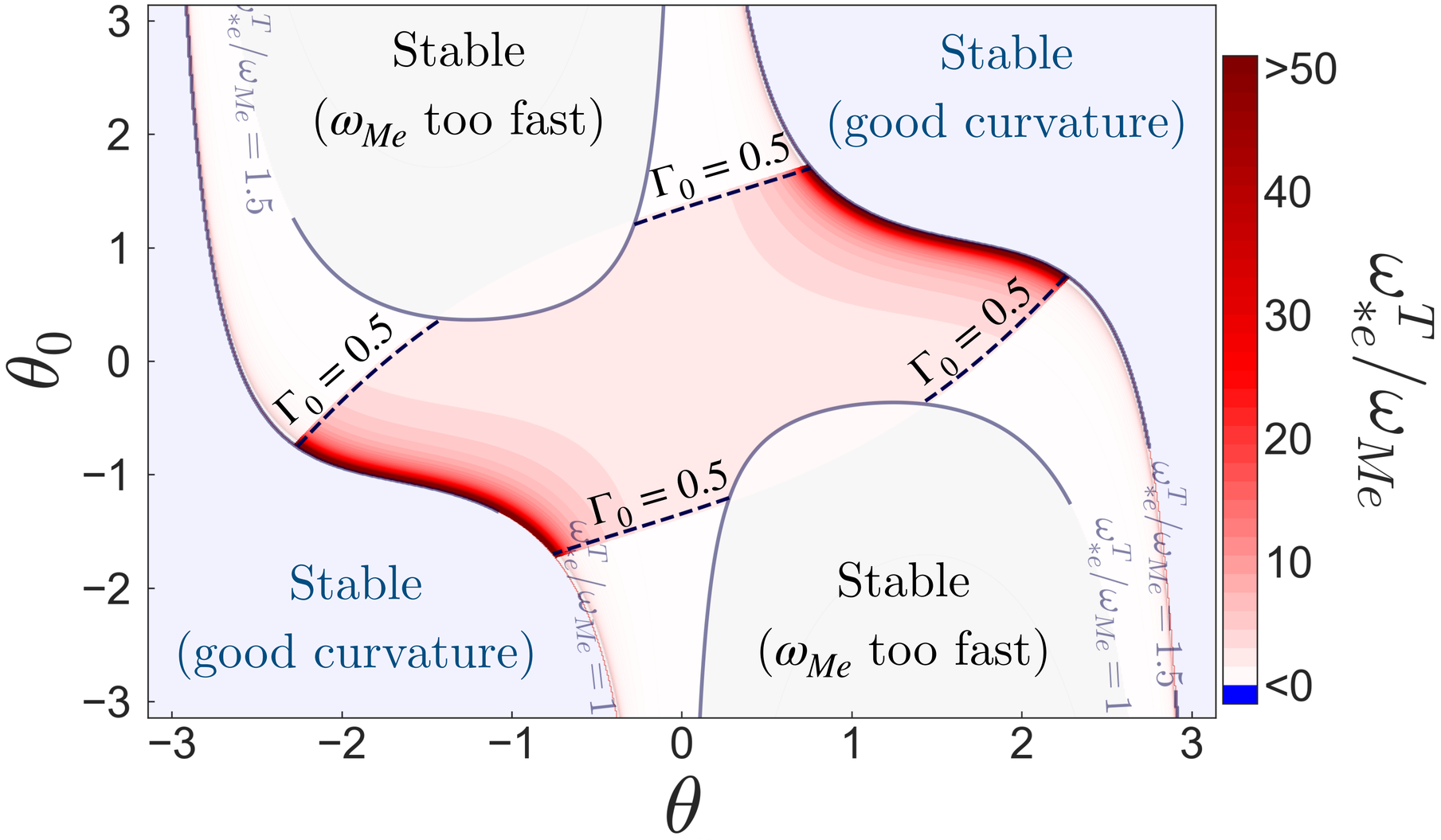

Linear core toroidal ETG physics

Combining magnetic drift and FLR constraints at $k_y\rho_e = 1$

stable

$\omega^T_{*e}/\omega_{Me} < 0$ <—> good curvature regions

stable

$0 < \omega^T_{*e}/\omega_{Me} \lesssim 1.5$ <—> bad curvature regions

highly unstable

$3 < \omega^T_{*e}/\omega_{Me} \lesssim 30$ <—> bad curvature regions

$3 \lesssim \omega^T_{*e}/\omega_{Me} \lesssim 30$
+
$\Gamma_0 \simeq 1$
<—>
most unstable region

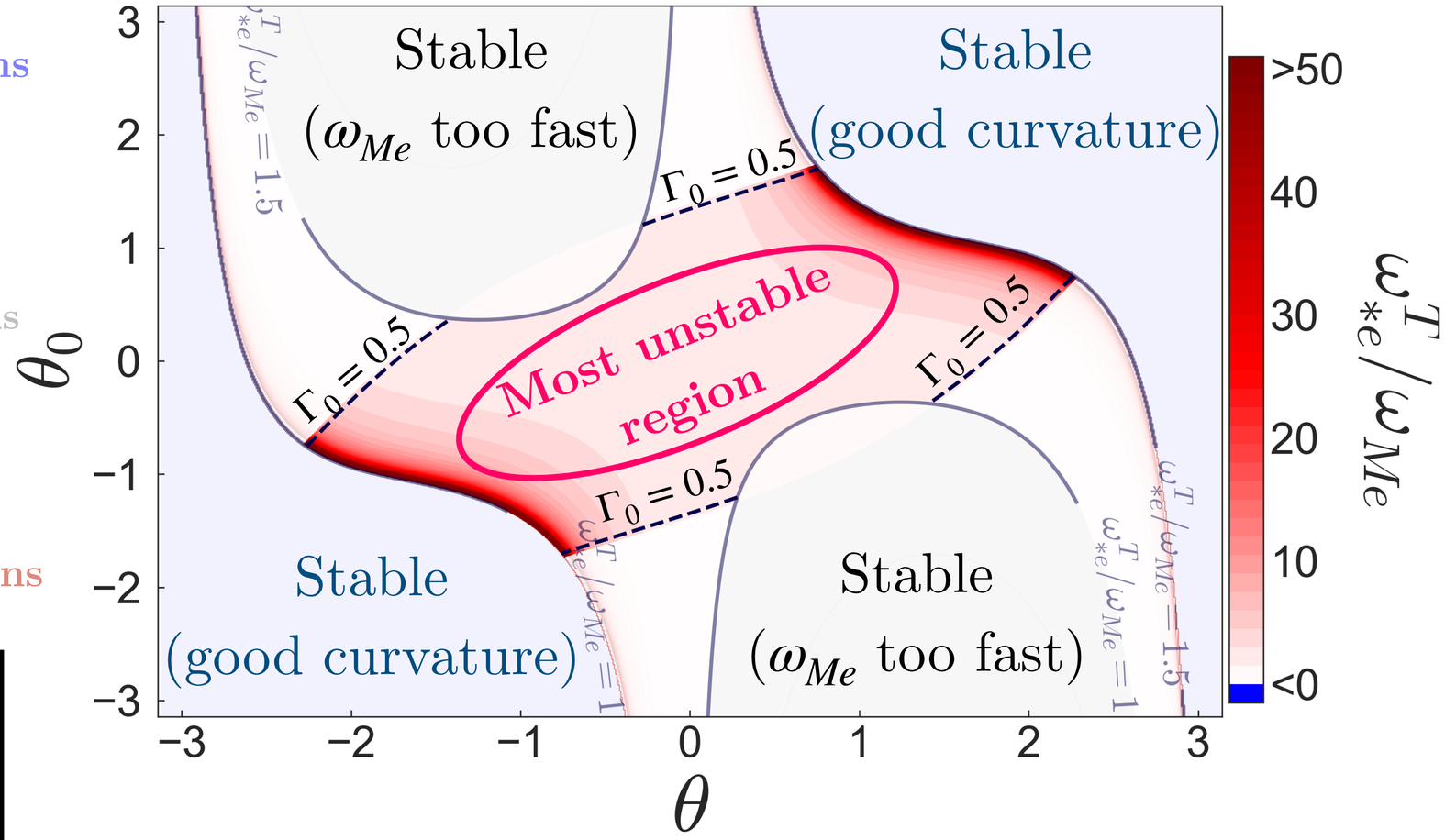

Linear pedestal toroidal ETG physics

Magnetic drifts in pedestal

- Take geometry for JET-ILW pedestal and plot $\omega_{*e}^{T}/\omega_{Me}$ versus θ and θ_0.

Linear pedestal toroidal ETG physics

Magnetic drifts in JET-ILW pedestal

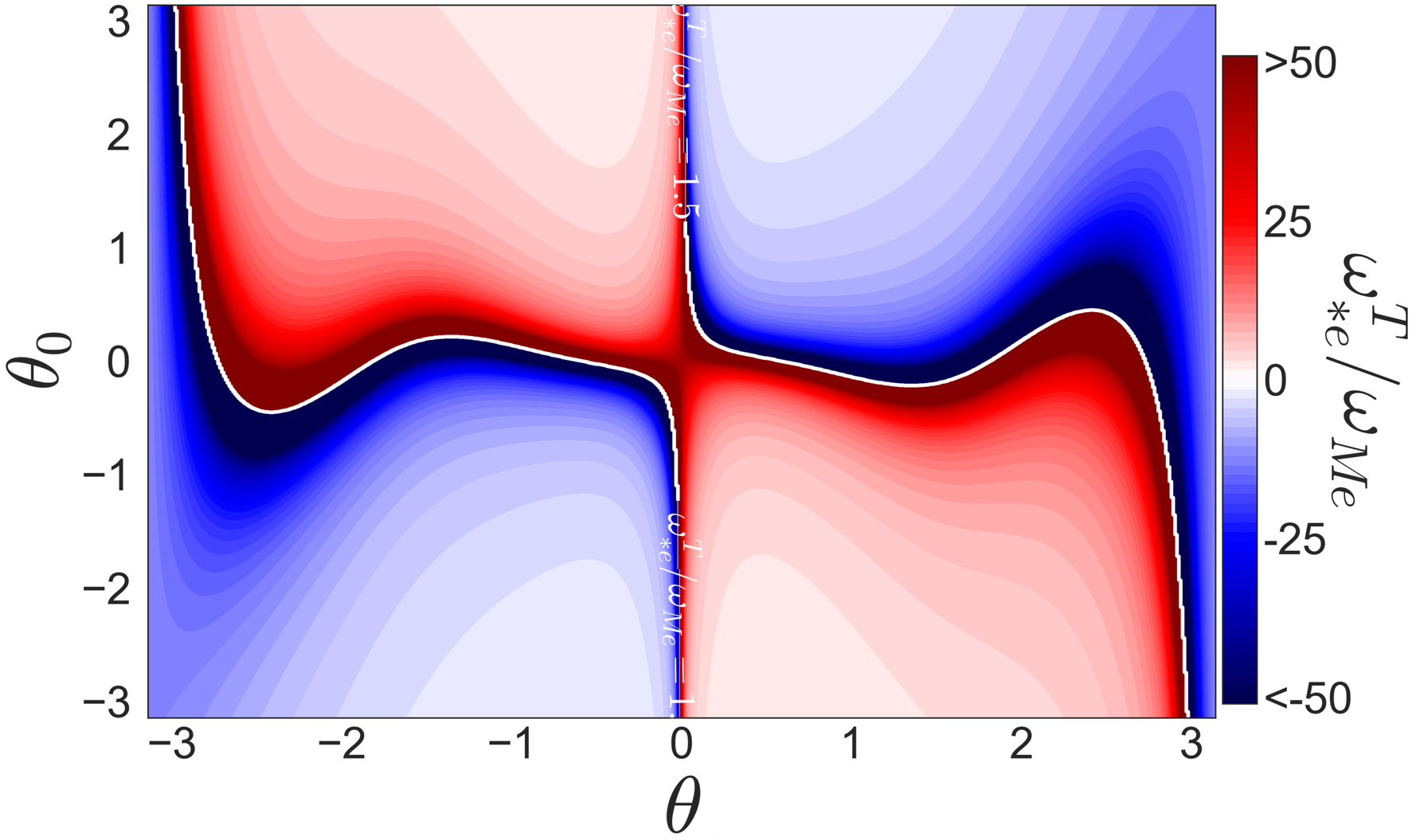

Linear pedestal toroidal ETG physics

Magnetic drifts in JET-ILW pedestal

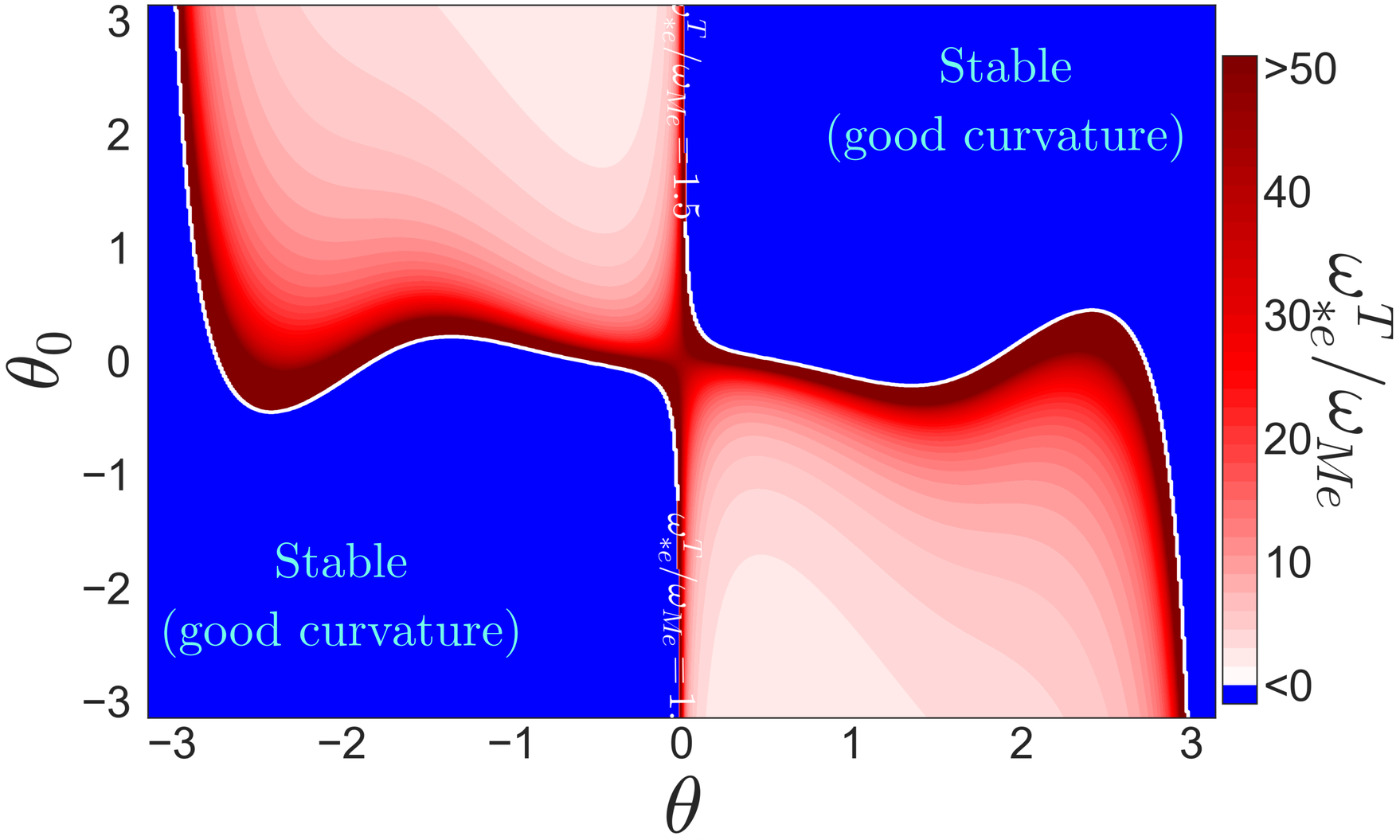

Linear pedestal toroidal ETG physics

Magnetic drifts in JET-ILW pedestal

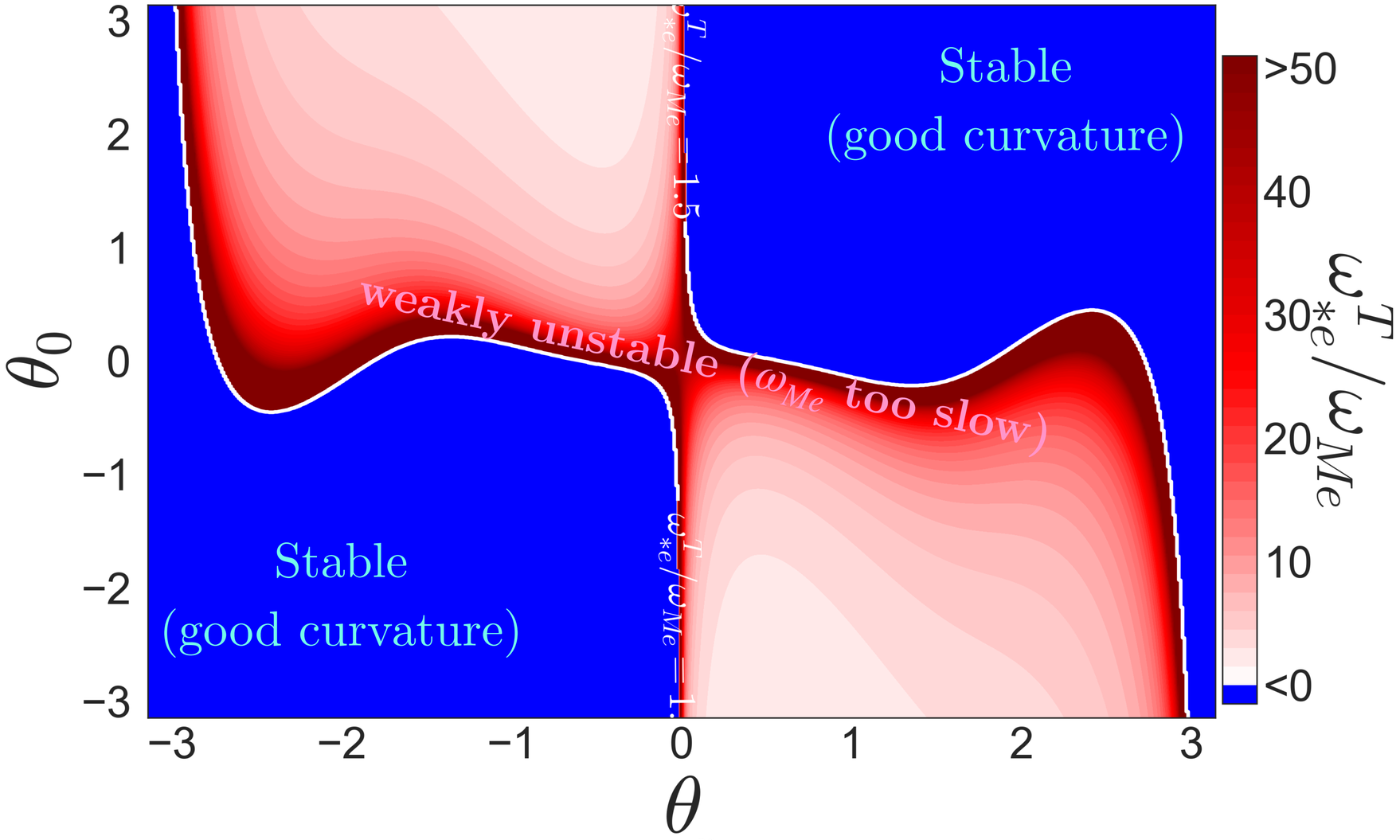

Linear pedestal toroidal ETG physics

Magnetic drifts in JET-ILW pedestal

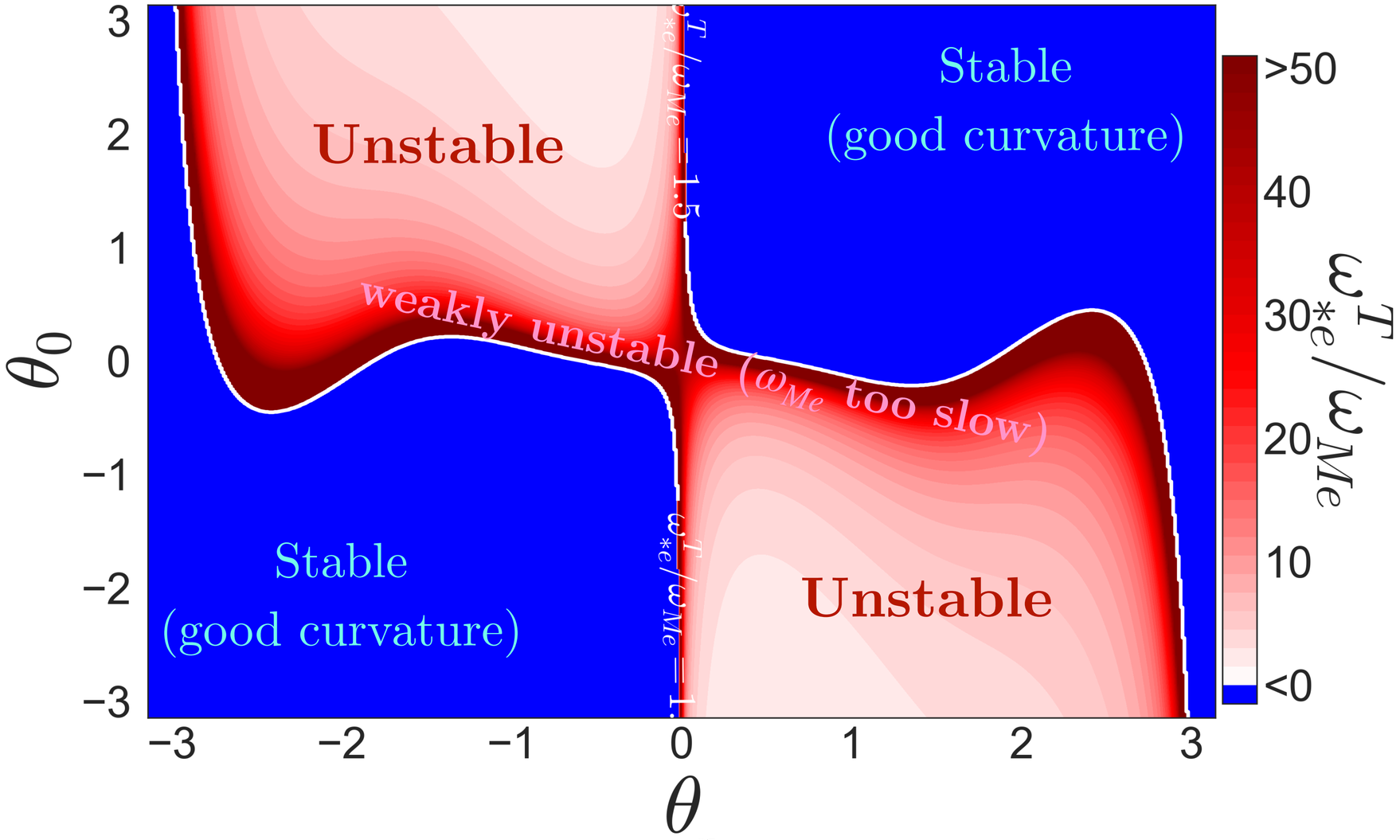

Linear pedestal toroidal ETG physics

Finite Larmor radius damping in JET-ILW pedestal at $k_y\rho_e = 1$

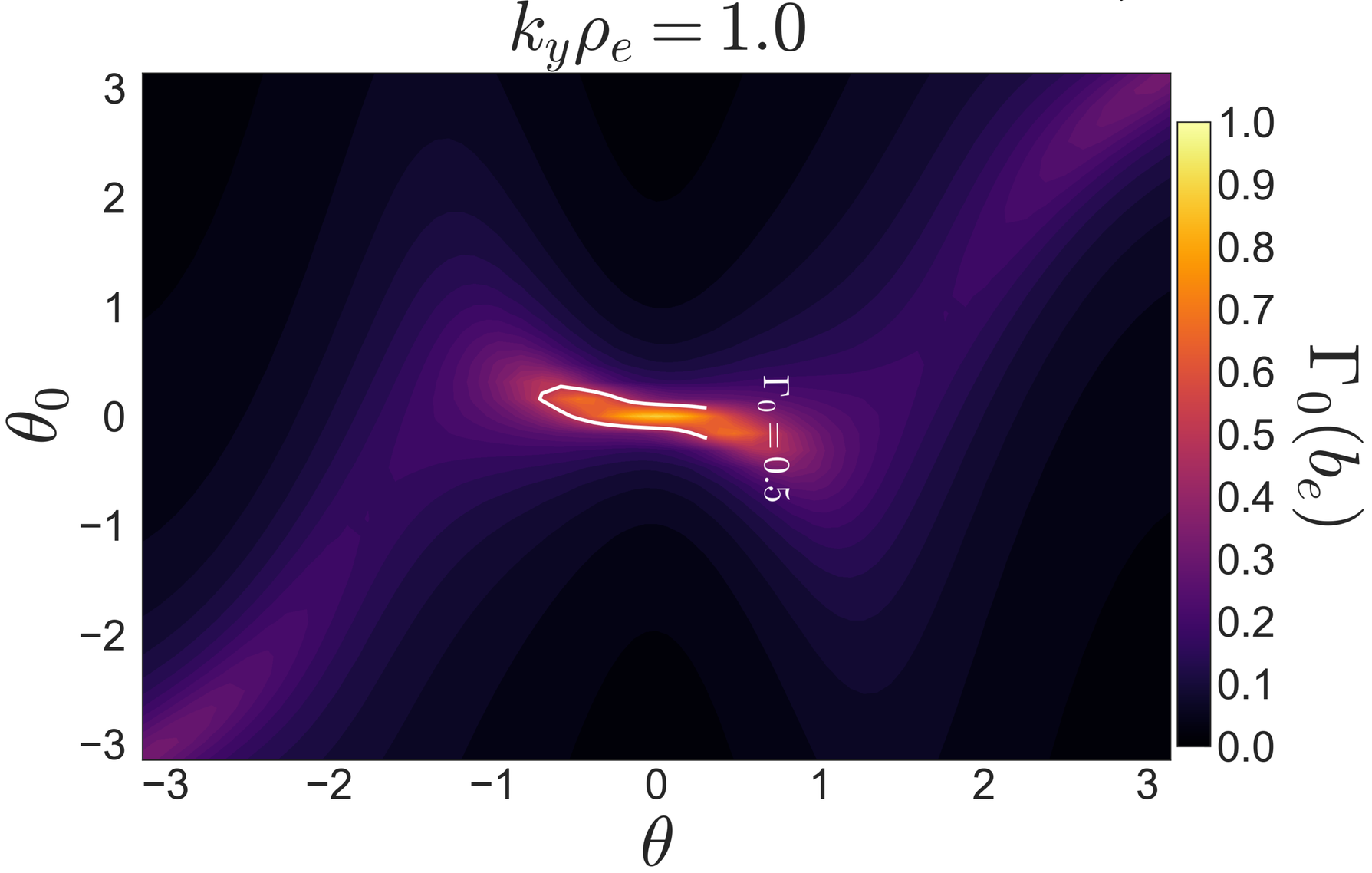

Linear pedestal toroidal ETG physics

Finite Larmor radius damping in JET-ILW pedestal at $k_y\rho_e = 1$

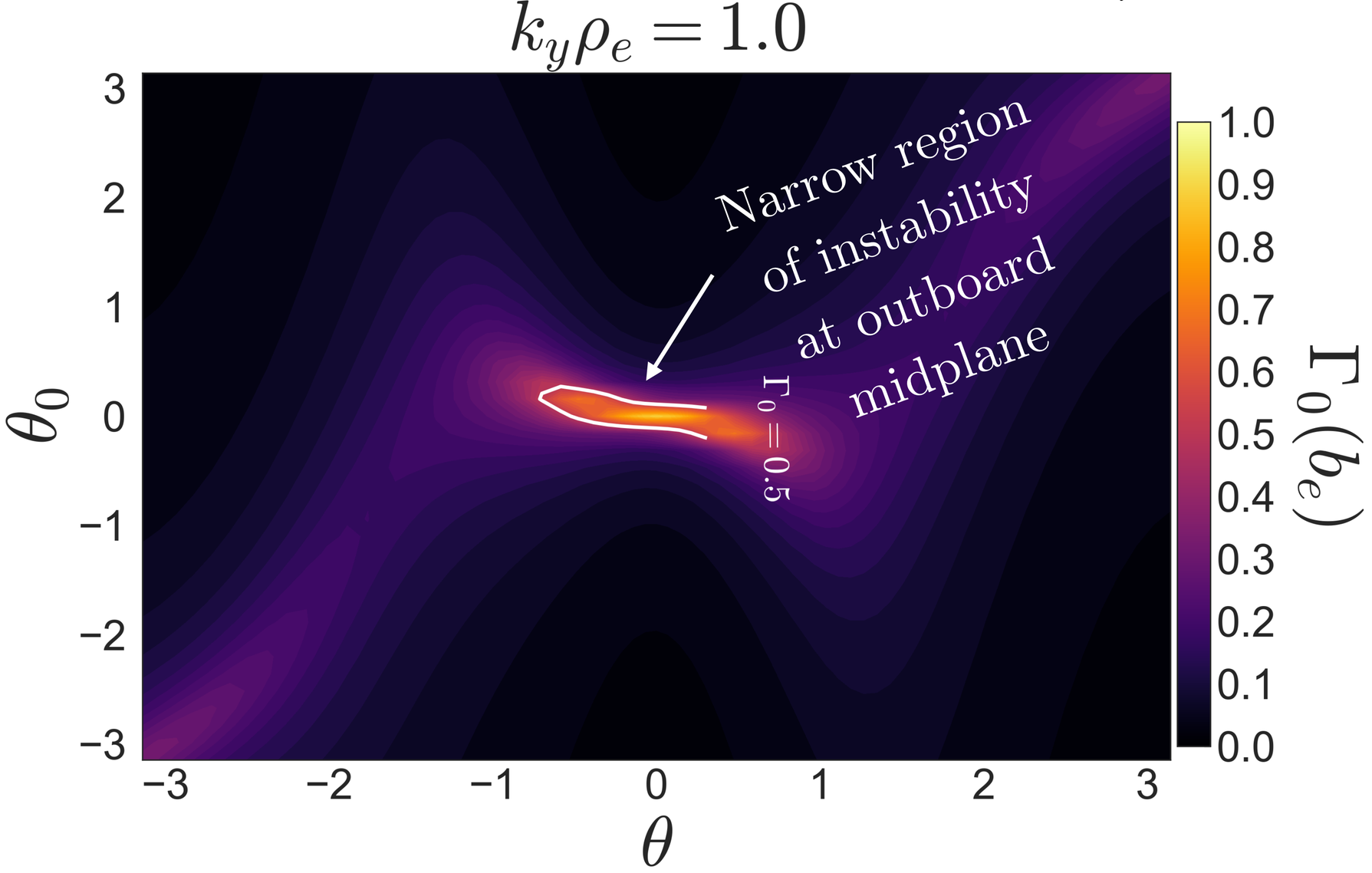

Linear pedestal toroidal ETG physics

Finite Larmor radius damping in JET-ILW pedestal at $k_y\rho_e = 1$

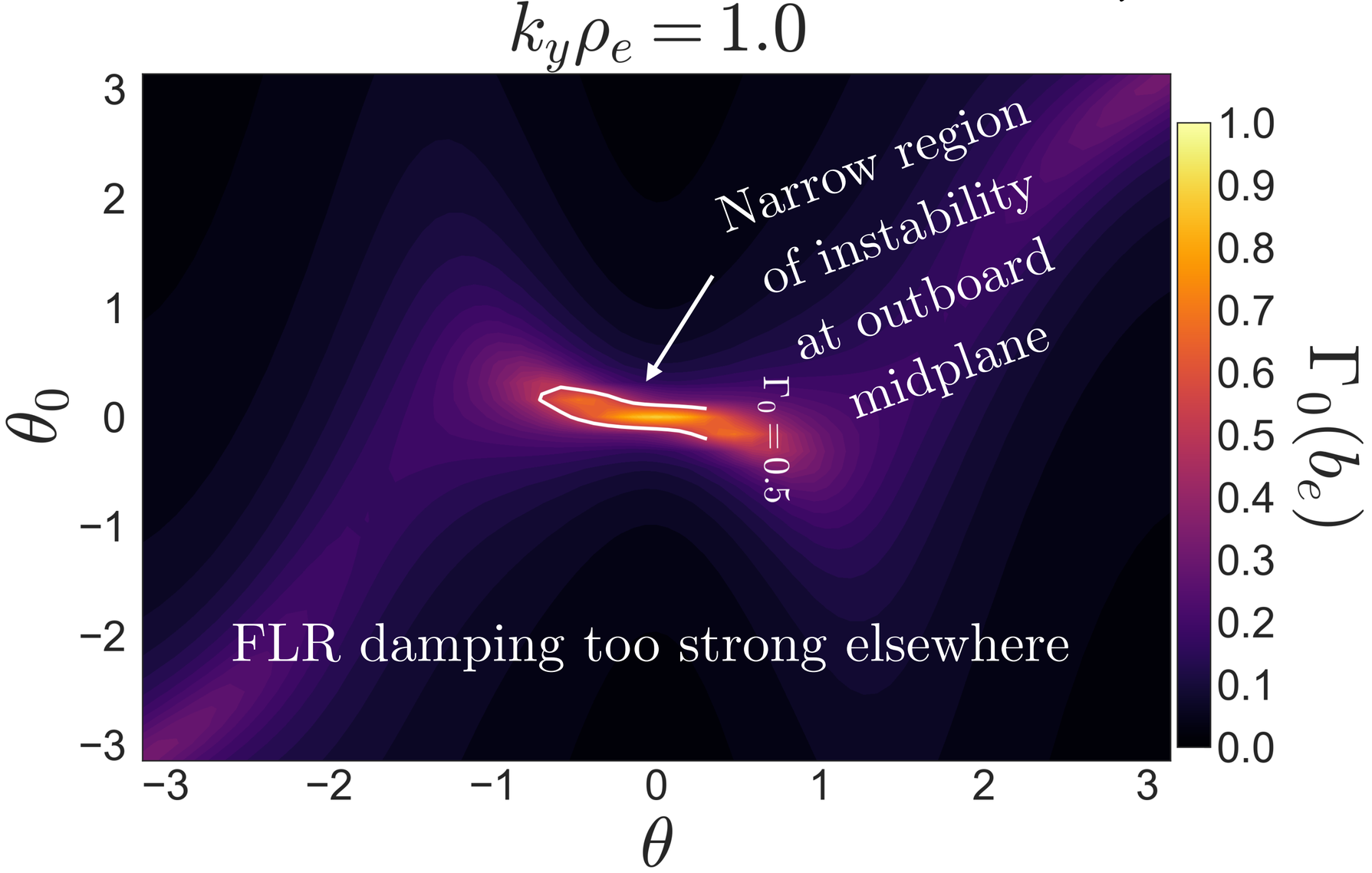

Linear core toroidal ETG physics

Combine constraints:

Magnetic drift constraint:

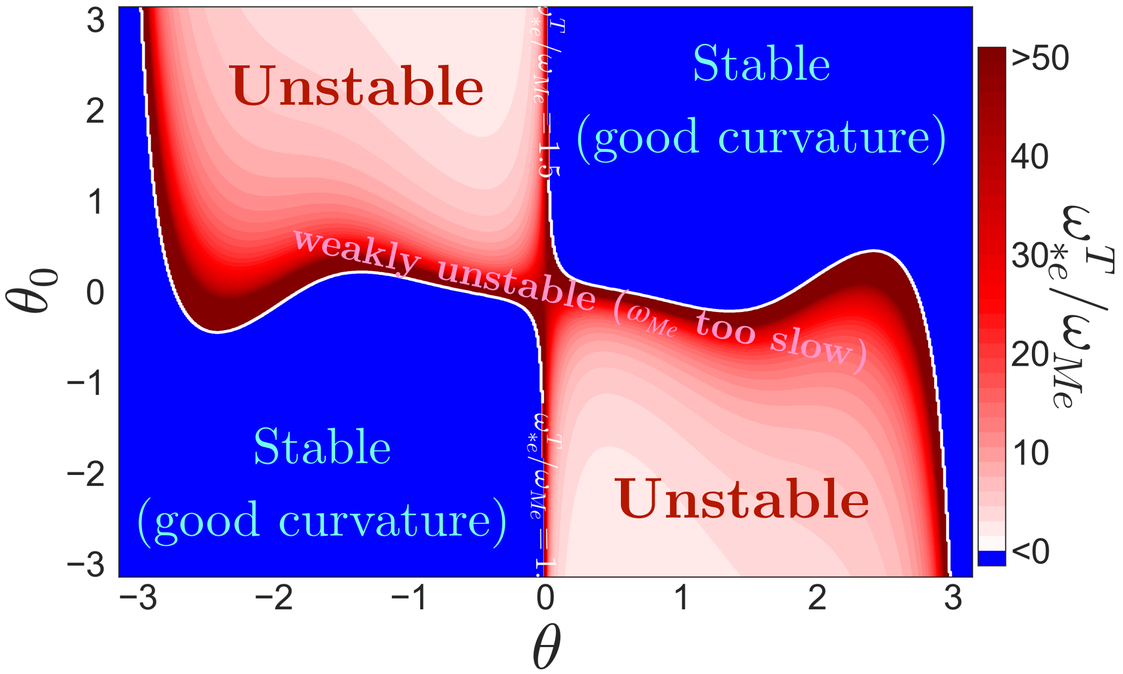

+

FLR damping constraint:

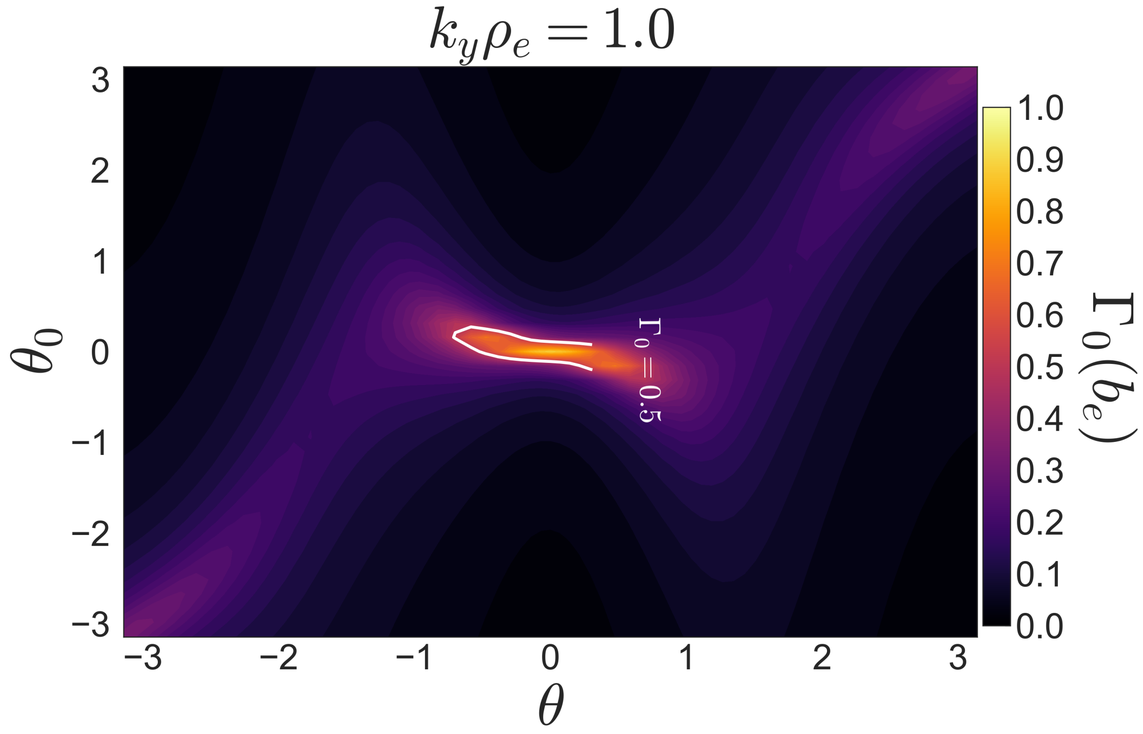

Linear pedestal toroidal ETG physics

Very weak toroidal ETG at $k_y\rho_e = 1$ in JET-ILW pedestal

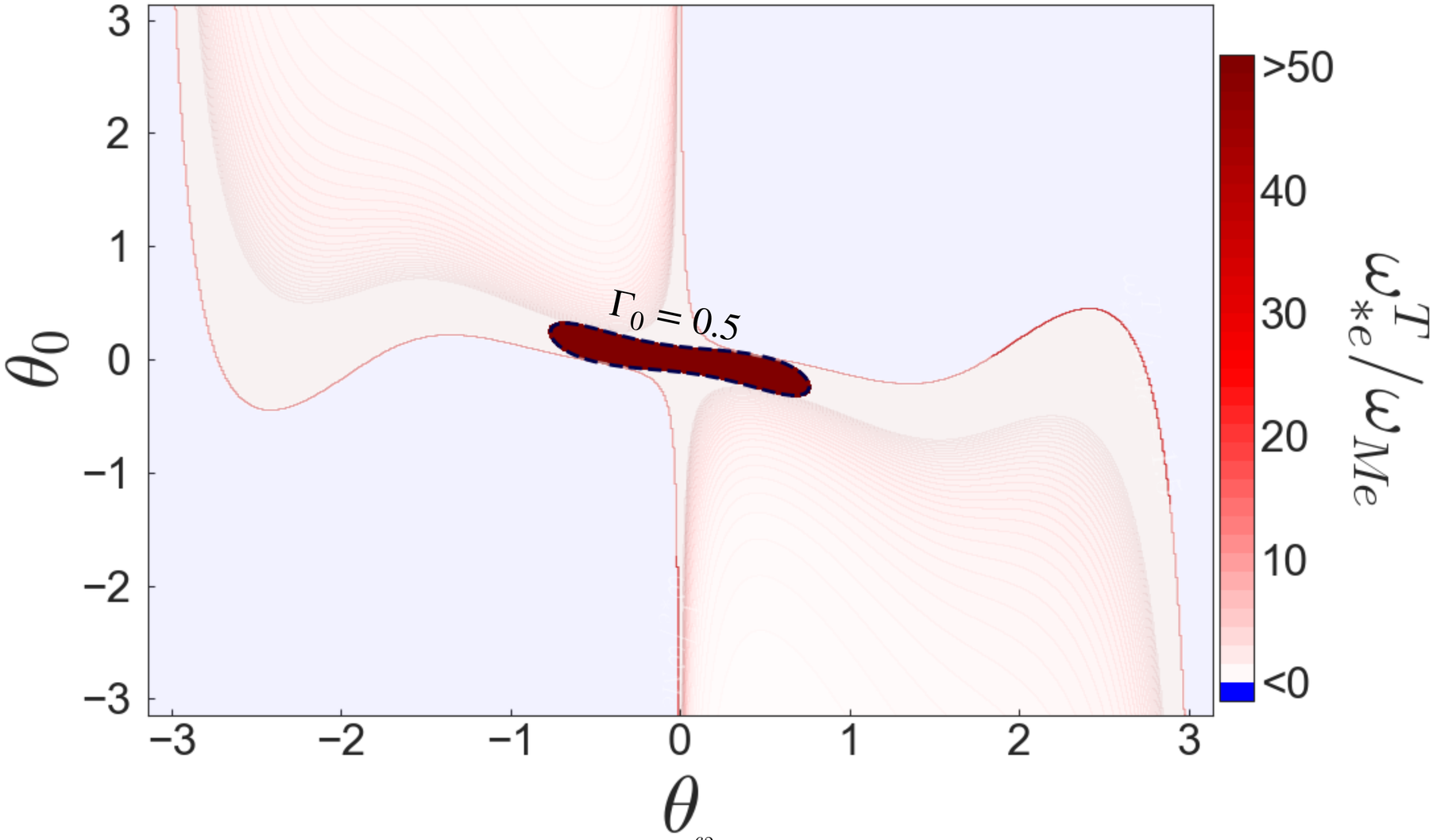

Linear pedestal toroidal ETG physics

Very weak toroidal ETG at $k_y\rho_e = 1$ in JET-ILW pedestal

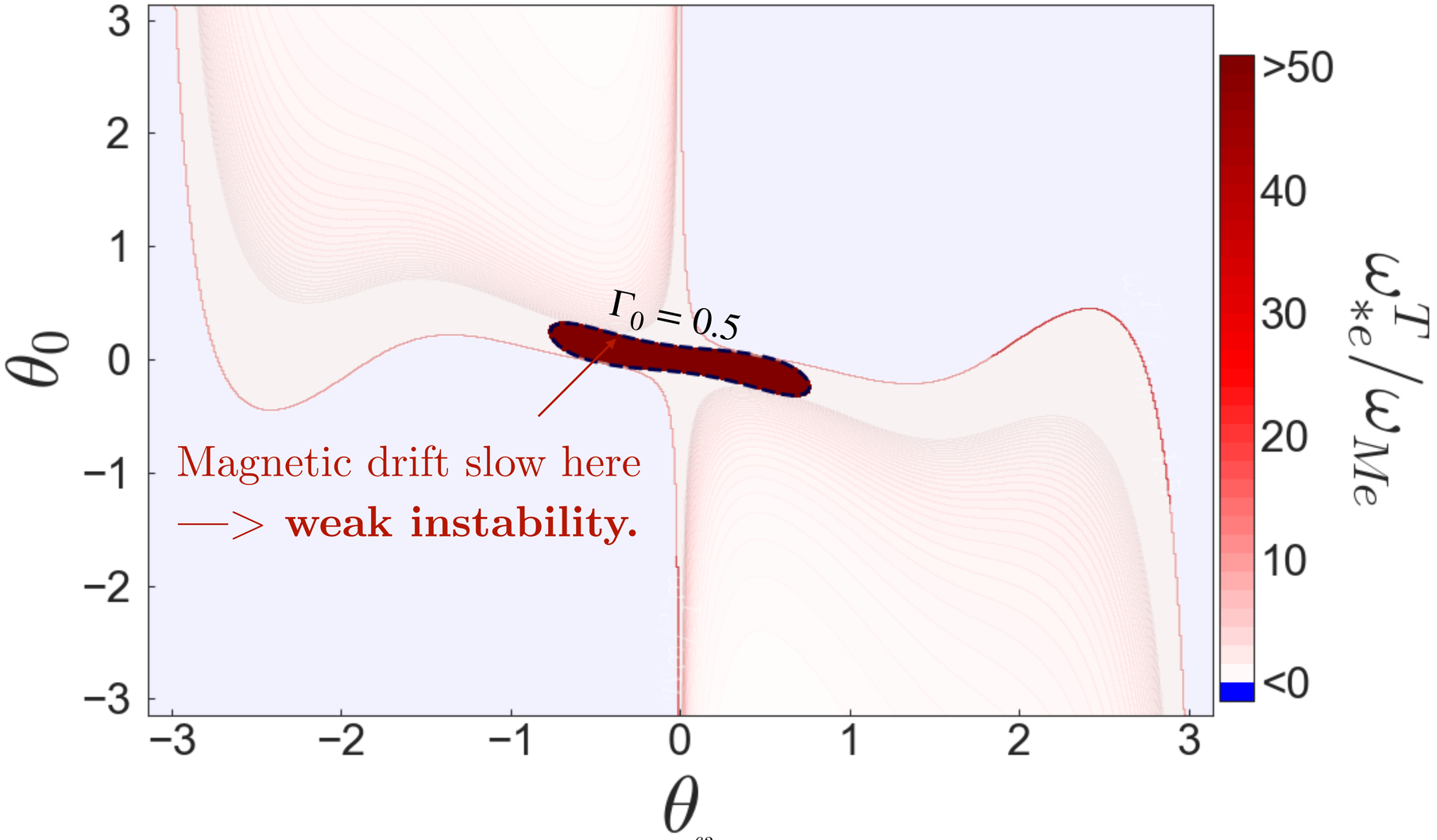

Linear pedestal toroidal ETG physics

Very weak toroidal ETG at $k_y\rho_e = 1$ in JET-ILW pedestal

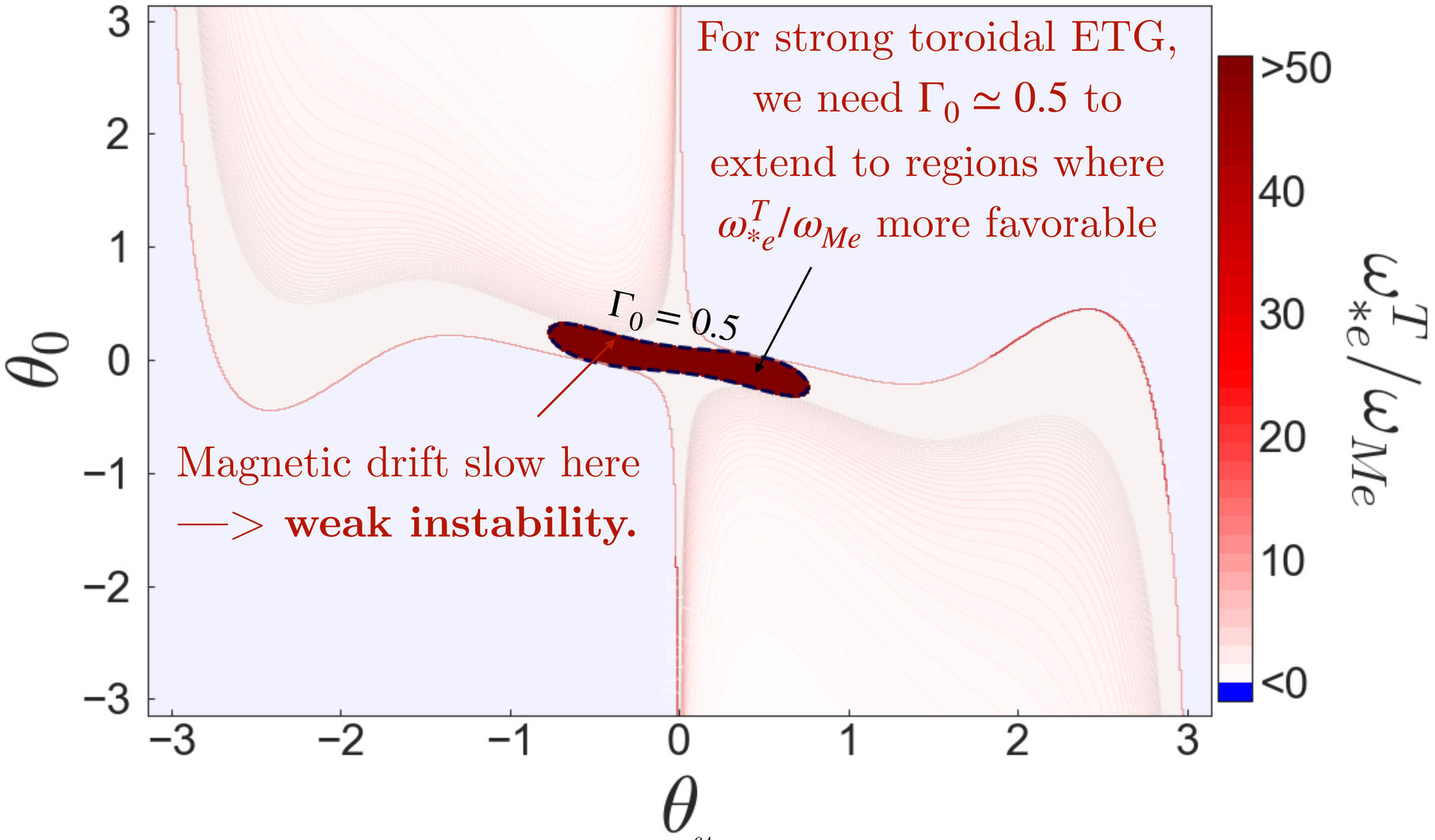

Finding $k_y\rho_e$ scale for strong toroidal ETG

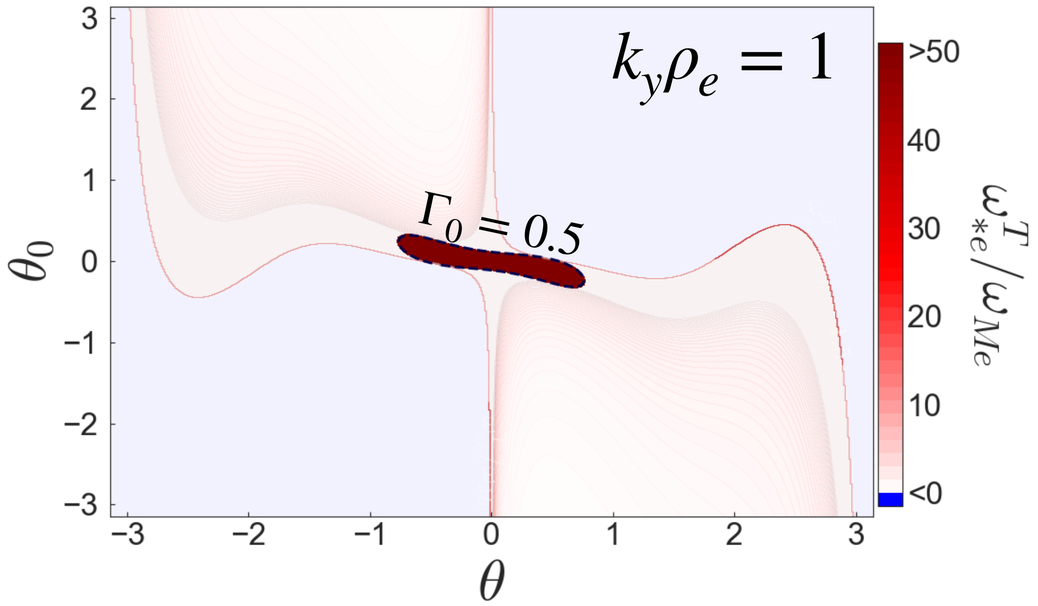

Finding $k_y\rho_e$ scale for strong toroidal ETG

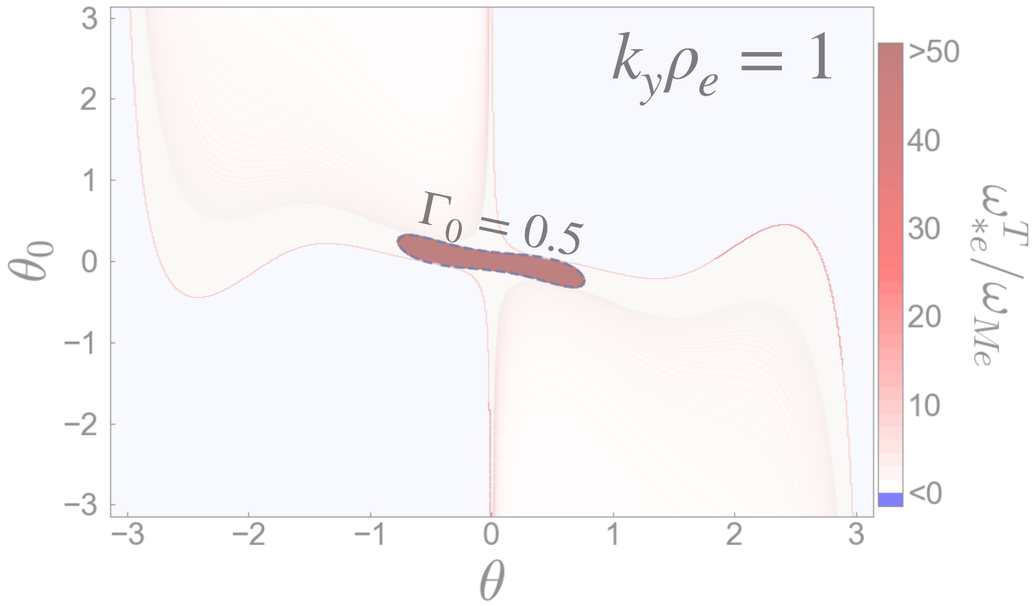

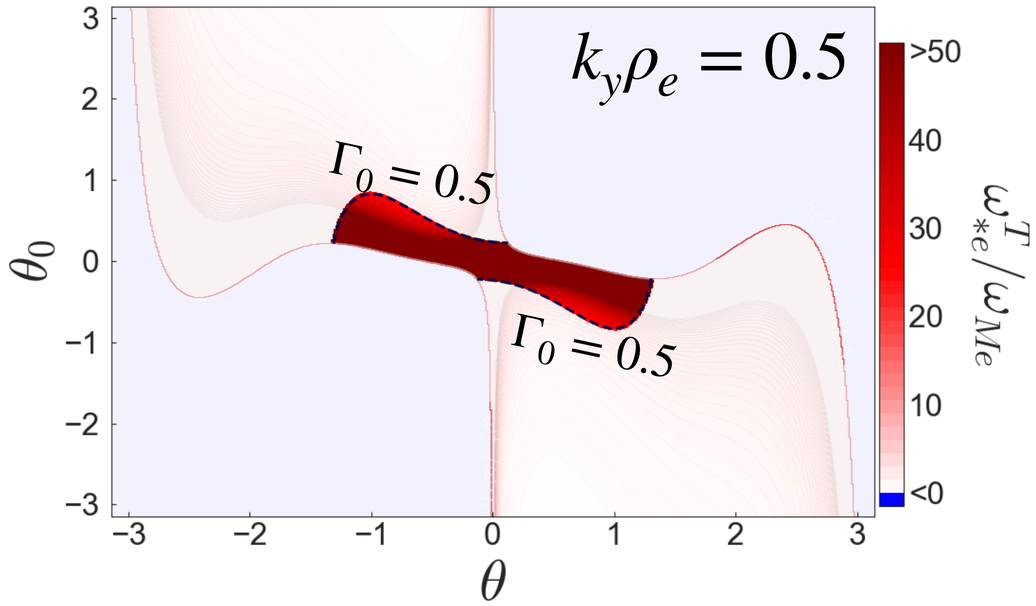

Finding $k_y\rho_e$ scale for strong toroidal ETG

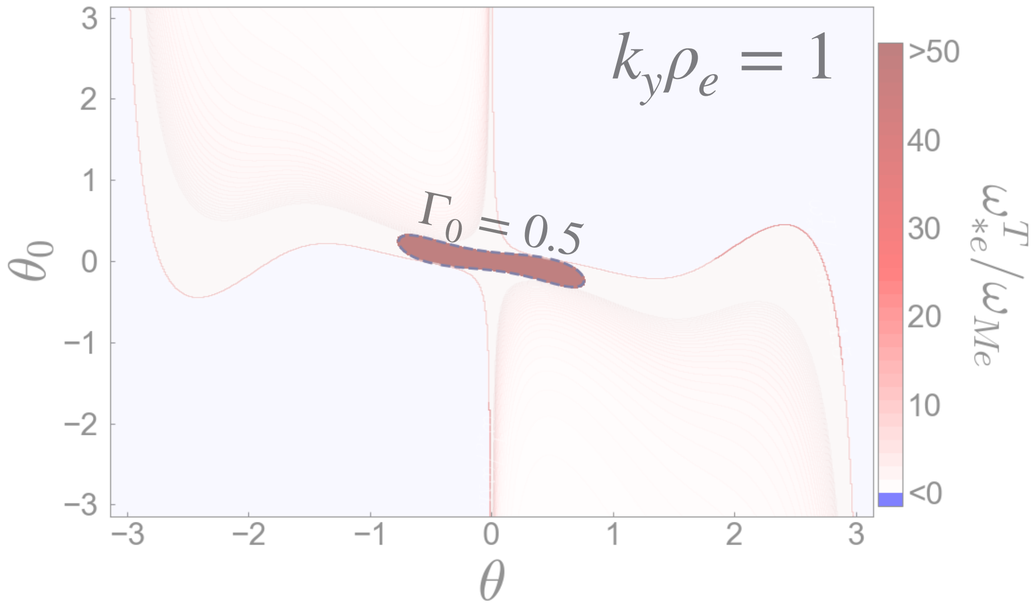

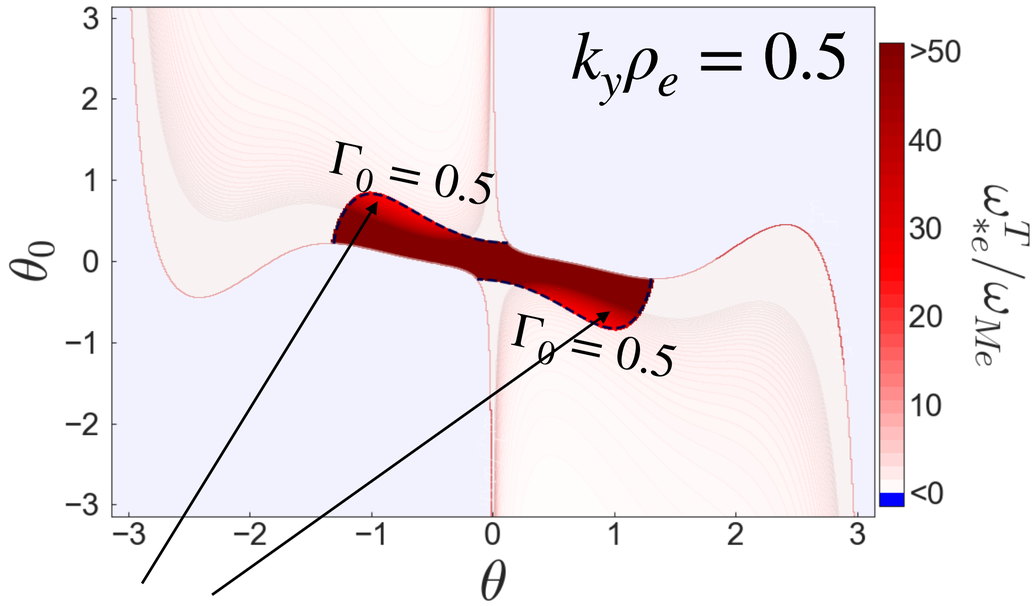

better $\omega^T_{*e}/\omega_{Me}$ regions appearing

Finding $k_y\rho_e$ scale for strong toroidal ETG

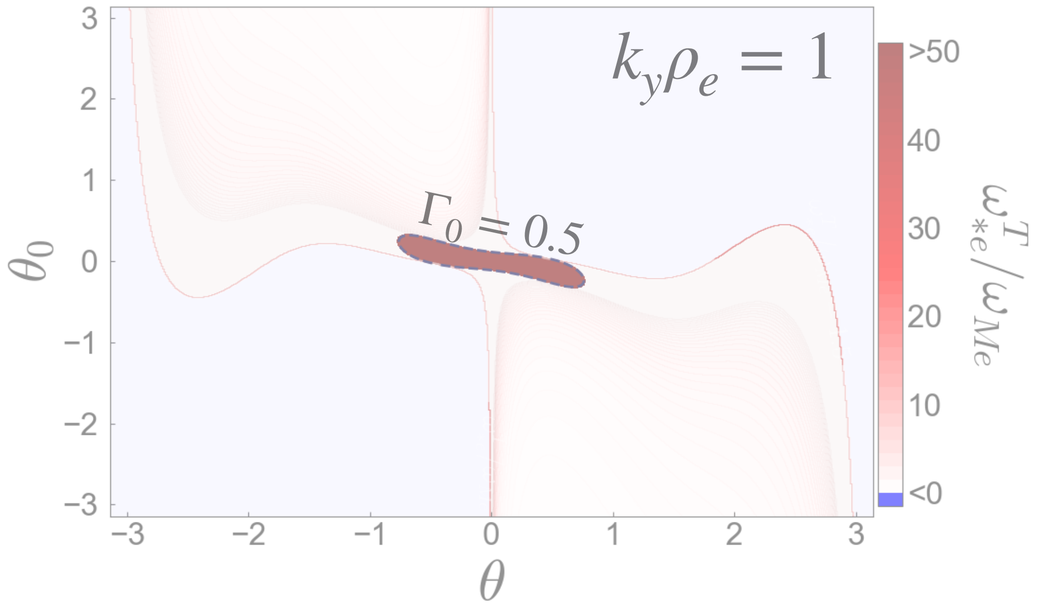

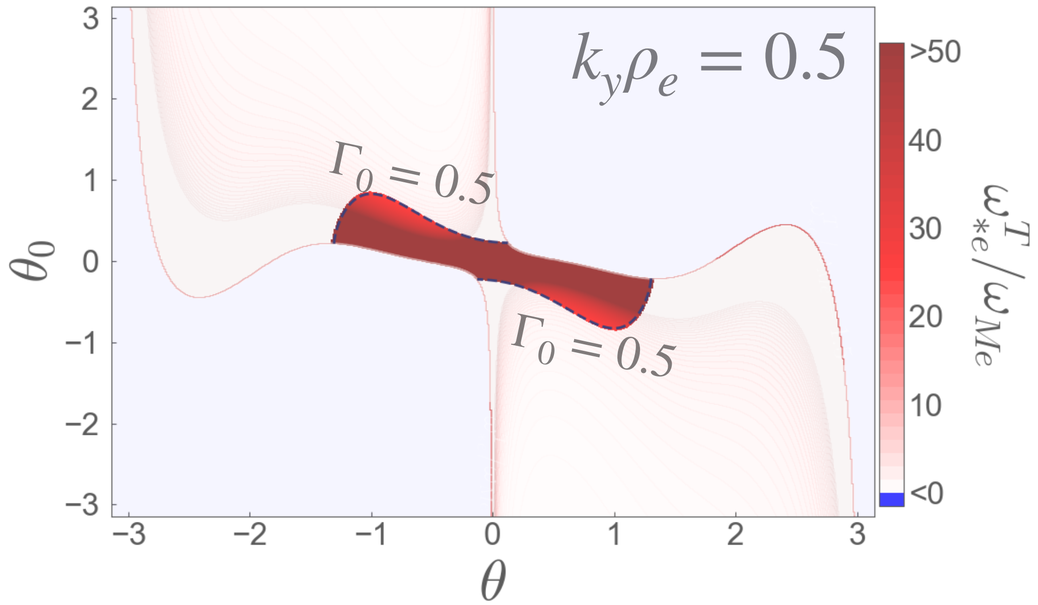

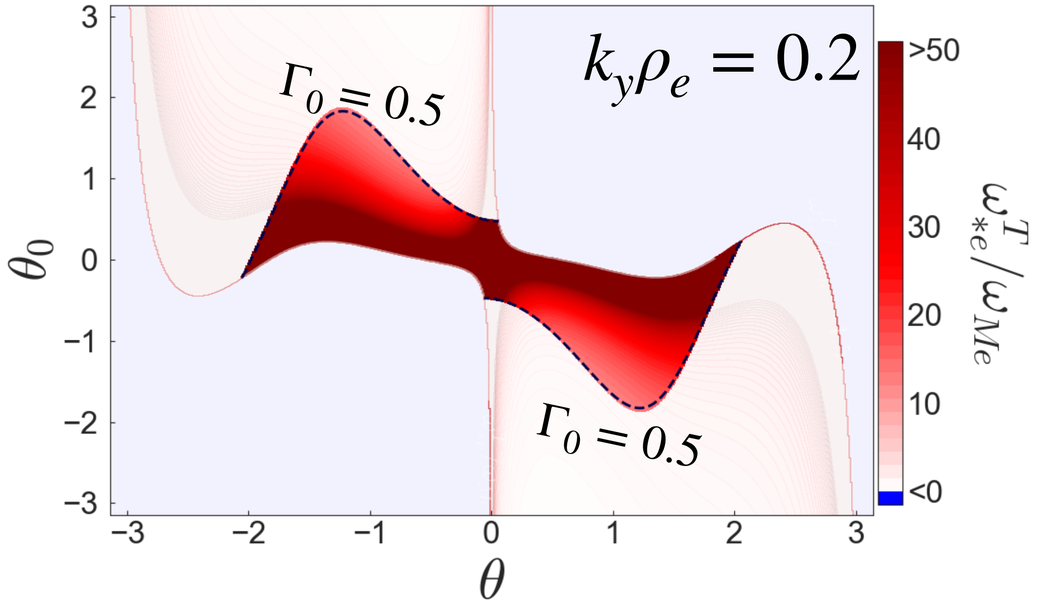

Finding $k_y\rho_e$ scale for strong toroidal ETG

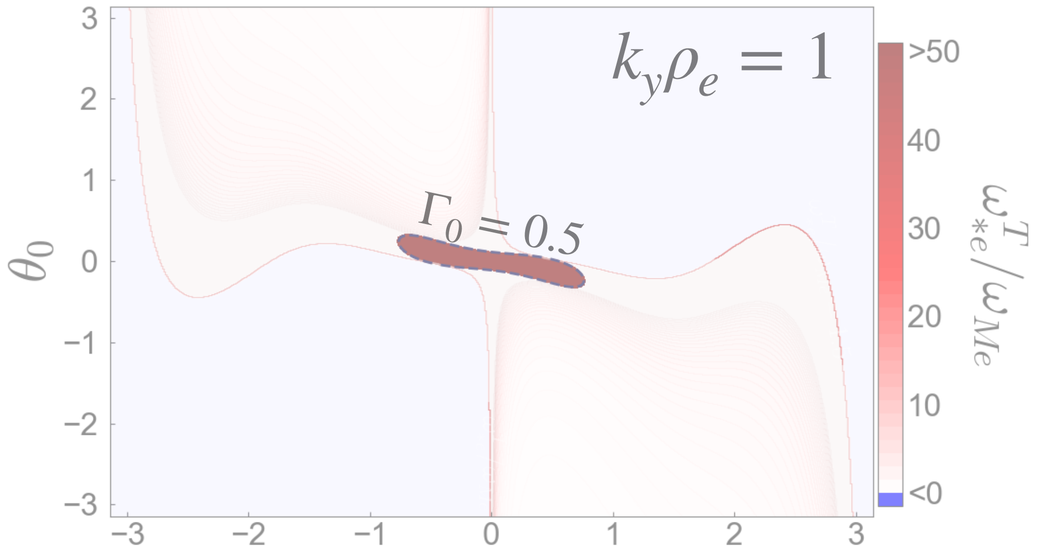

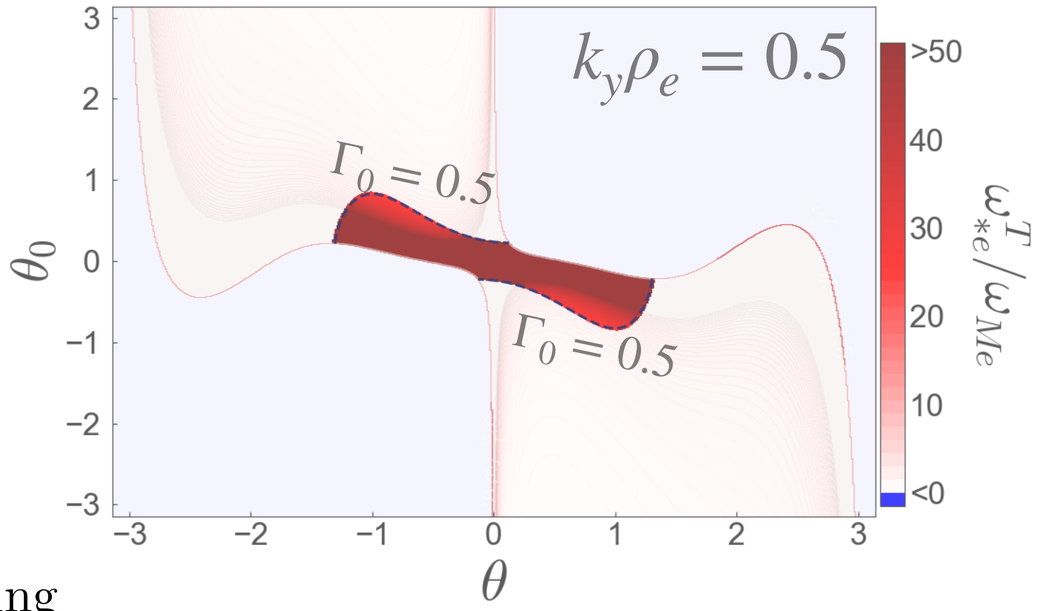

much better $\omega^T_{*e}/\omega_{Me}$ regions appearing

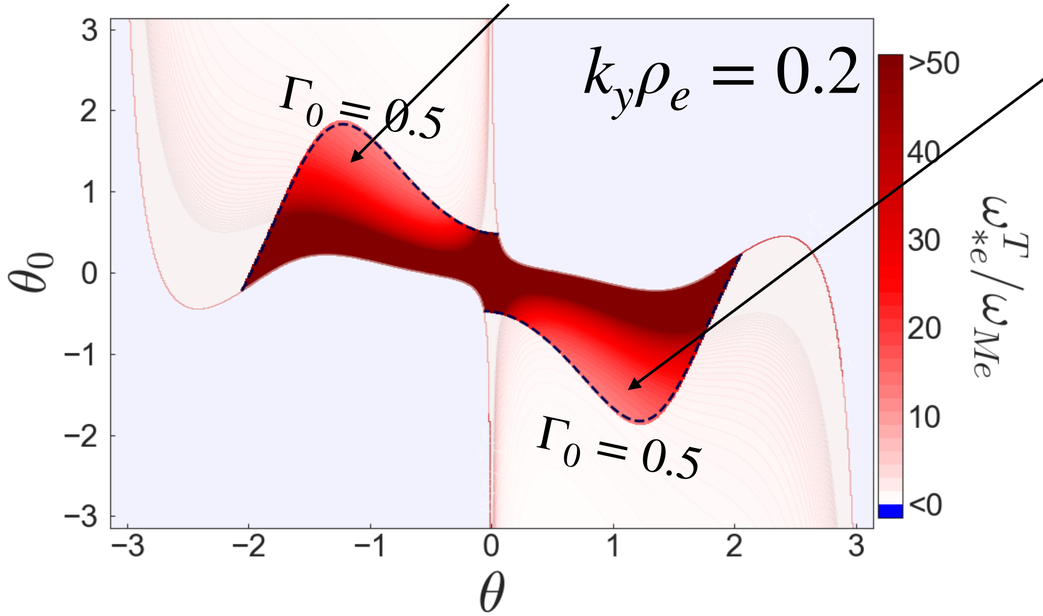

Finding $k_y\rho_e$ scale for strong toroidal ETG

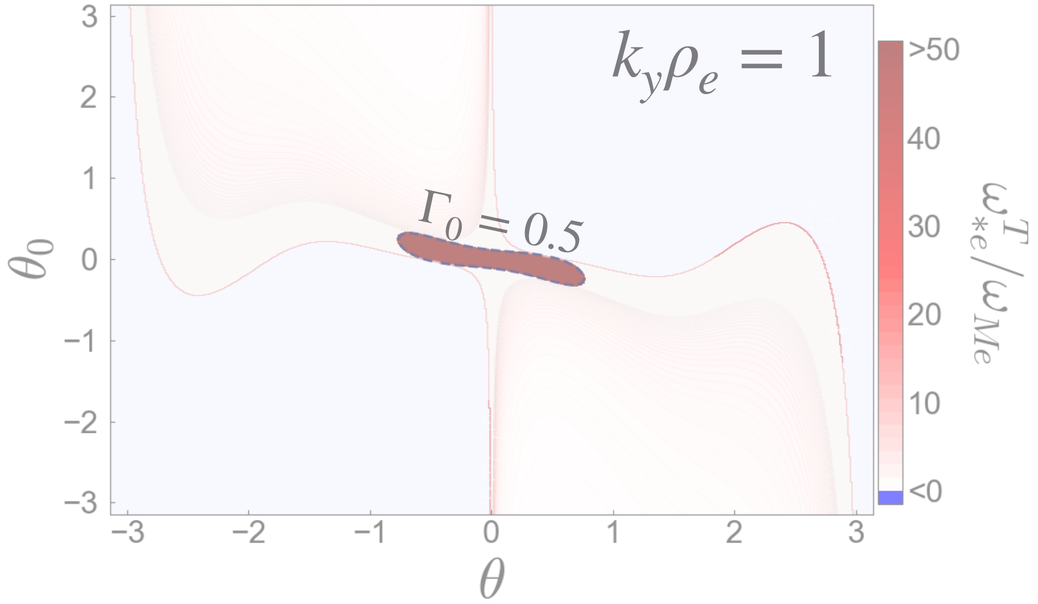

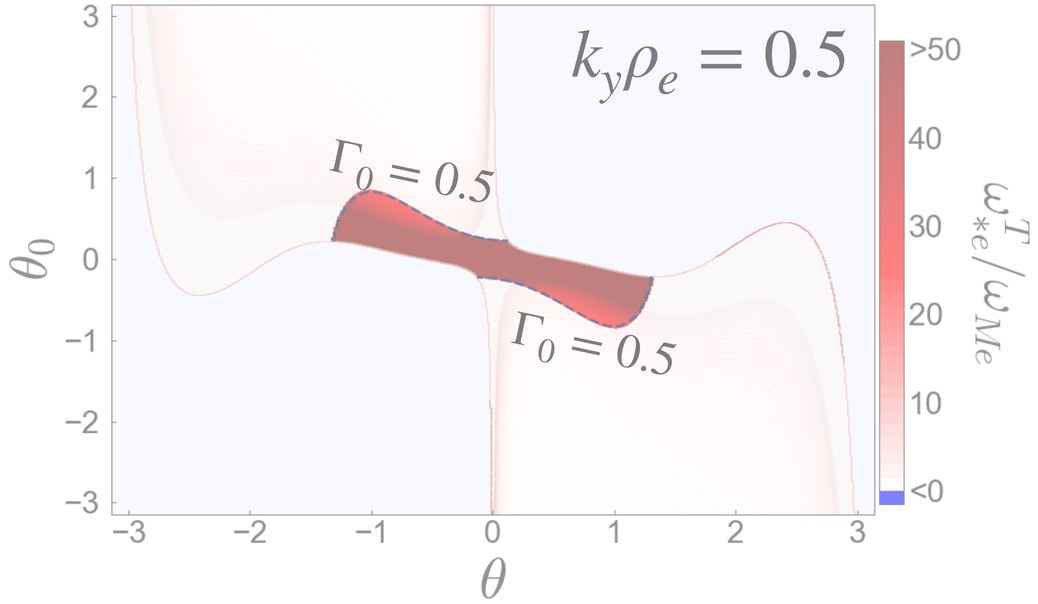

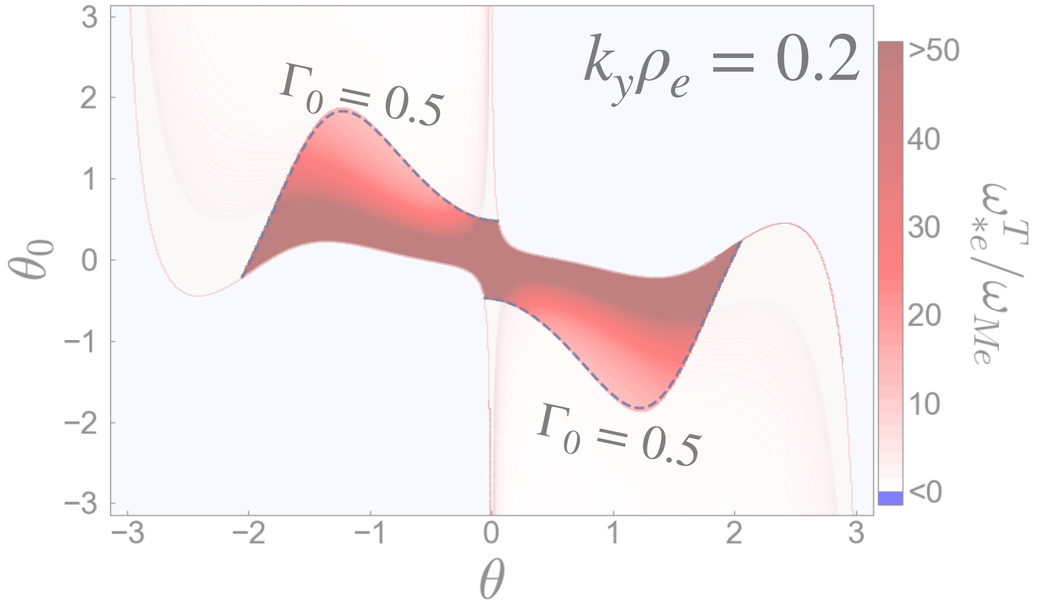

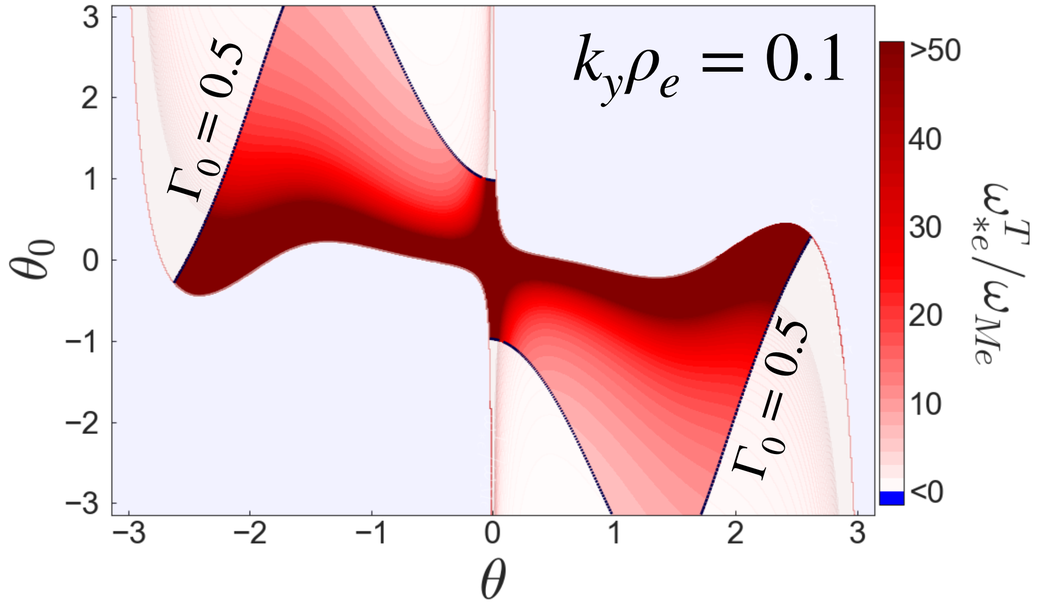

Finding $k_y\rho_e$ scale for strong toroidal ETG

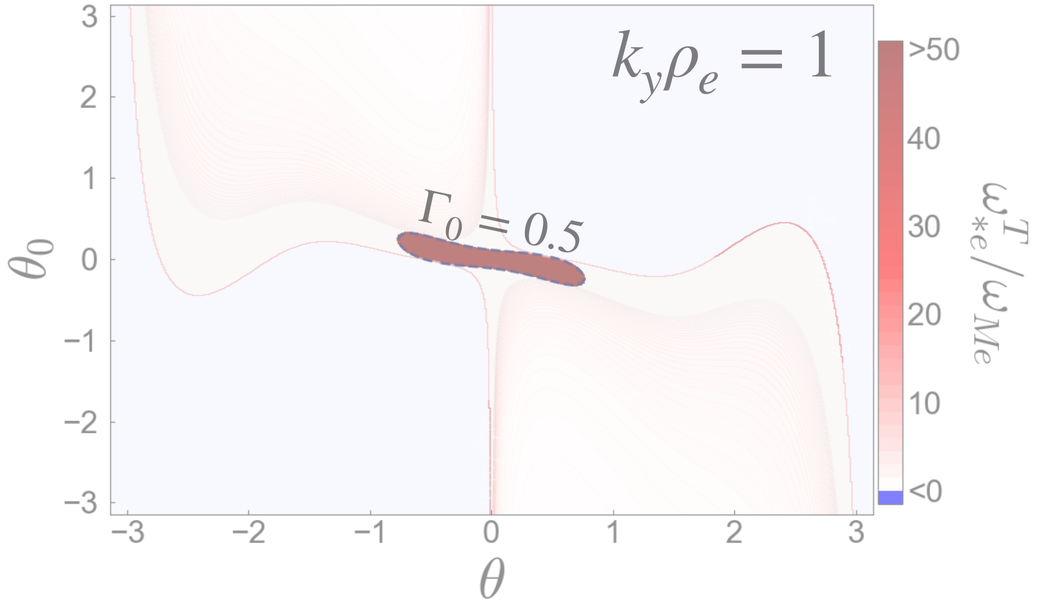

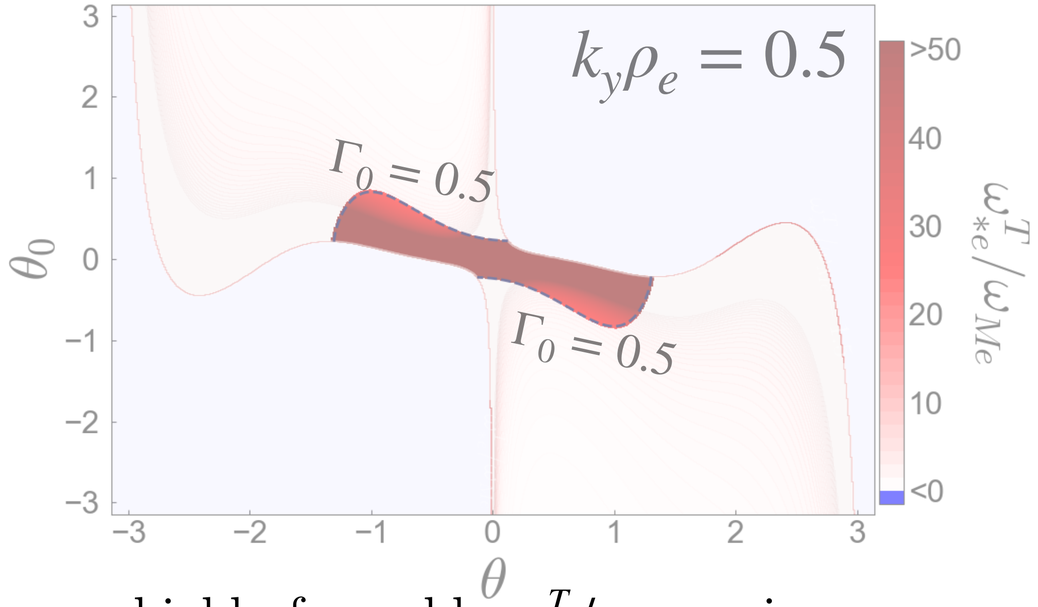

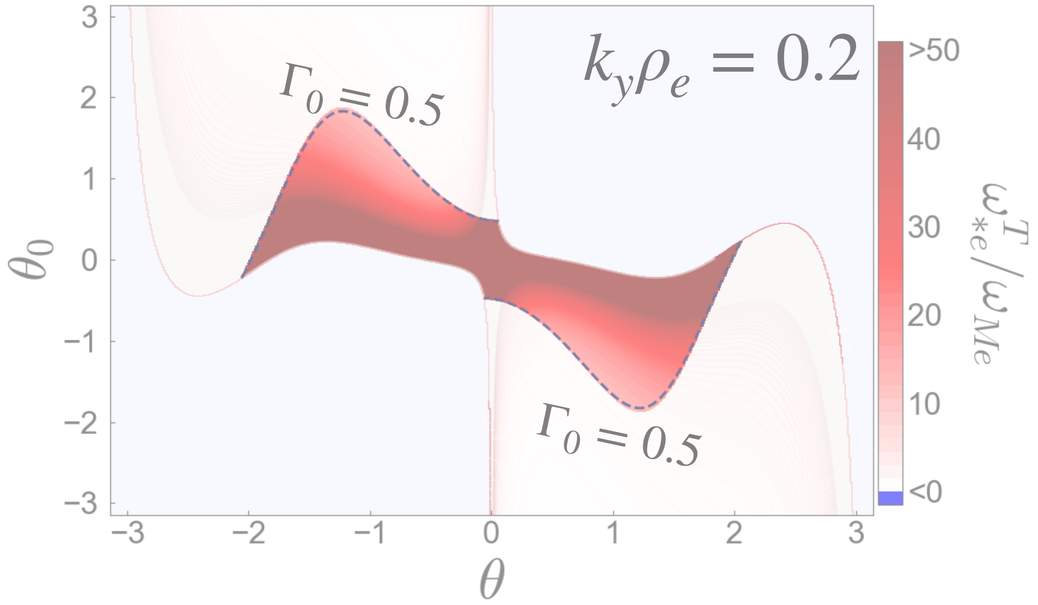

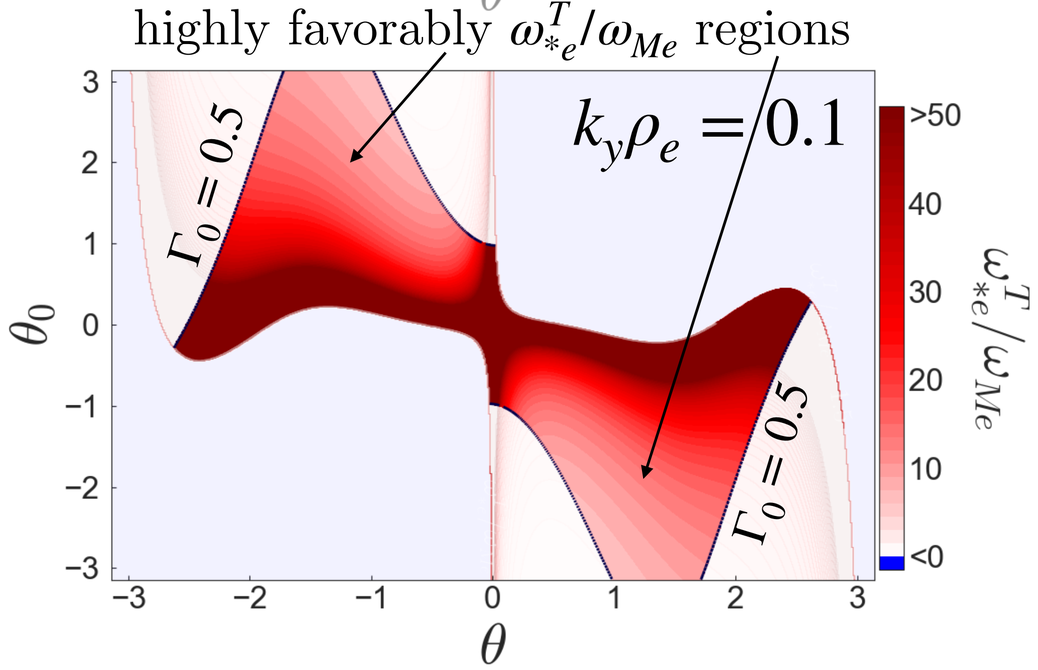

Linear pedestal toroidal ETG physics

Magnetic drifts and FLR damping at $k_y\rho_e = 0.1$.

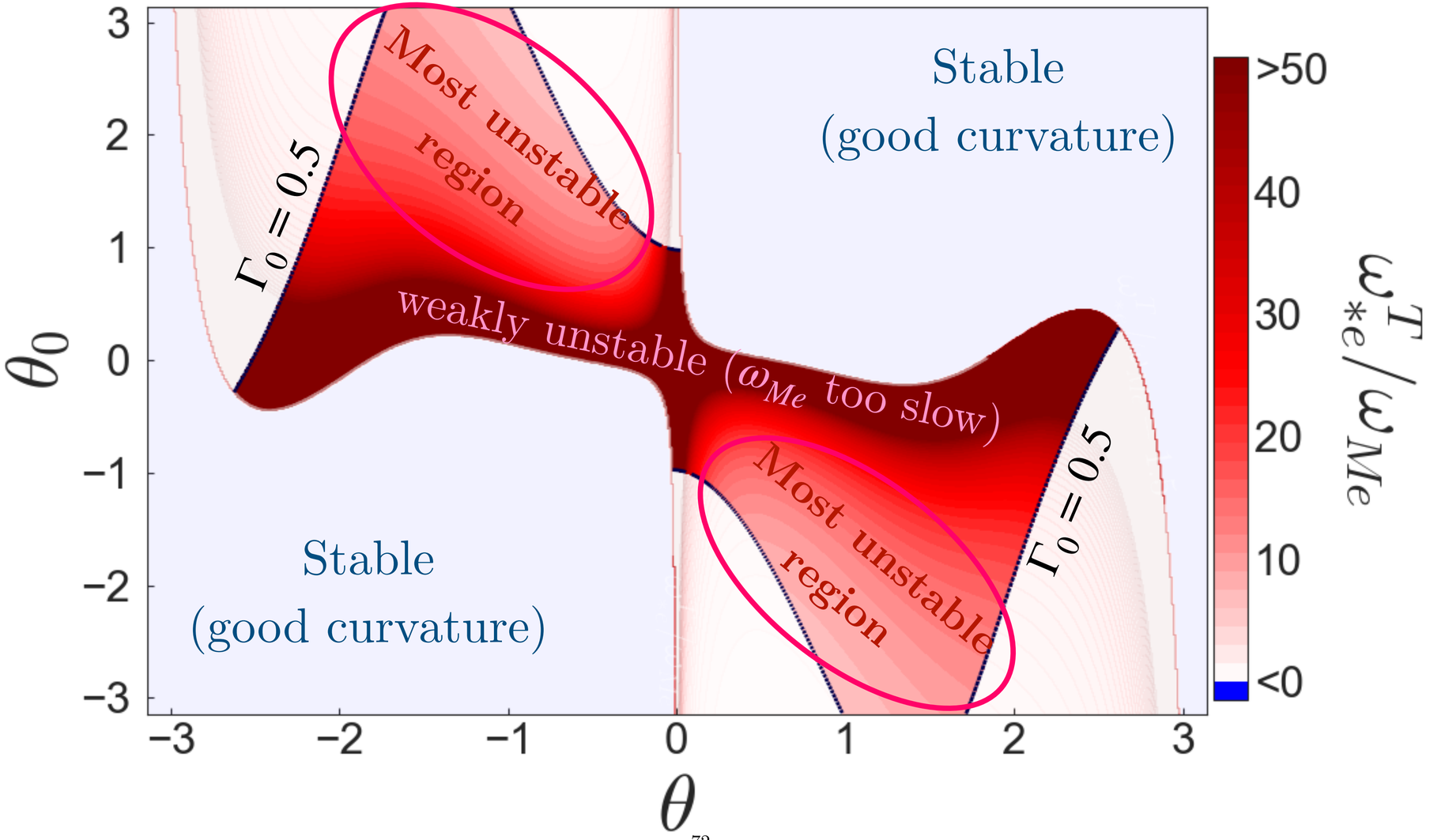

Linear pedestal toroidal ETG physics

Core and Pedestal Comparison

Core

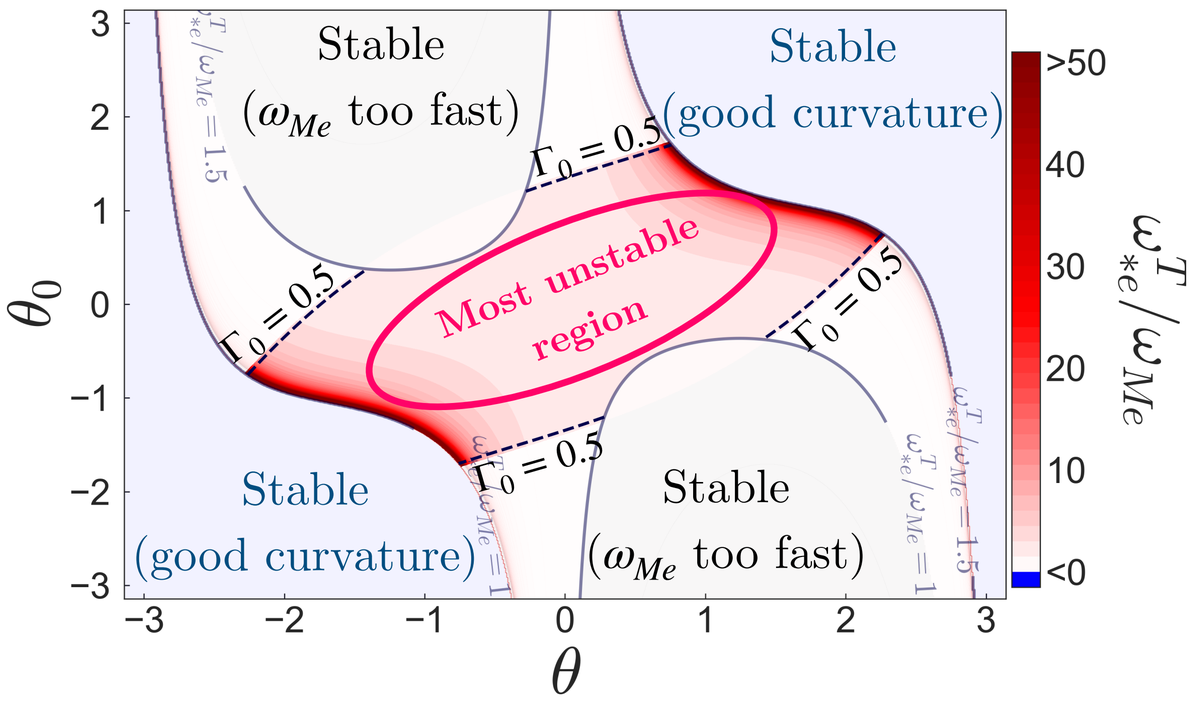

JET Pedestal

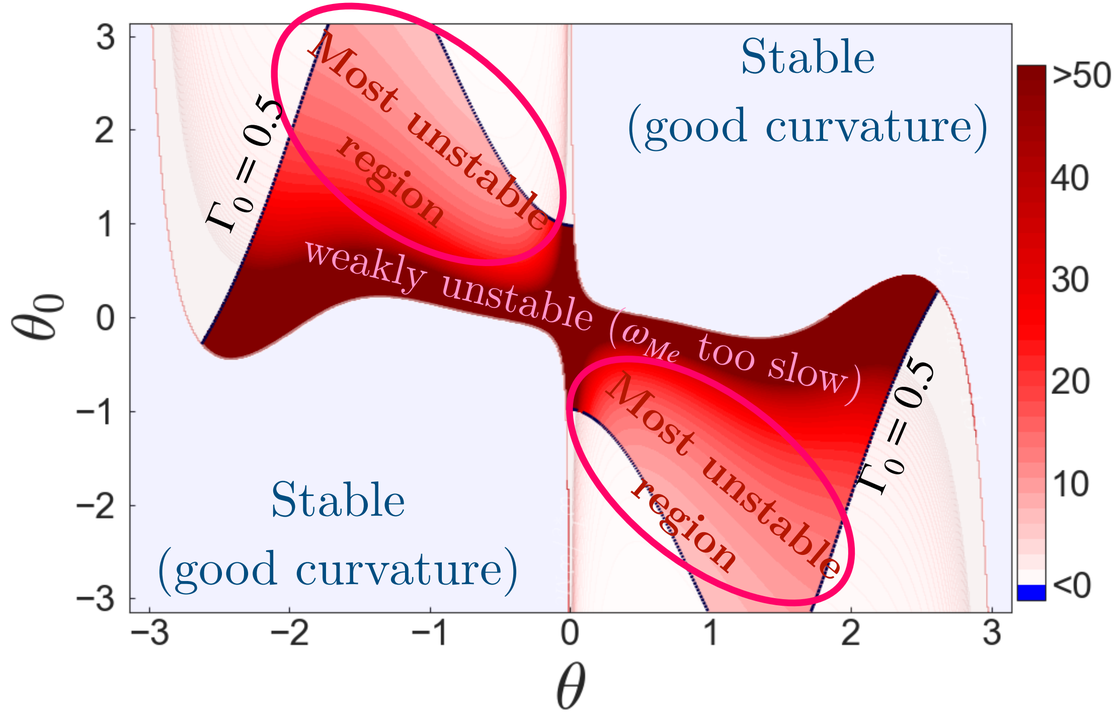

Linear pedestal toroidal ETG physics

Core and Pedestal Comparison

Core

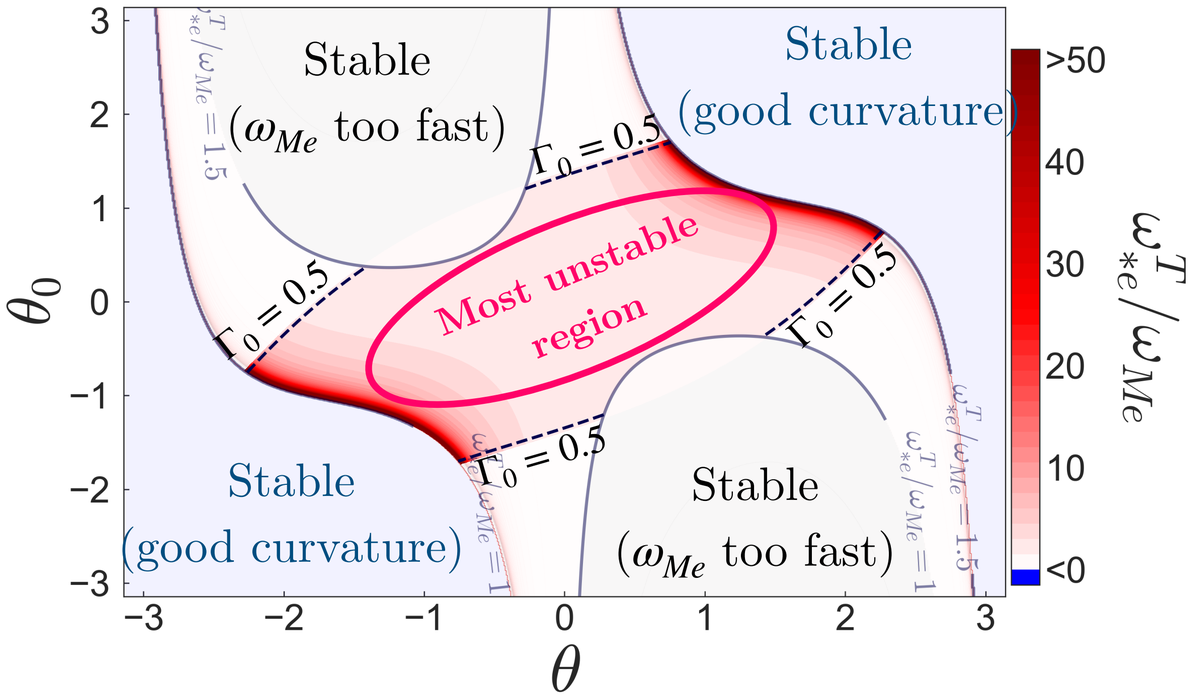

JET Pedestal

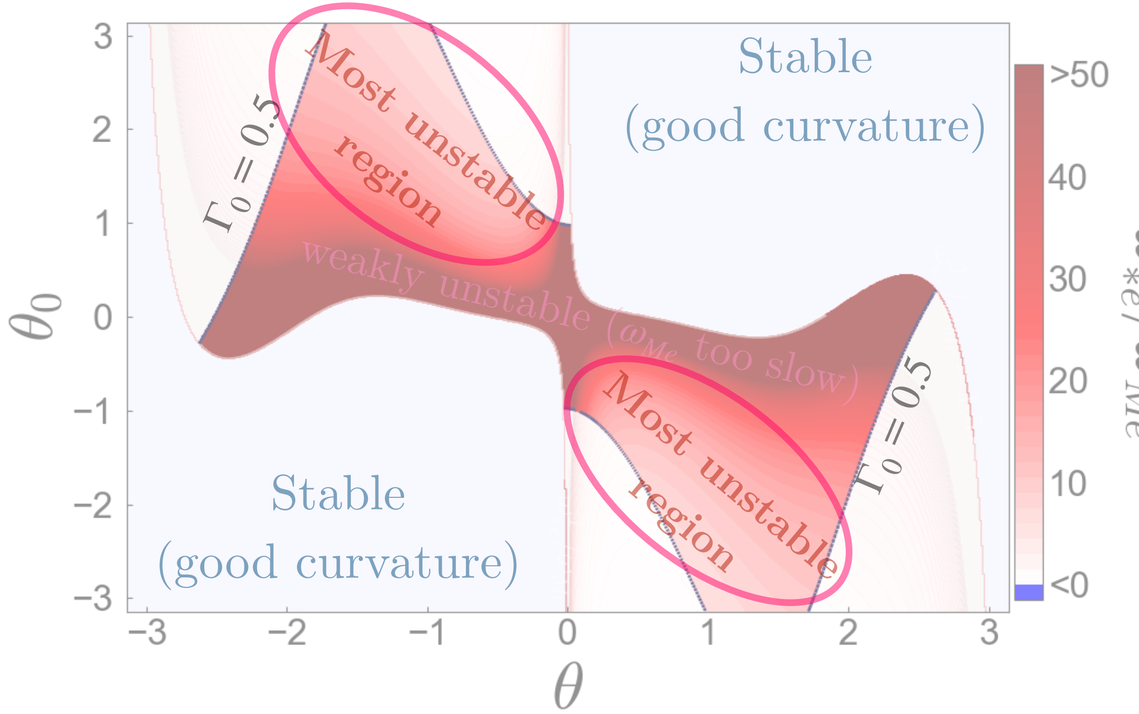

Expect toroidal ETG turbulence at $k_y\rho_e \sim 1$,
amplitude peaked at outboard midplane,
smoothly decreases in parallel direction.

—> **linear core toroidal ETG physics 2d**

Linear pedestal toroidal ETG physics

Core and Pedestal Comparison

Core

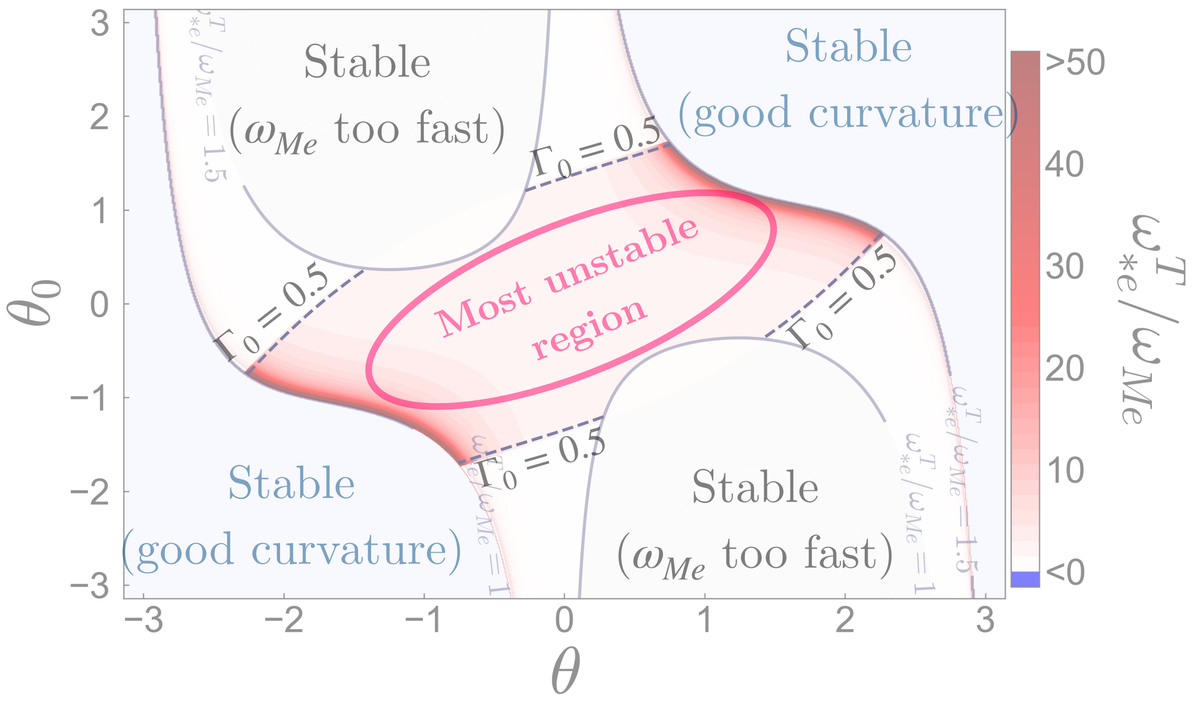

Expect toroidal ETG turbulence at $k_y\rho_e \sim 1$,
amplitude peaked at outboard midplane,
smoothly decreases in parallel direction.

—> **linear core toroidal ETG physics 2d**

JET Pedestal

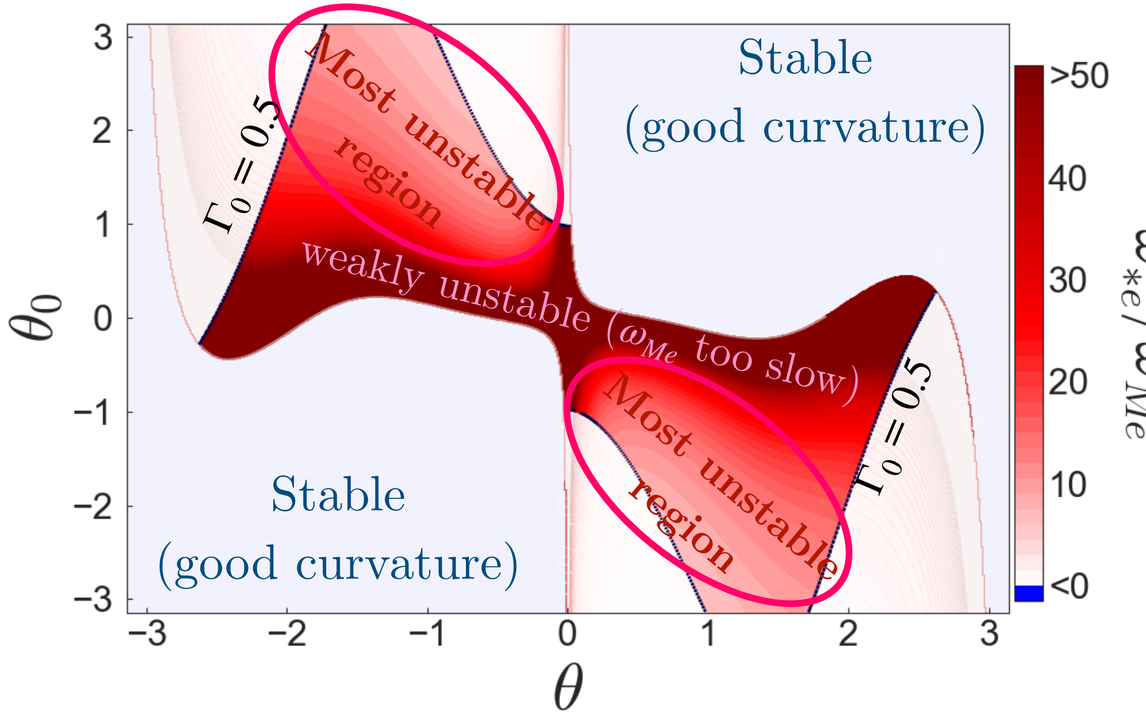

Expect toroidal ETG turbulence at $k_y\rho_e \sim 0.1$,
amplitude peaked at $\theta \simeq \pm\,\pi/2$.

—> **linear pedestal toroidal ETG physics 3d**

Nonlinear ETG simulations parallel comparison

Core

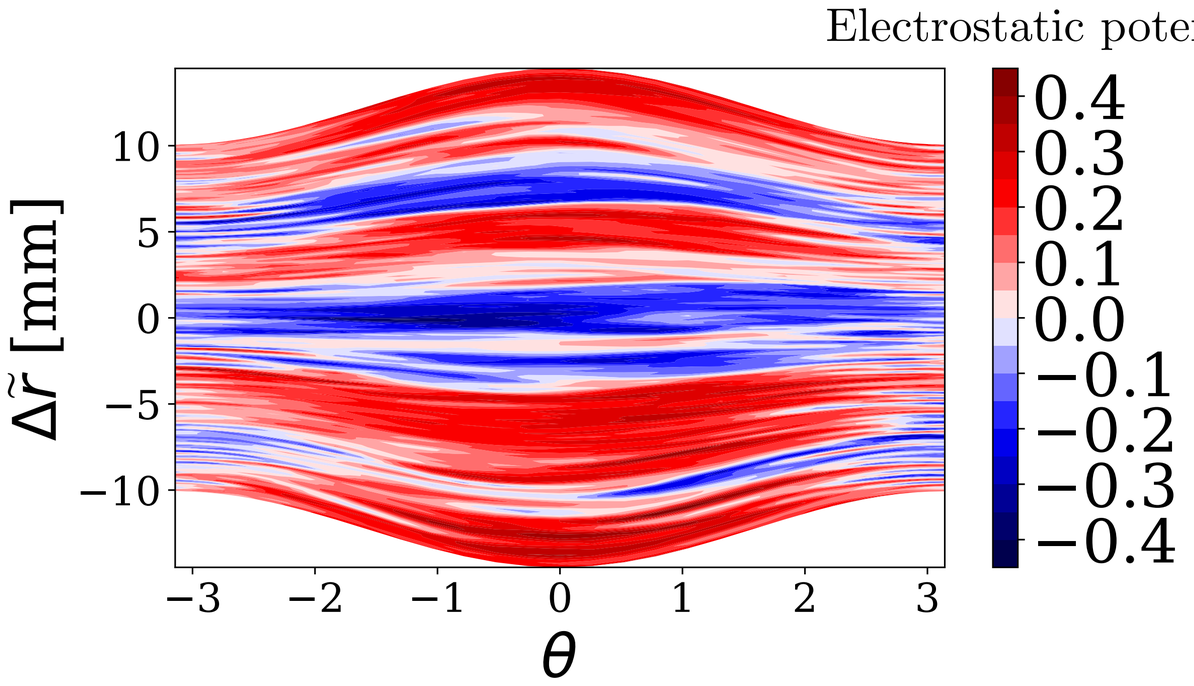

Core ETG turbulence extended smoothly in parallel direction, peaked at outboard midplane.

JET Pedestal

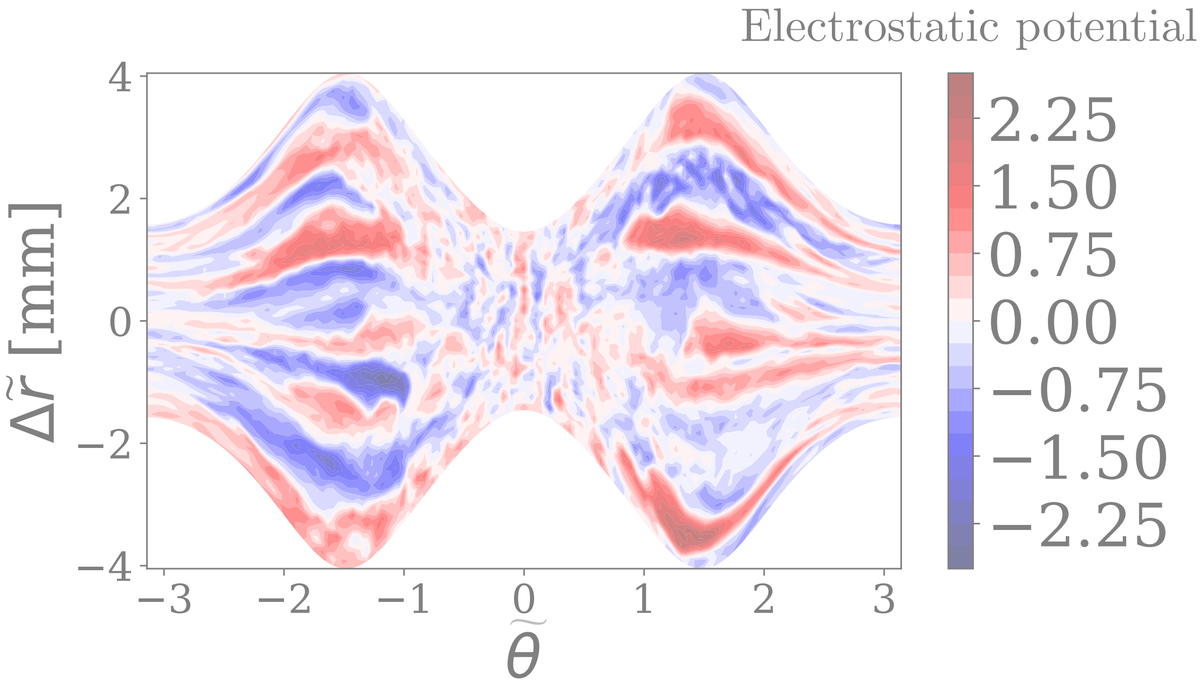

Pedestal ETG turbulence peaked at $\theta \simeq \pm\,\pi/2$.

$\Delta\tilde{r} \sim 1/B_{\text{poloidal}}$ is a radial coordinate that captures flux expansion.

Nonlinear ETG simulations parallel comparison

Core

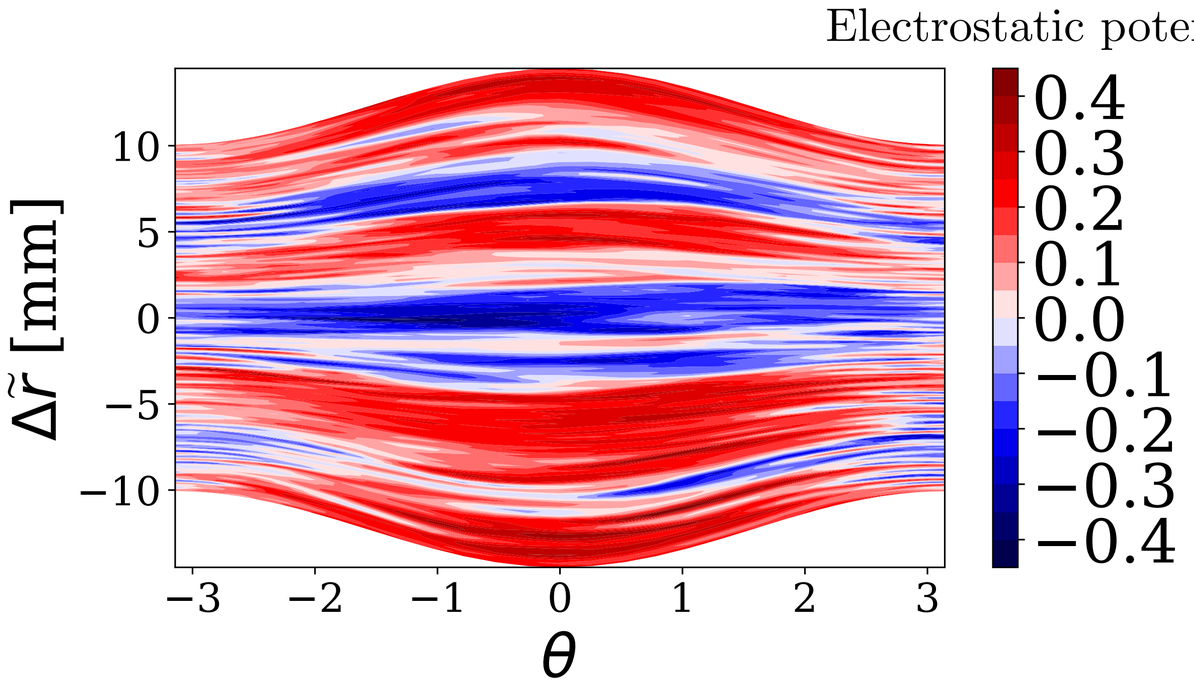

Core ETG turbulence extended smoothly in parallel direction, peaked at outboard midplane.

JET Pedestal

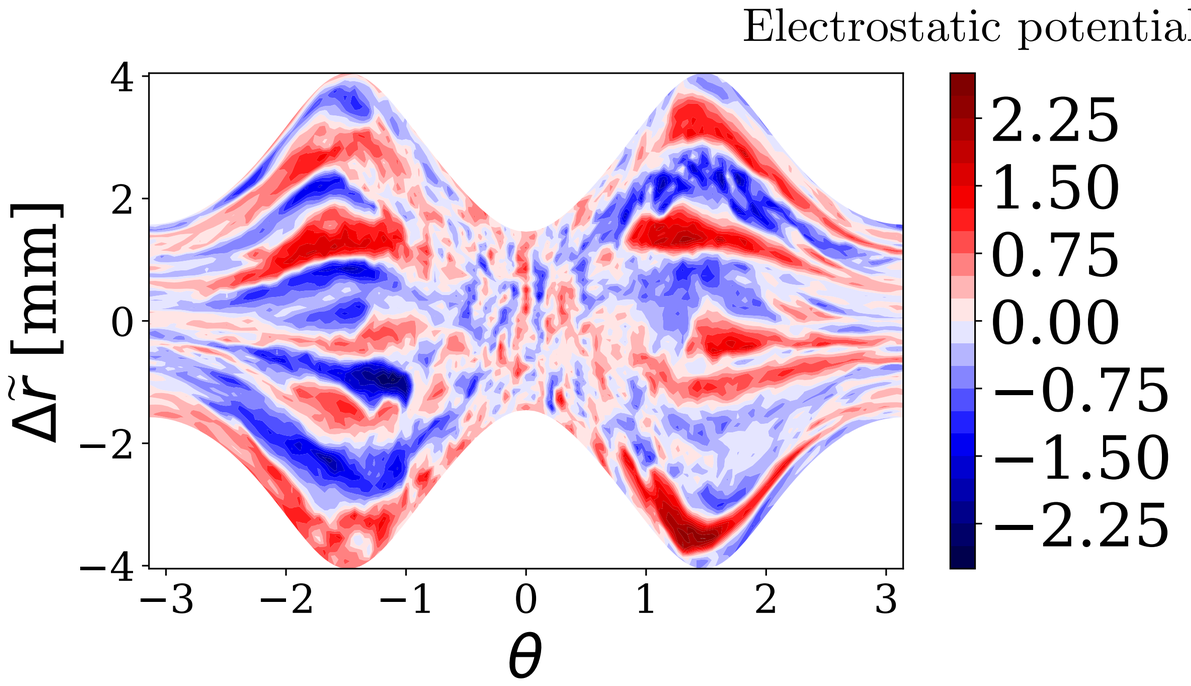

Pedestal ETG turbulence peaked at $\theta \simeq \pm\,\pi/2$.

$\Delta\tilde{r} \sim 1/B_{\text{poloidal}}$ is a radial coordinate that captures flux expansion.

Prior numerical evidence of 3-dimensional turbulence in pedestal

Linear

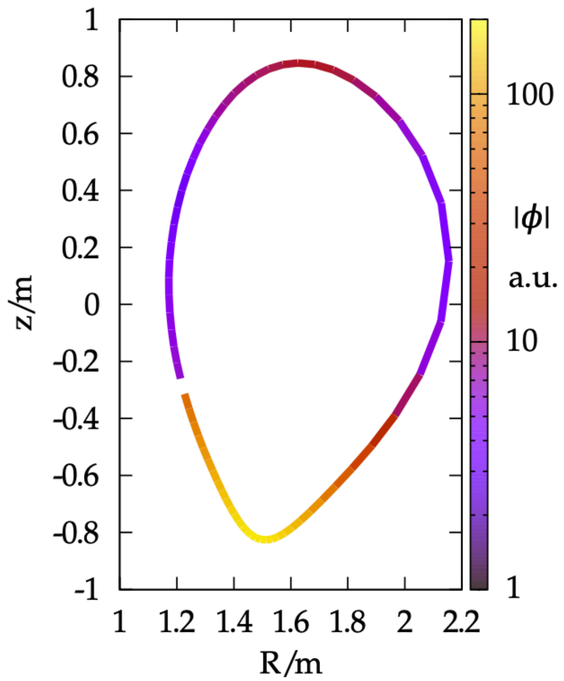

Told et al., PoP, **15,** 10 (2008): Parallel ϕ structure for linear ETG mode in ASDEX discharge.

Nonlinear

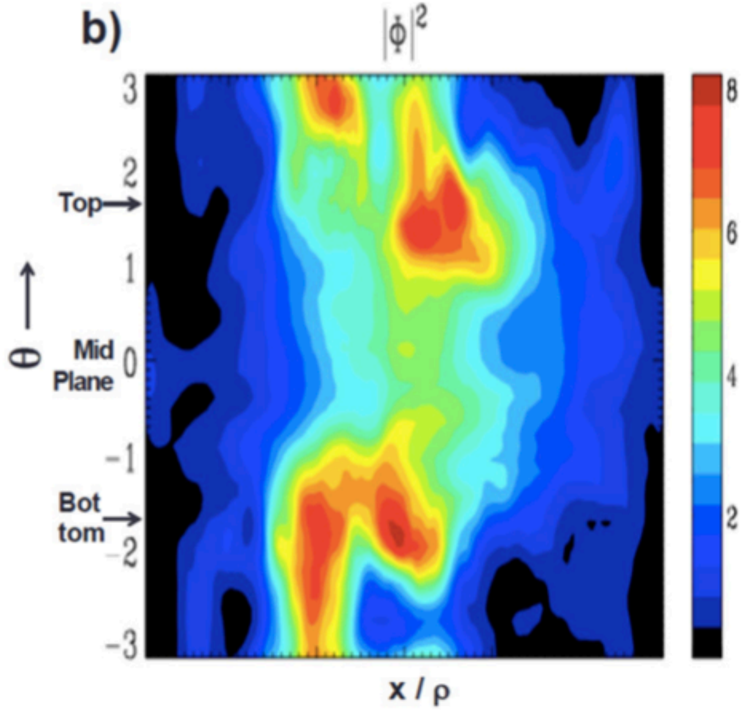

Kotschenreuther et al., NF, **57**, 064001 (2017): $|\phi|^2$ versus radial coordinate x and poloidal angle θ for global JET-ILW nonlinear simulation.

Core versus pedestal toroidal ETG summary

	Core	**JET Pedestal**
Geometry	Instability peaked at outboard midplane	Instability peaked away from outboard midplane
Geometry	Dominant linear instability at $k_y\rho_e \sim 1$	Dominant linear instability at $k_y\rho_e \ll 1$
Outer Scale	Outer scale at $k_y\rho_i \sim \frac{1}{q}\frac{L_{Te}}{R}\frac{\rho_i}{\rho_e} \gg 1$	Outer scale at $k_y\rho_i \sim \frac{1}{q}\frac{L_{Te}}{R}\frac{\rho_i}{\rho_e} \sim 1$

Similar considerations also apply to slab ETG. For more, see
[Dorland, PRL, **85**, 5579 (2000)], [Jenko, PoP, **7**, 5 (2000)], [Idomura, **7**, 2456 (2000)],
[Ishizawa, PFR, **6** (2011)], [Parisi, Thesis, 2020], [Chapman, 2022 (in prep)].

Numerical results: Linear physics

Linear growth rate

Most linear modes in JET-ILW pedestal simulations peak away from outboard midplane

For lower and higher wavenumbers, highest growth rates γ often at $\theta_0 \neq 0$, where $\theta_0 = k_x/k_y\hat{s}$

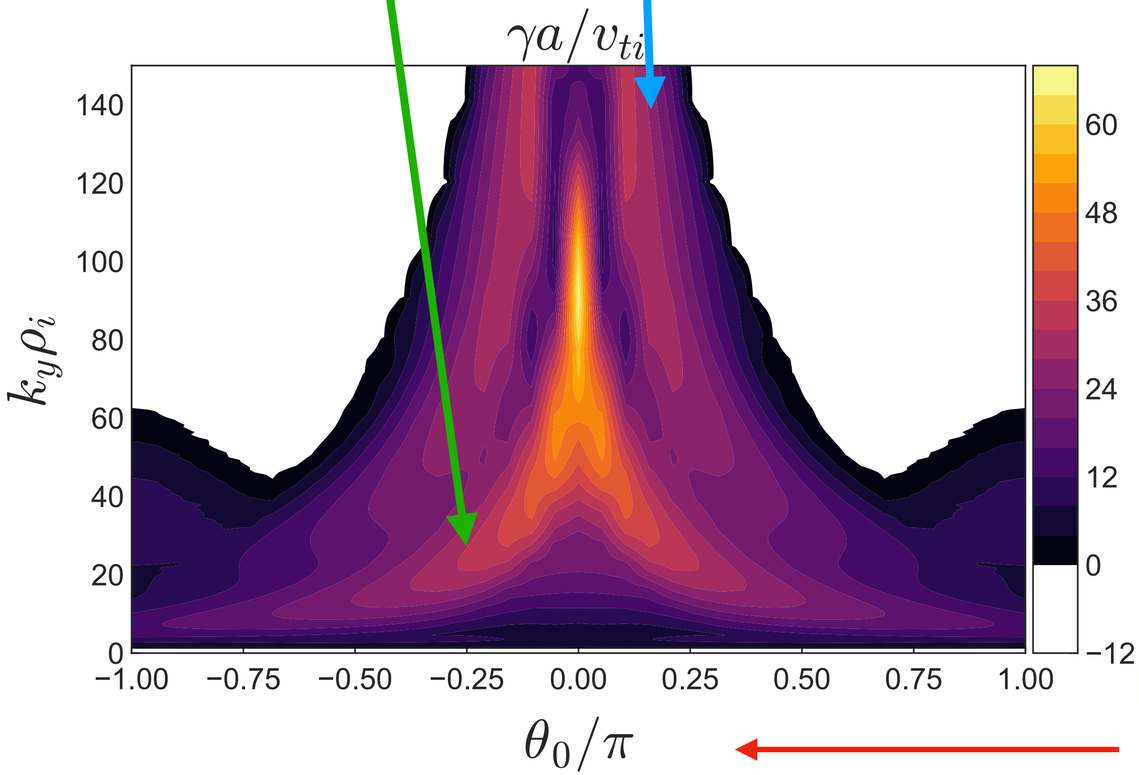

a) Growth rates γ for fastest growing modes in steep gradient region of JET-ILW pedestal

Most linear modes have largest amplitude away from outboard midplane

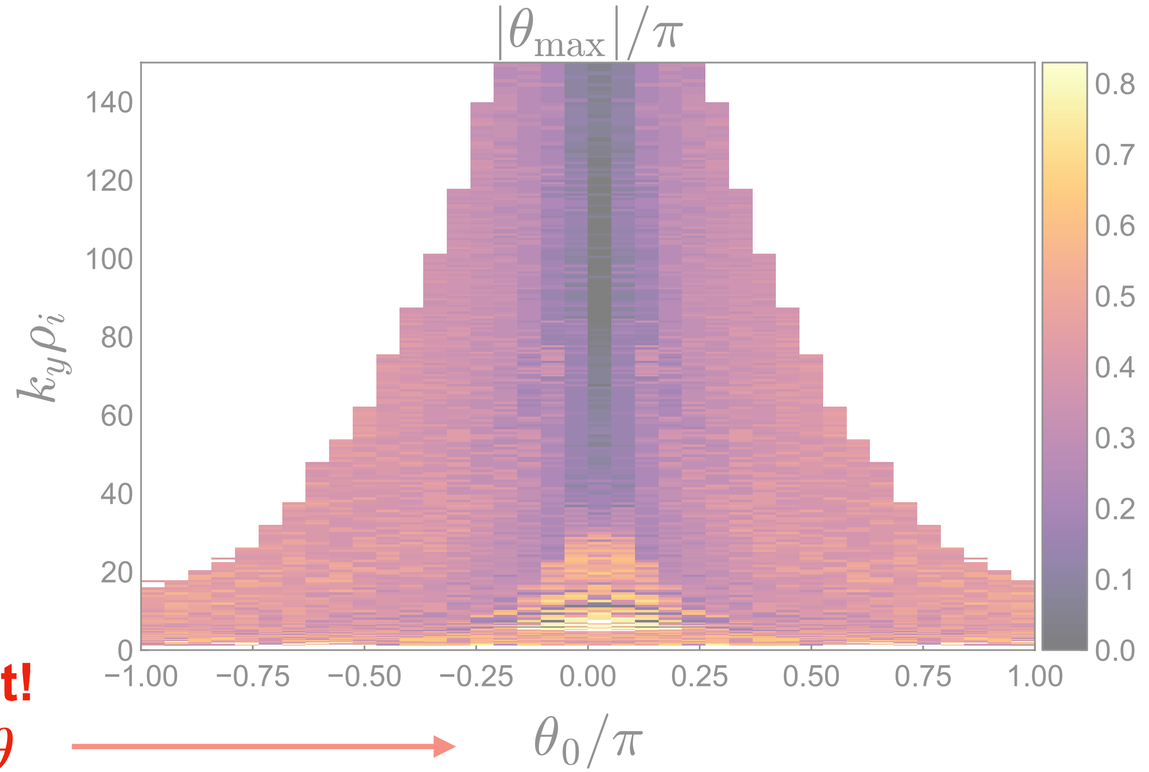

b) Poloidal location $\theta_{\max}$ for fastest growing modes in steep gradient region of JET-ILW pedestal

Important!
θ_0, not θ

Linear growth rate

Most linear modes in JET-ILW pedestal simulations peak away from outboard midplane

For lower and higher wavenumbers, highest growth rates γ often at $\theta_0 \neq 0$, where $\theta_0 = k_x/k_y\hat{s}$

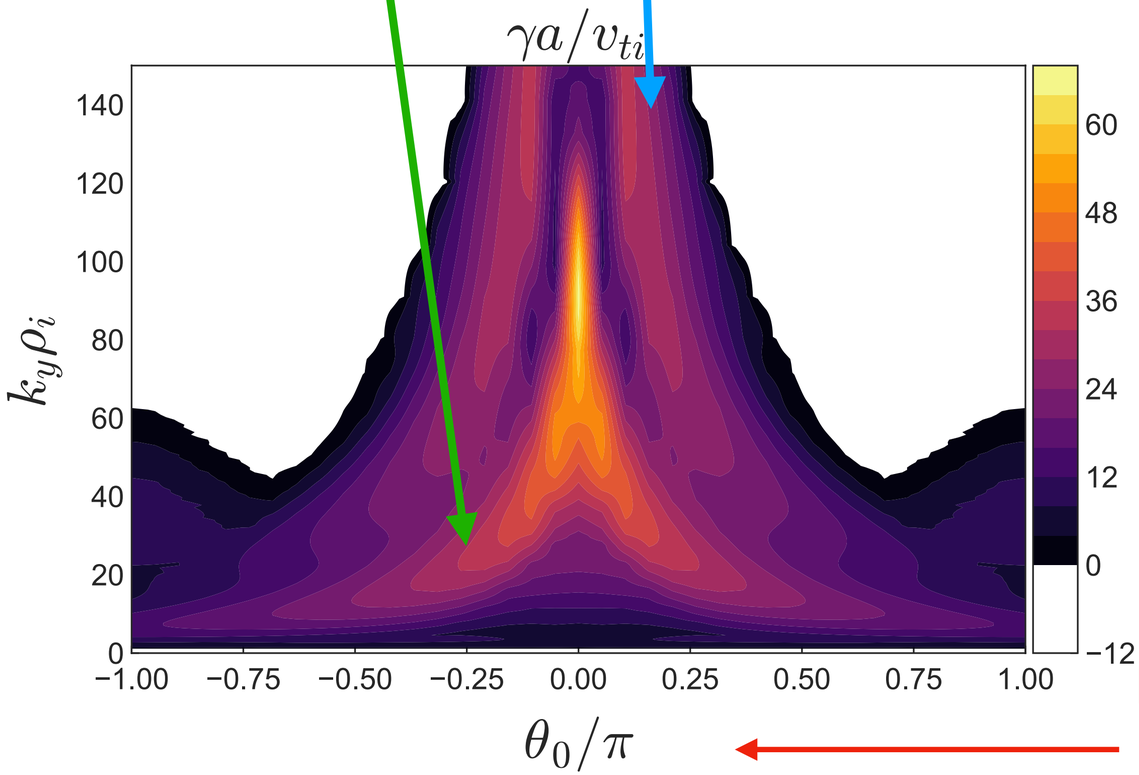

a) Growth rates γ for fastest growing modes in steep gradient region of JET-ILW pedestal

Most linear modes have largest amplitude away from outboard midplane

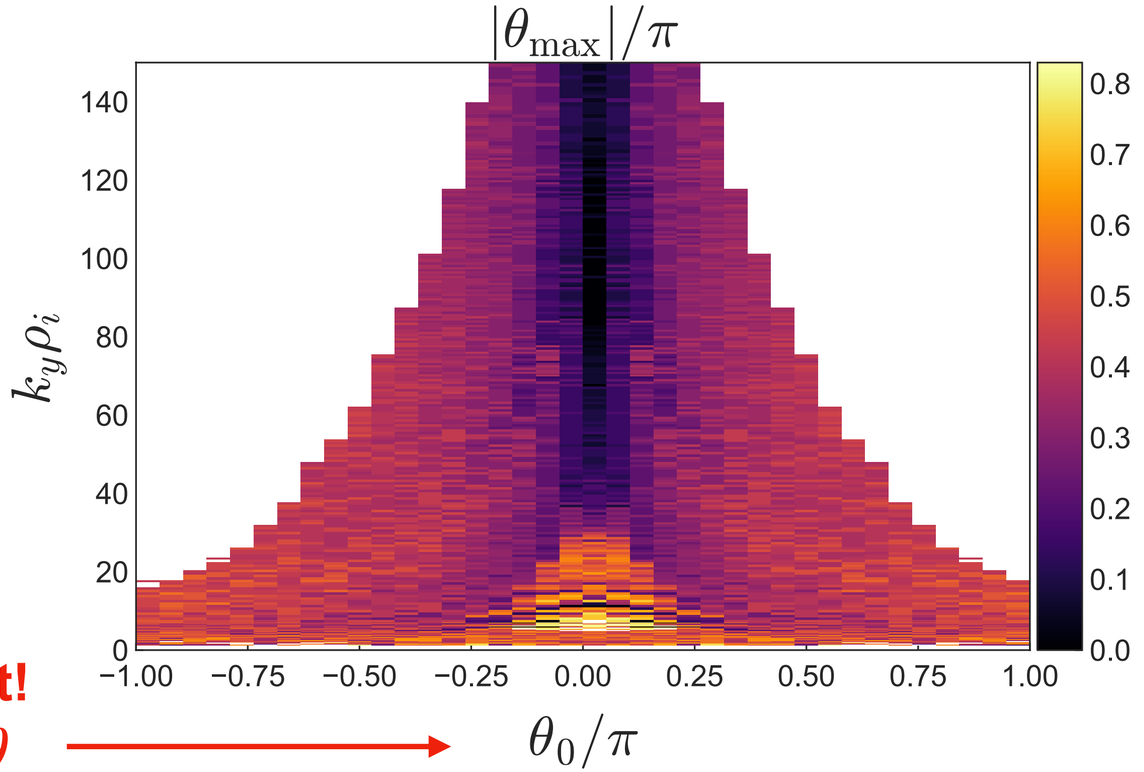

b) Poloidal location $\theta_{\max}$ for fastest growing modes in steep gradient region of JET-ILW pedestal

Important!
θ_0, not θ

Linear growth rate

Important to resolve all θ locations in pedestal simulations

Most linear modes have largest amplitude away from outboard midplane

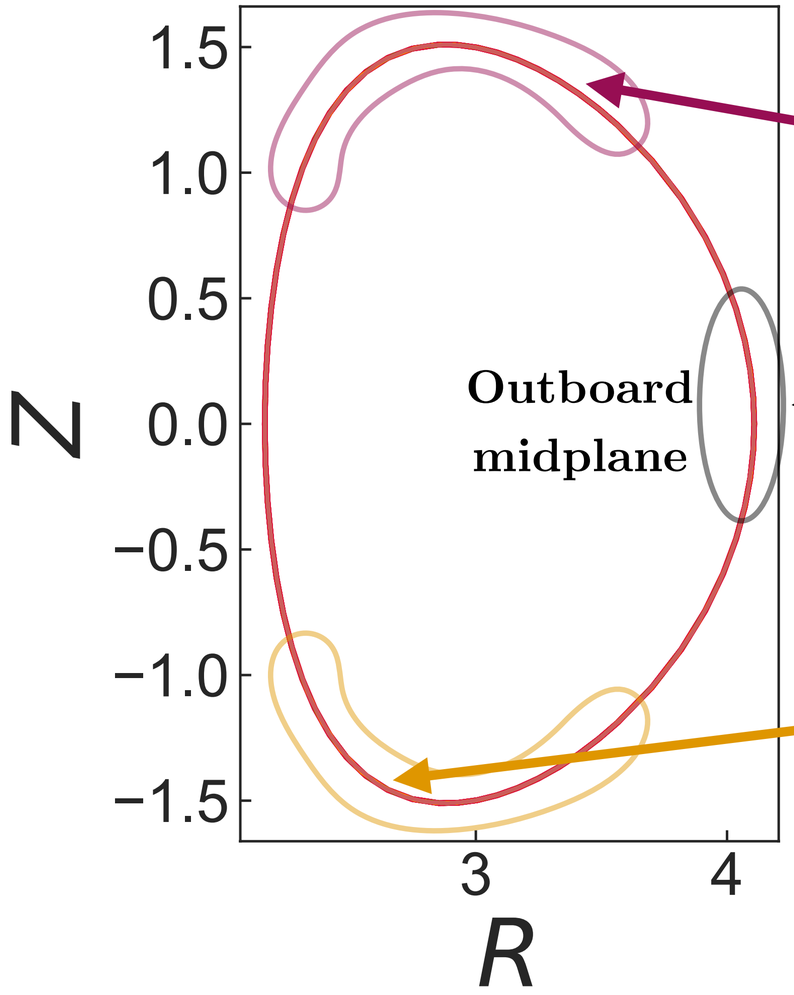

a) Poloidal location for fastest growing modes.

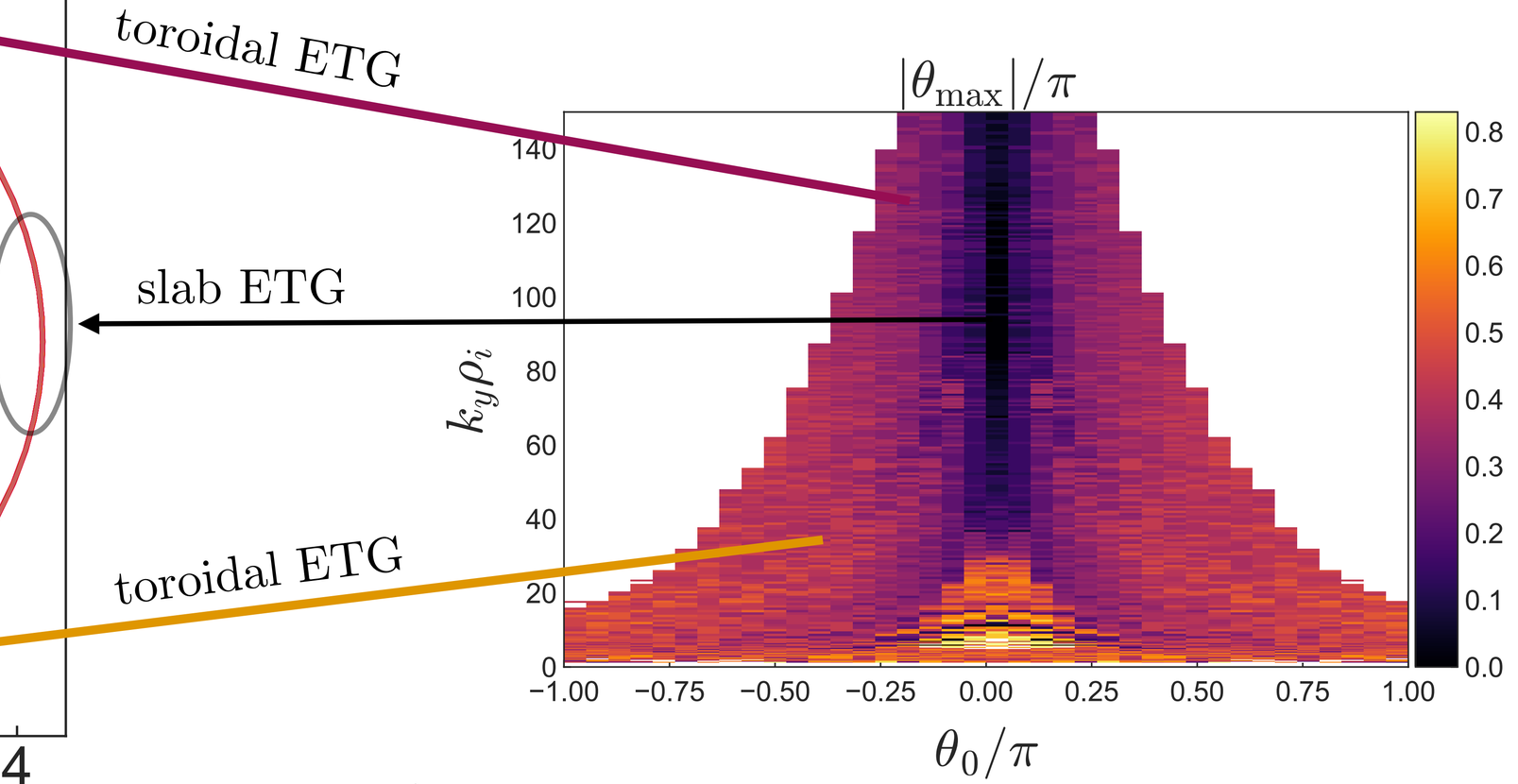

b) Poloidal location $\theta_{\max}$ for fastest growing modes in steep gradient region of JET-ILW pedestal

Linear growth rate

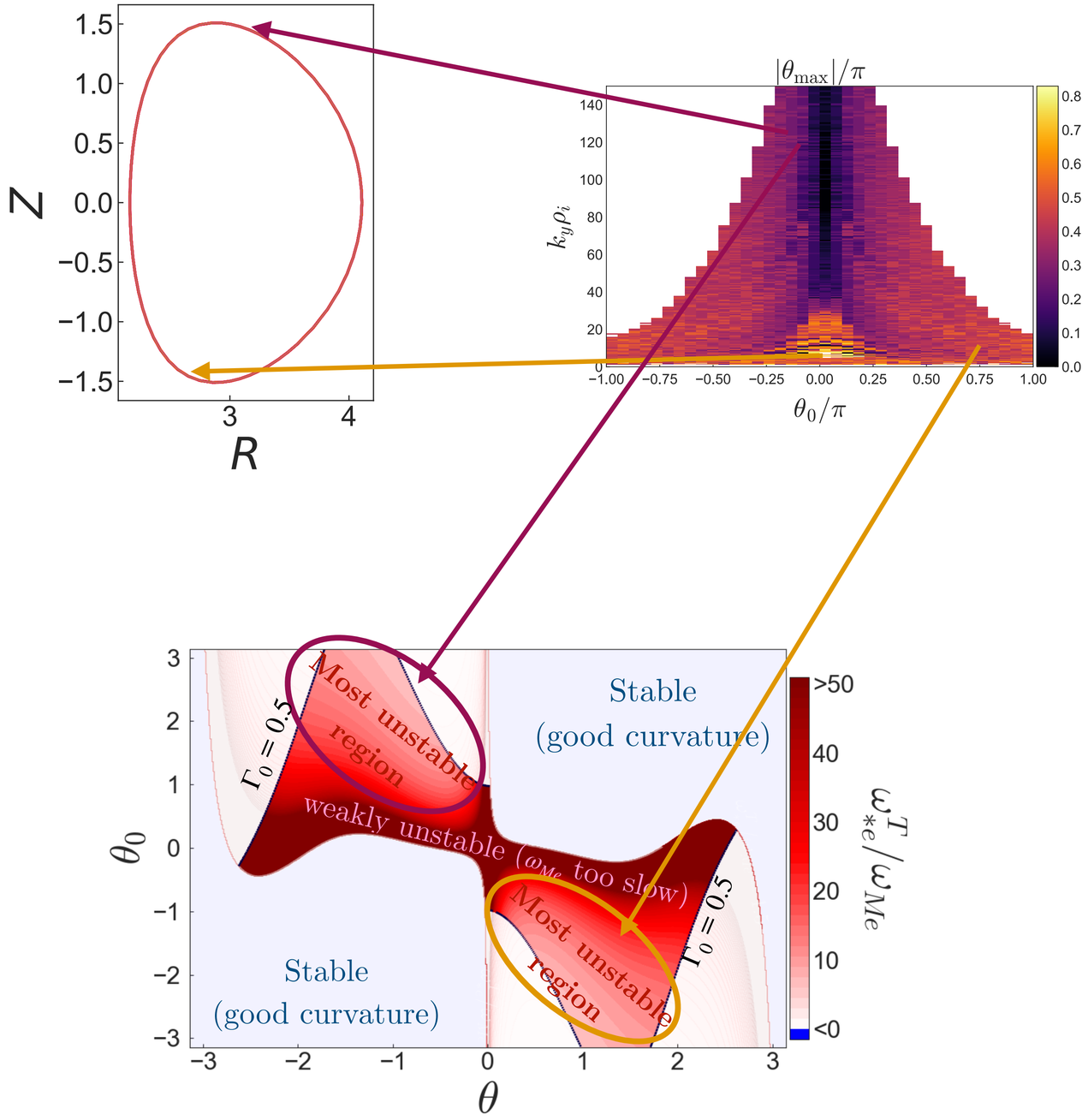

Linear growth rate

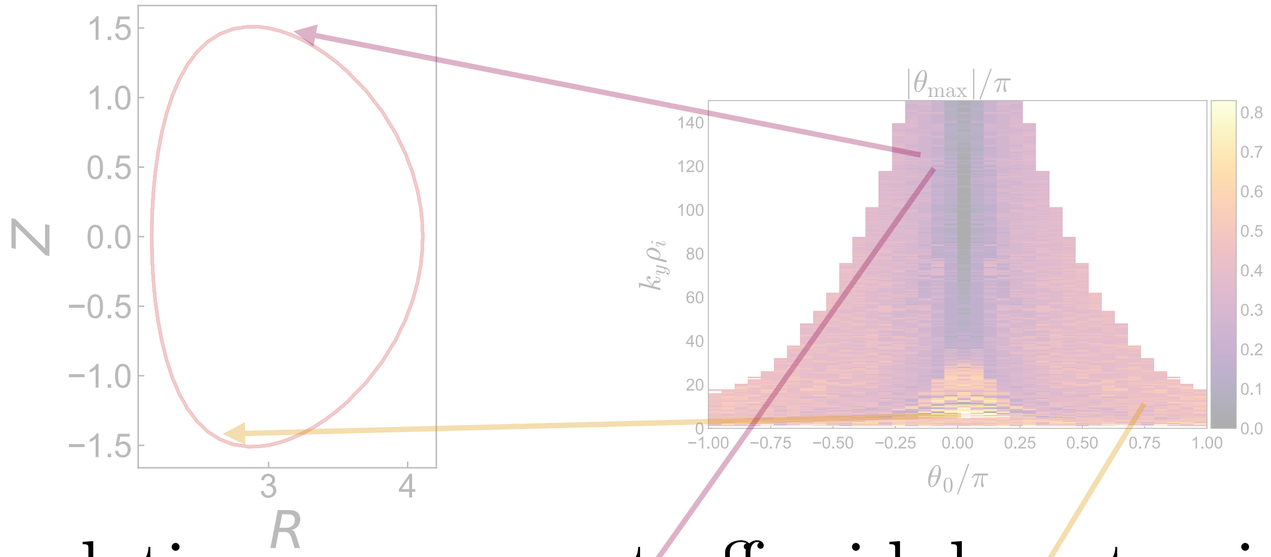

$\longrightarrow$ in nonlinear simulations, we expect off-midplane toroidal ETG turbulence and transport.

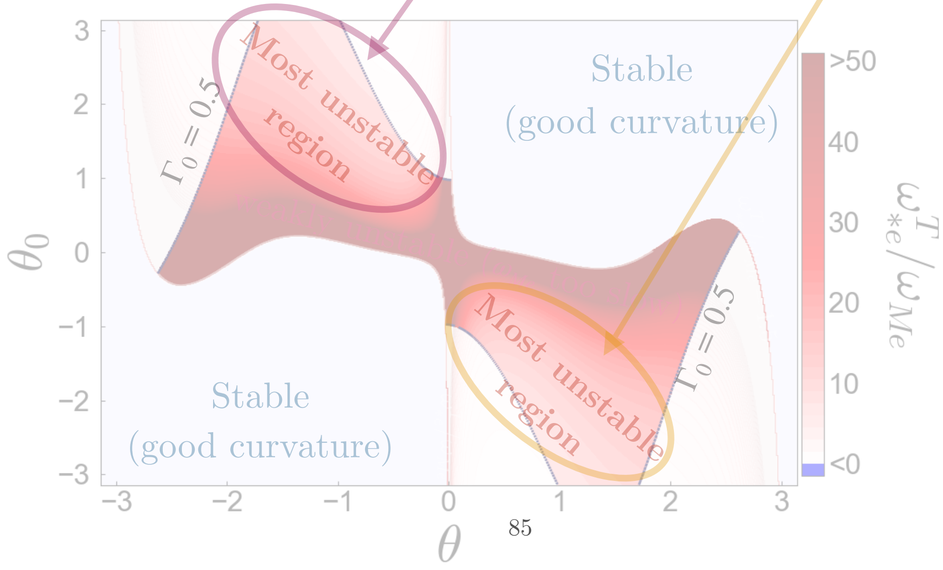

Numerical results: Nonlinear physics

Nonlinear simulation

Parameters: resolving all relevant scales is numerically challenging

- We perform electrostatic nonlinear gyrokinetic simulations using stella [Barnes, 2019].
- Steep gradient region of JET-ILW pedestal, $R/L_{Te} \simeq 130$.
- 150 poloidal modes, 70 radial modes, 128 parallel gridpoints, 64 $v_{\parallel}$ gridpoints, 12 μ gridpoints, some hyperviscosity, kinetic ions and electrons, Miller geometry fit to JET shot 92174. 'Experimental' $E \times B$ shear needed to stabilize streamers.
- Minimum poloidal wavenumber $k_y \rho_i = 0.7$, minimum radial wavenumber $k_x \rho_i = 1.6$.
- Run simulation for roughly 2000 a/v_{te} times (∼40 linear growth times of slowest dominant linear modes in our box).

Nonlinear simulation Split into early and late times

- **Early** times: slab ETG modes dominate (electron-scale slab modes grow and saturate faster).
- **Late** times: ion-scale ETG modes have relatively large amplitudes, reduce electron-scale transport.

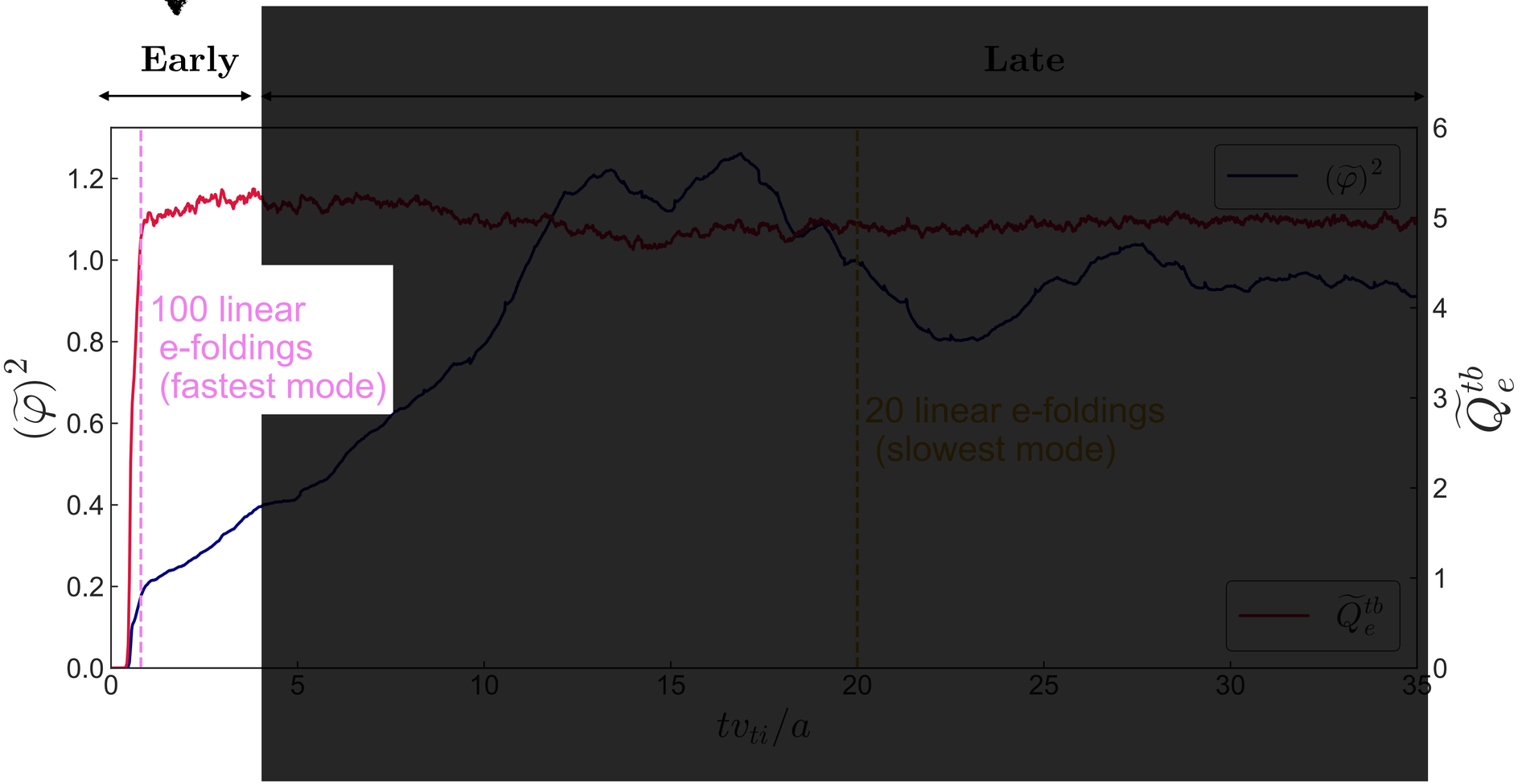

Normalization conventions:

Heat flux:

$$\widetilde{Q}_e^{tb} = Q_e^{tb}/Q_{gB,i}$$

Electrostatic potential:

$$\widetilde{\varphi} = e\phi^{tb}/T_i\rho_{*i}$$

Nonlinear simulation Split into early and late times

- **Early** times: slab ETG modes dominate (electron-scale slab modes grow and saturate faster).
- **Late** times: ion-scale ETG modes have relatively large amplitudes, reduce electron-scale transport.

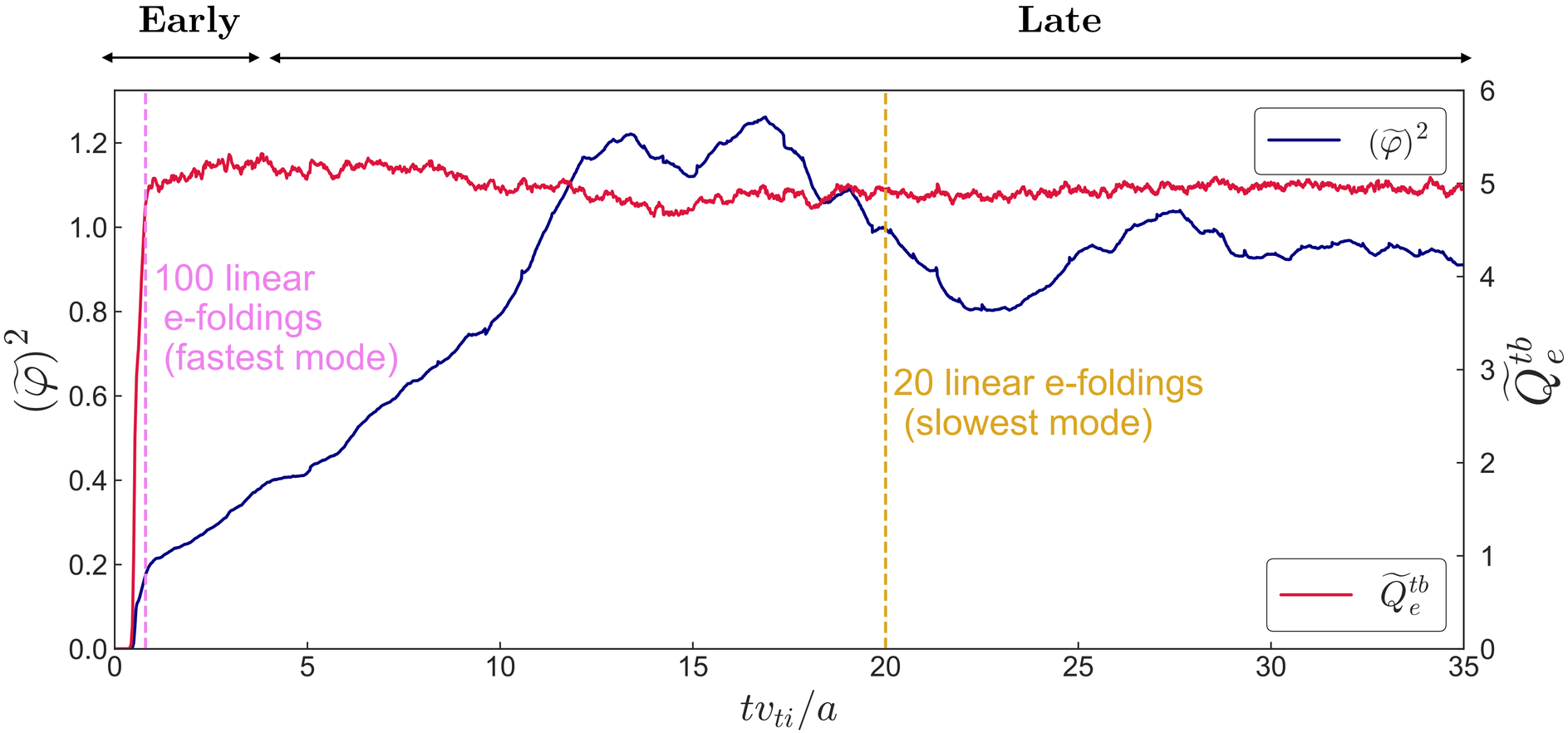

Normalization conventions:

Heat flux:

$$\widetilde{Q}_e^{tb} = Q_e^{tb}/Q_{gB,i}$$

Electrostatic potential:

$$\widetilde{\varphi} = e\phi^{tb}/T_i\rho_{*i}$$

Pedestal ETG turbulence has complex 3-dimensional structure

Wait sufficiently long, **off-midplane non-ballooning ion-scale** toroidal ETG modes grow to dominate.

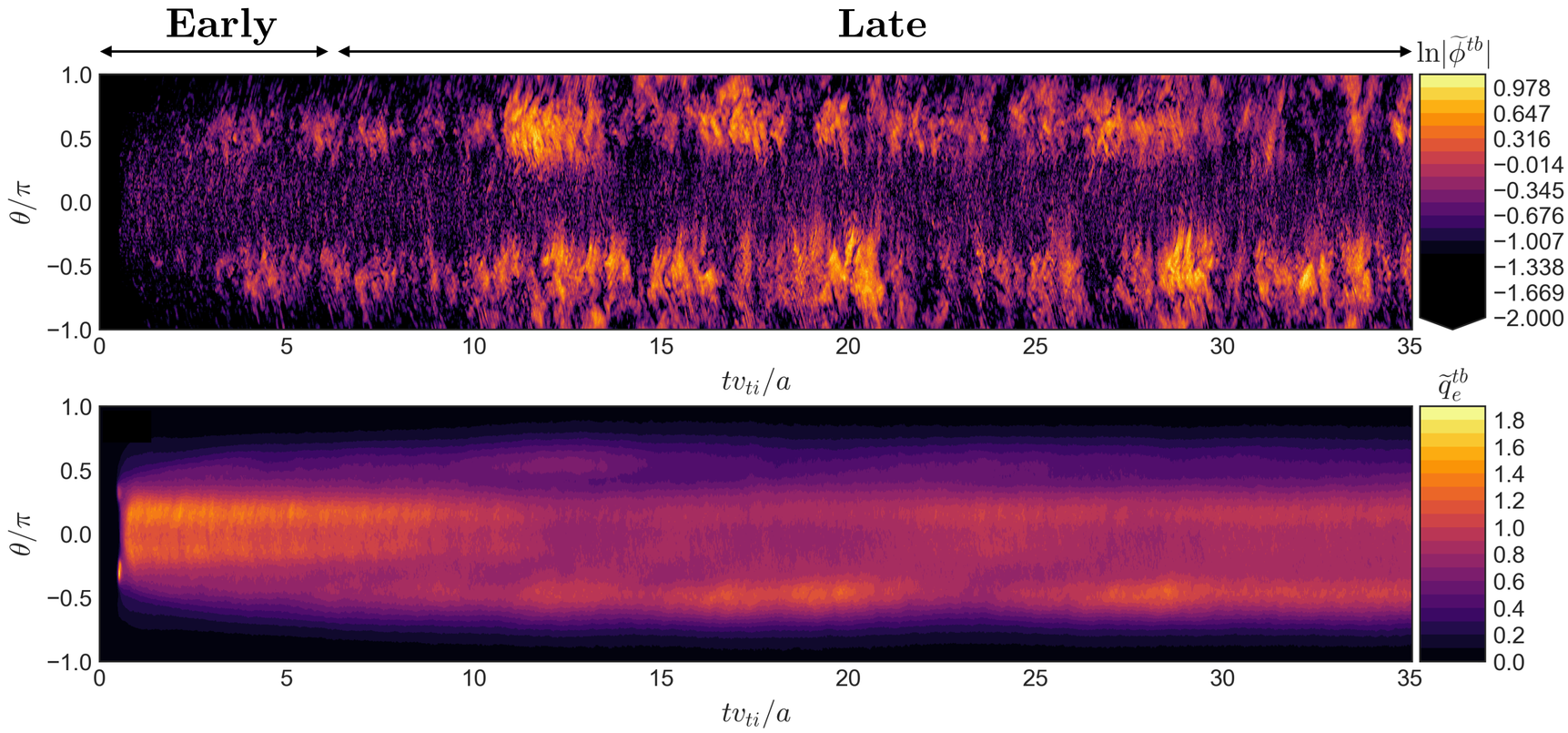

Pedestal ETG turbulence has complex 3-dimensional structure

Wait sufficiently long, **off-midplane non-ballooning ion-scale** toroidal ETG modes grow to dominate.

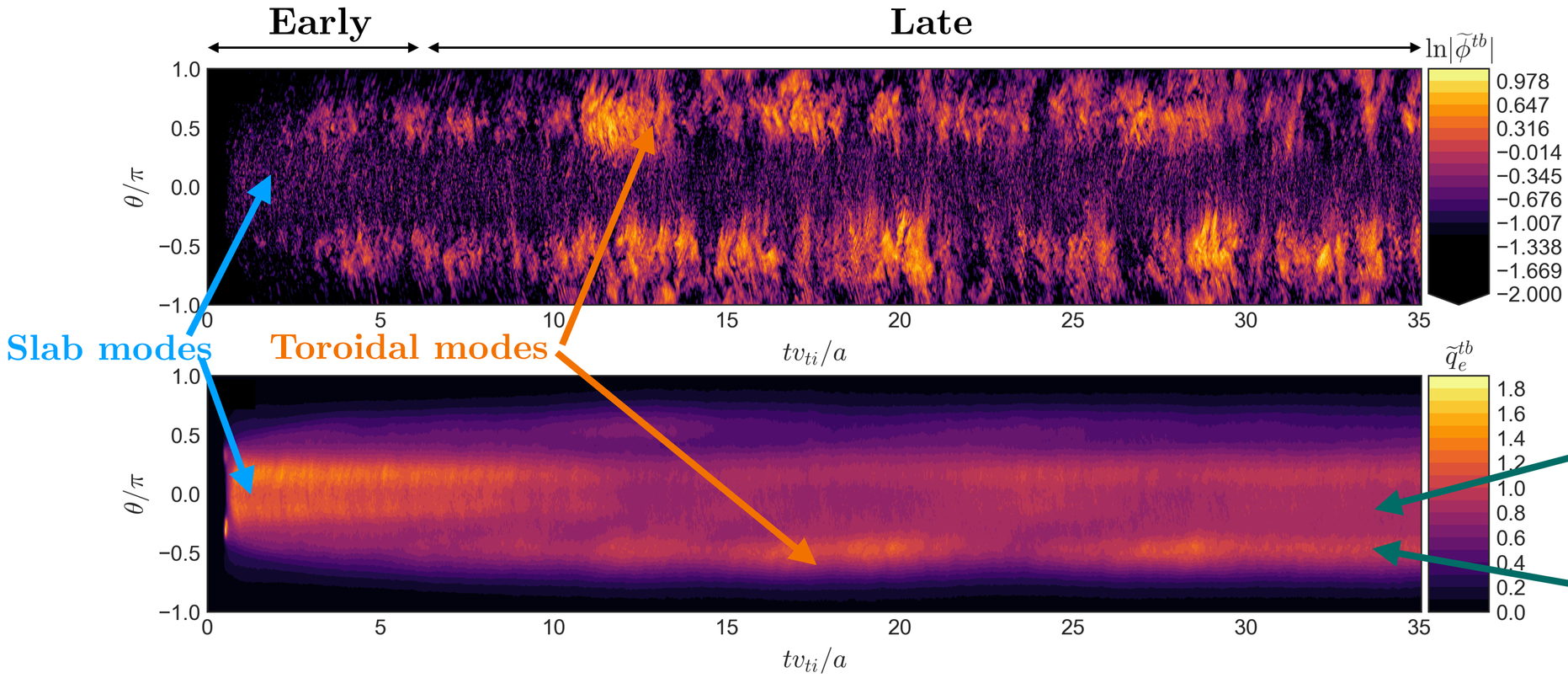

Pedestal ETG turbulence has complex 3-dimensional structure

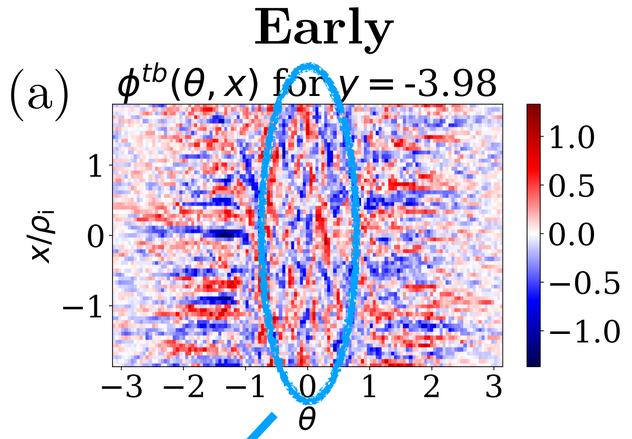

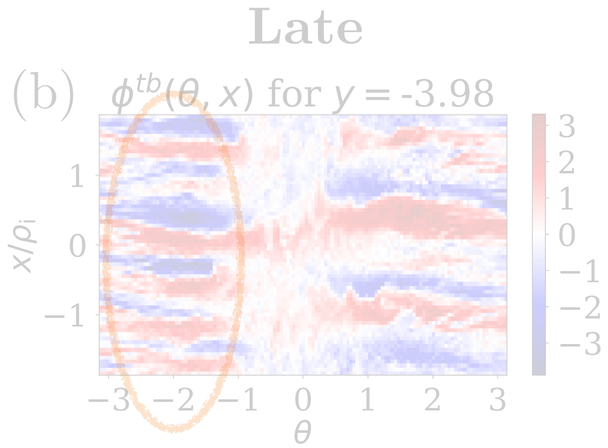

Figures: electrostatic potential versus radial coordinate and θ at fixed y for (a) Early times and (b) Late times.

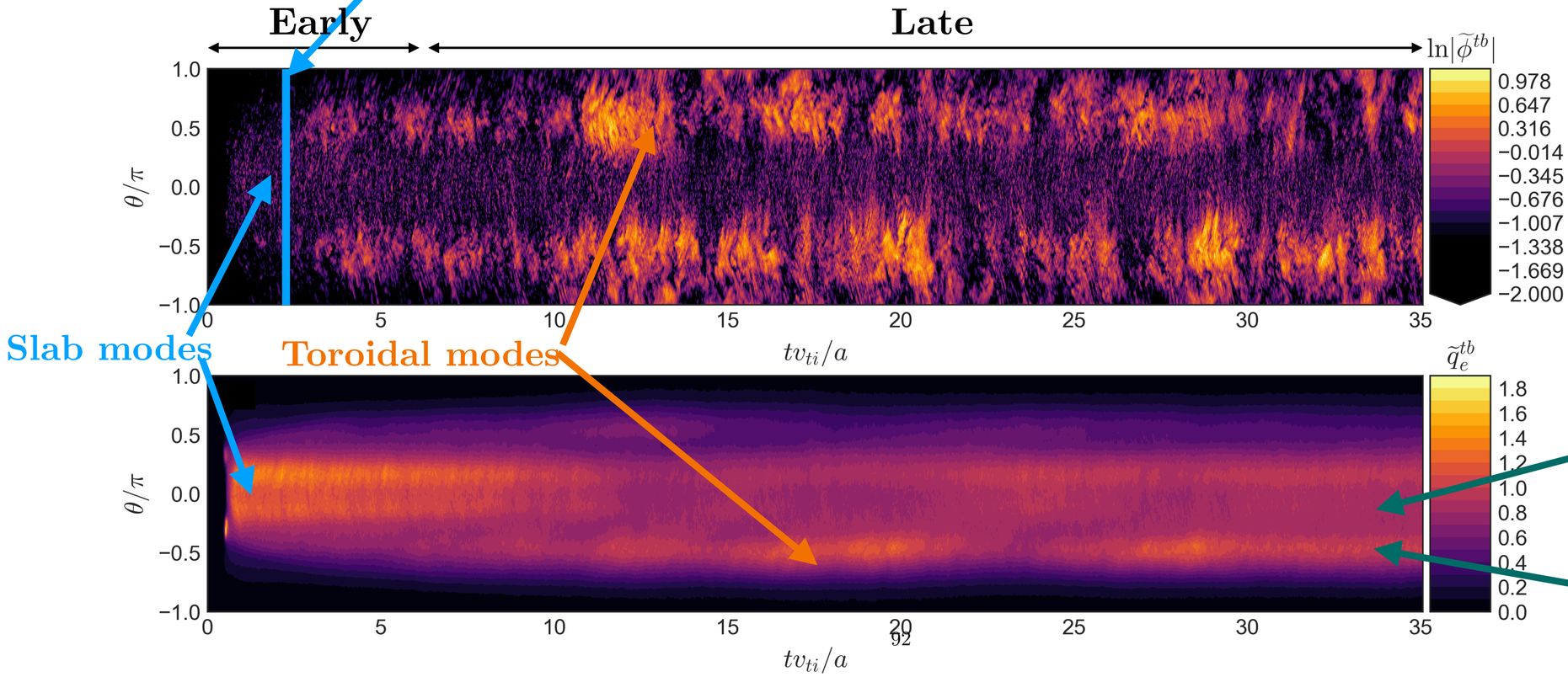

Reduction of slab transport at outboard midplane

Toroidal transport

Pedestal ETG turbulence has complex 3-dimensional structure

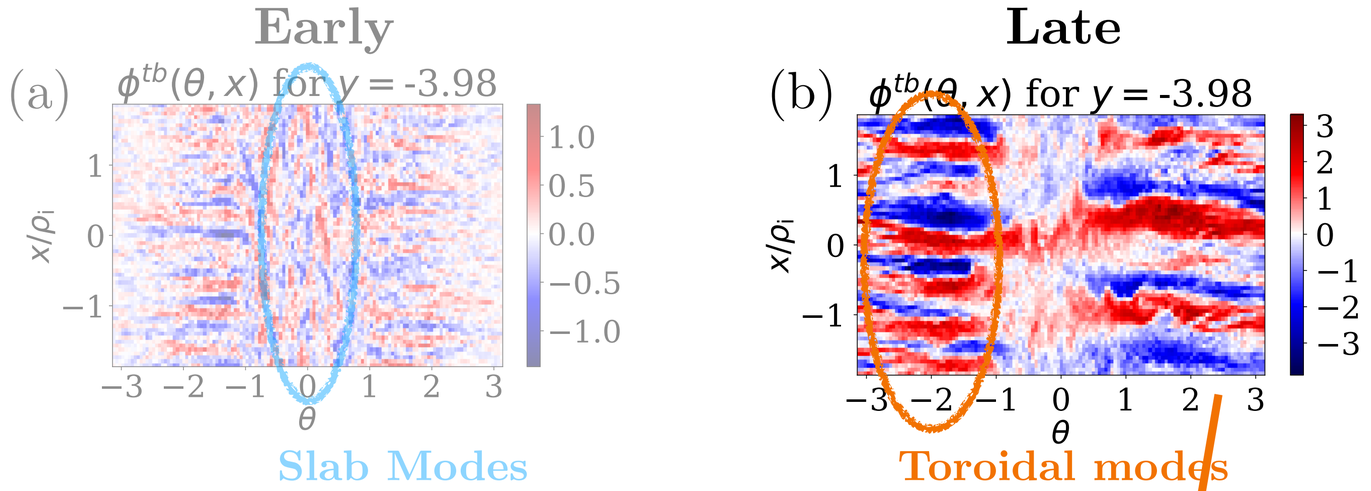

Figures: electrostatic potential versus radial coordinate and θ at fixed y for (a) Early times and (b) Late times.

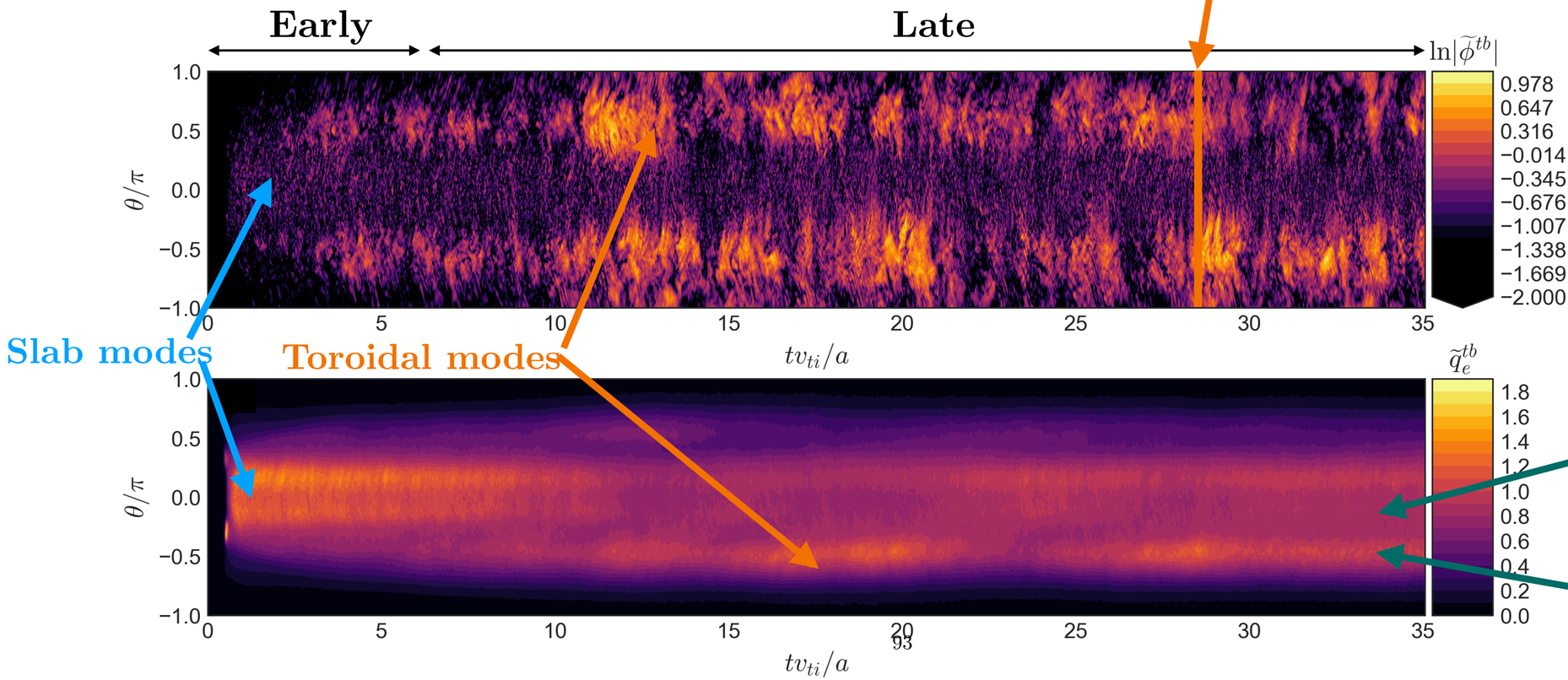

Reduction of slab transport at outboard midplane

Toroidal transport

Nonlinear results

Heat flux spectrum time evolution

- Heat flux spectra changes significantly with time. At early times, electron heat flux dominated by fast growing, electron-scale modes near outboard midplane ($\theta = 0.0$).

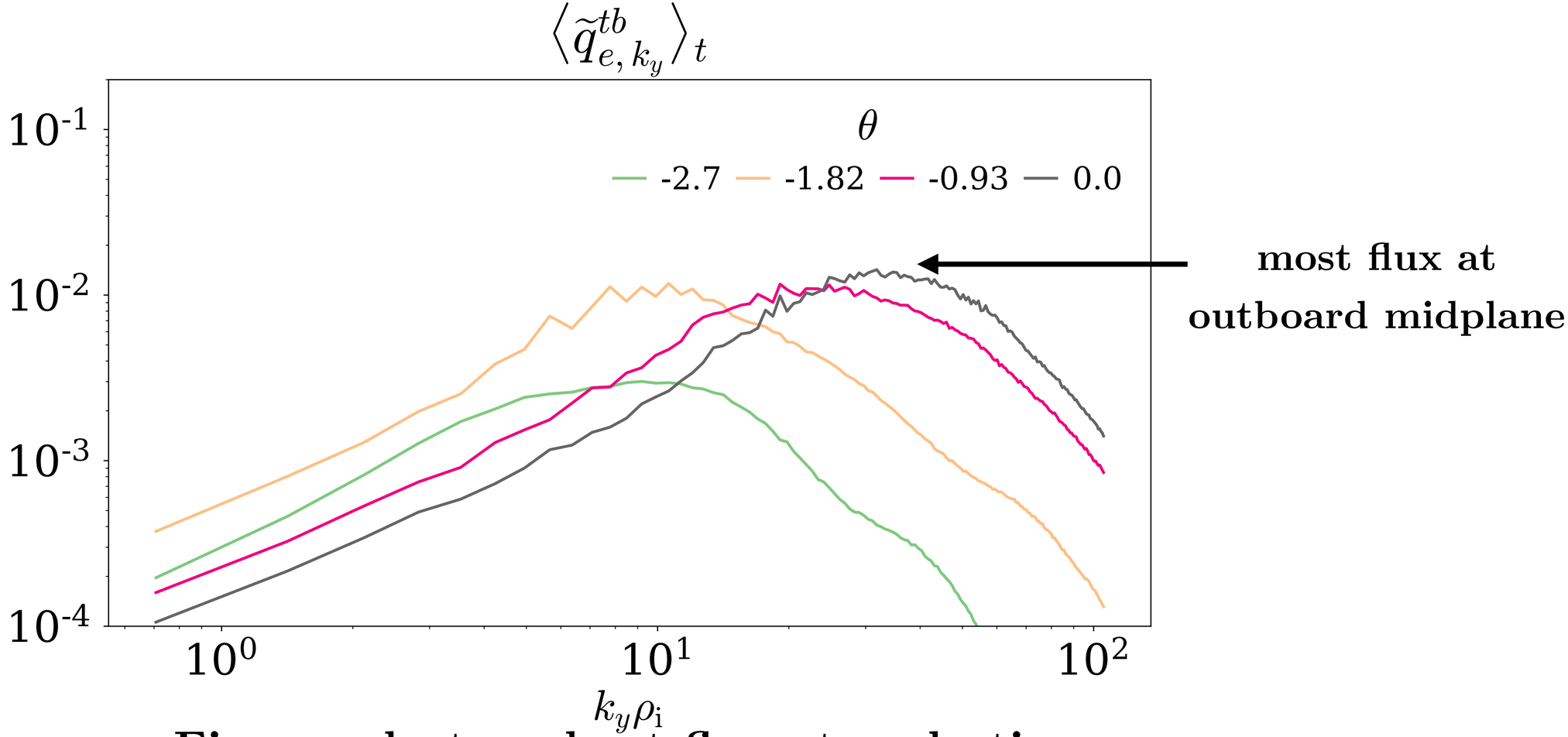

Figure: electron heat flux at early times.

Nonlinear results

Heat flux spectrum time evolution

- At late times, electron heat flux also has significant ion-scale contribution away from outboard midplane.

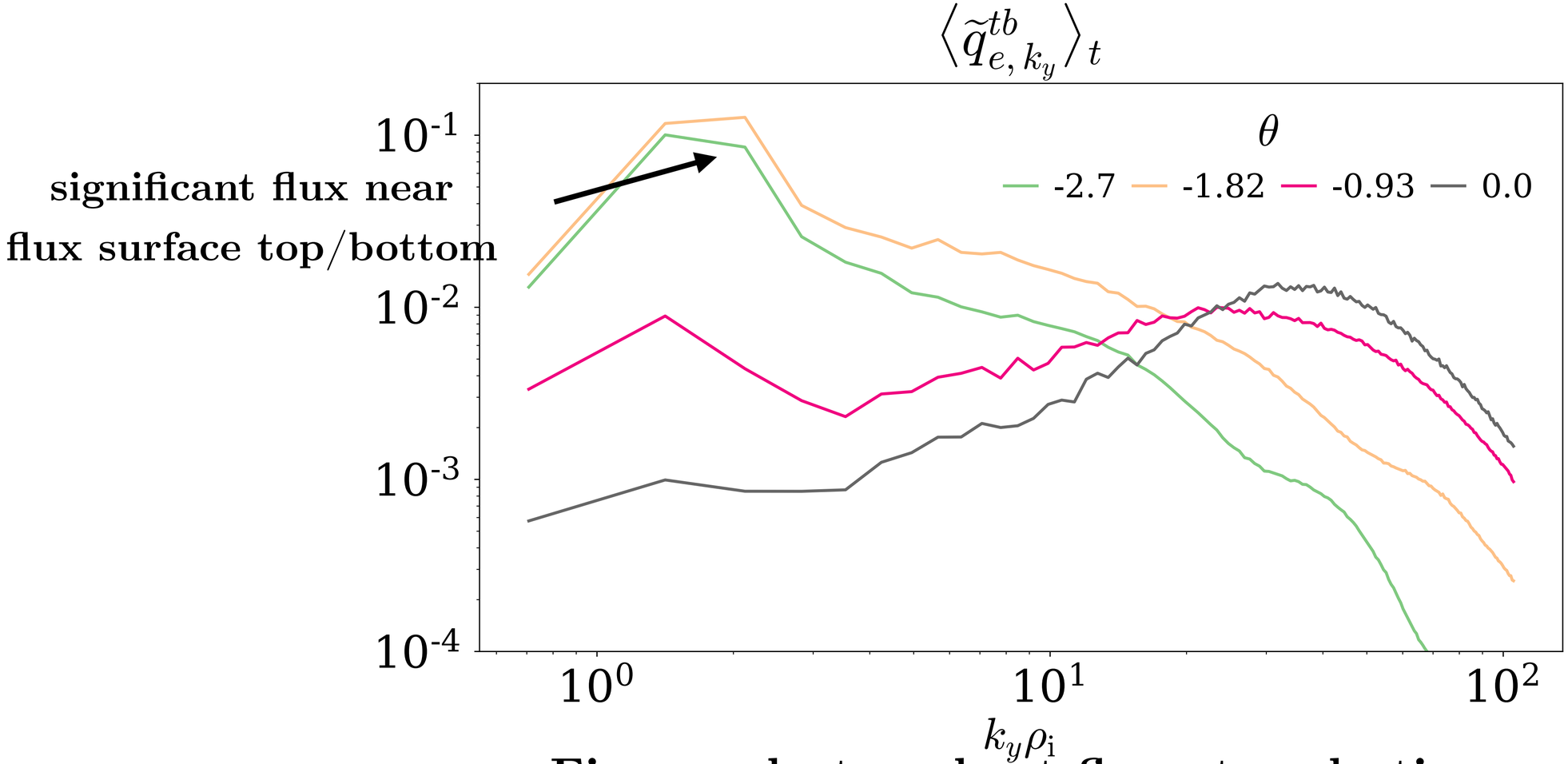

Figure: electron heat flux at early times.

Nonlinear results

Heat flux spectrum time evolution

- Ion-scale heat flux contribution away from outboard midplane.

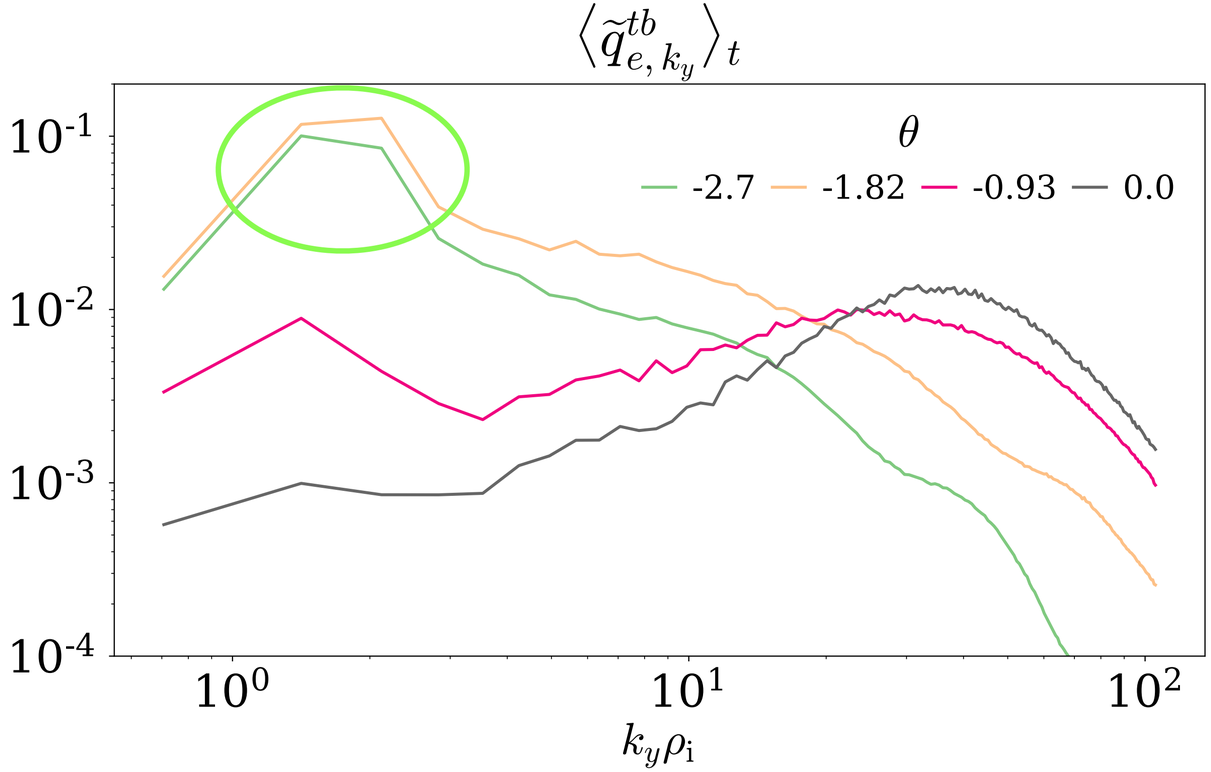

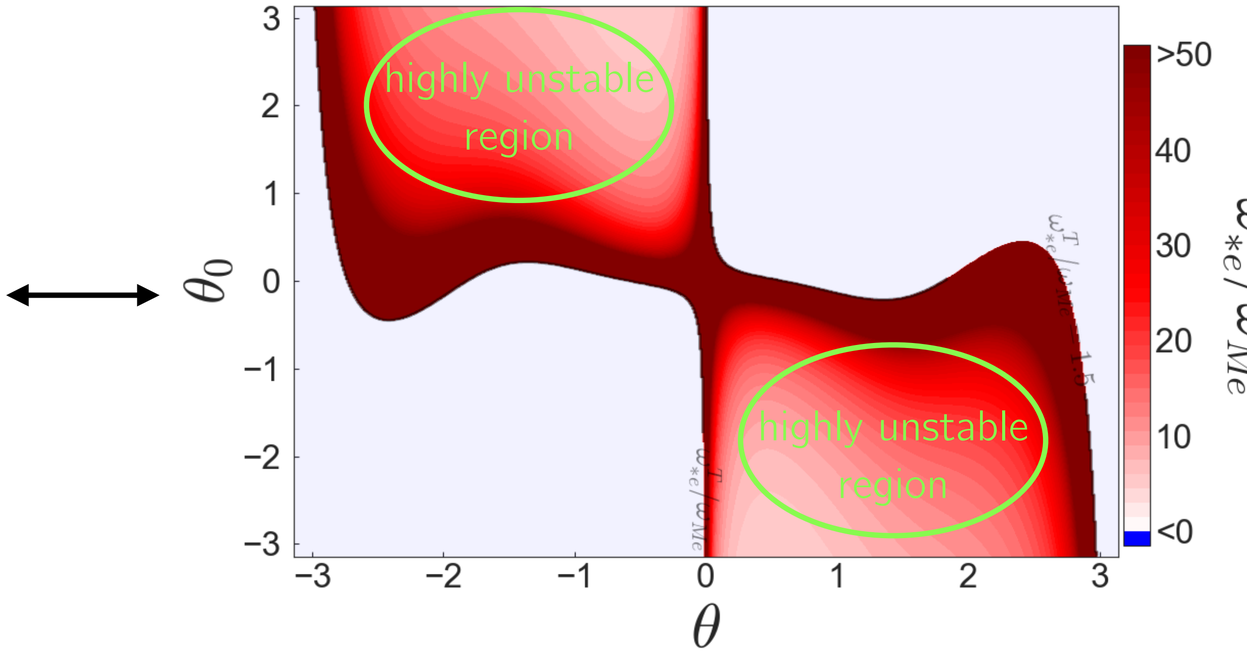

Nonlinear results

Heat flux spectrum time evolution

- Ion-scale heat flux contribution away from outboard midplane.

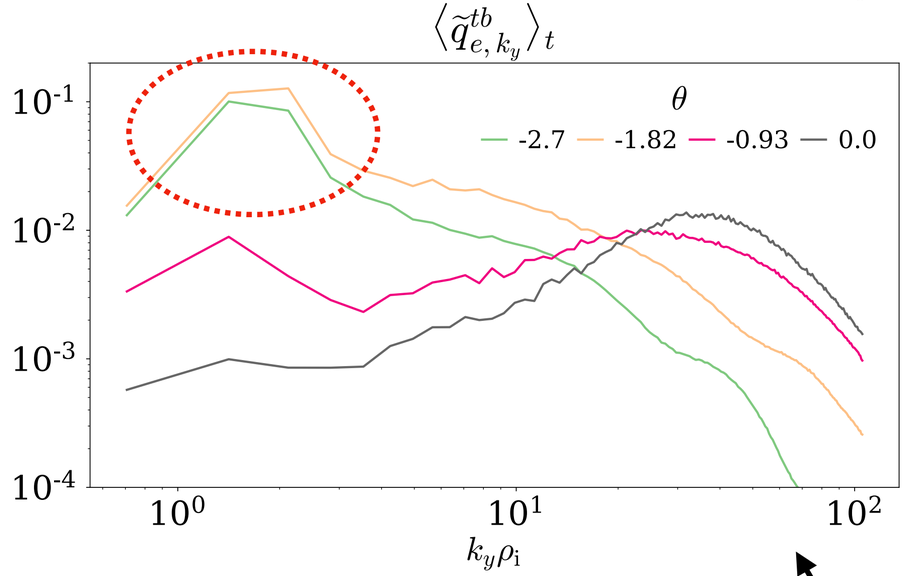

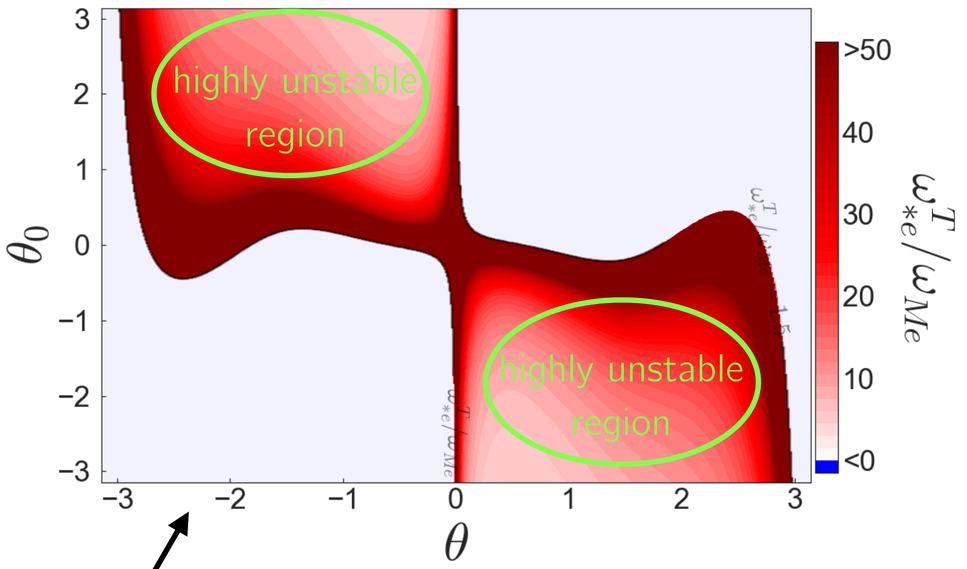

Toroidal ETG turbulence

$k_y\rho_i = 1.4$

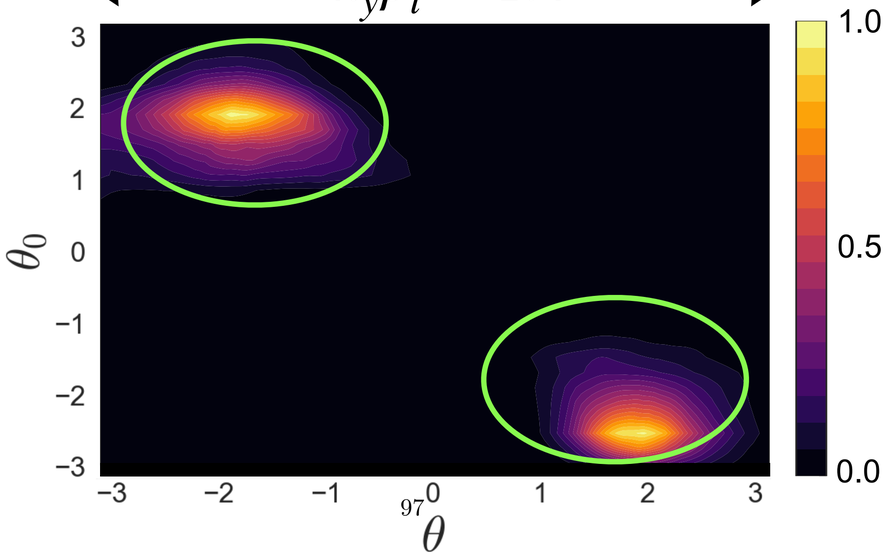

$|\phi^{tb}|^2$
(Arb. units)

Nonlinear results

Heat flux spectrum time evolution

- Electron-scale slab ETG heat flux contribution near outboard midplane.

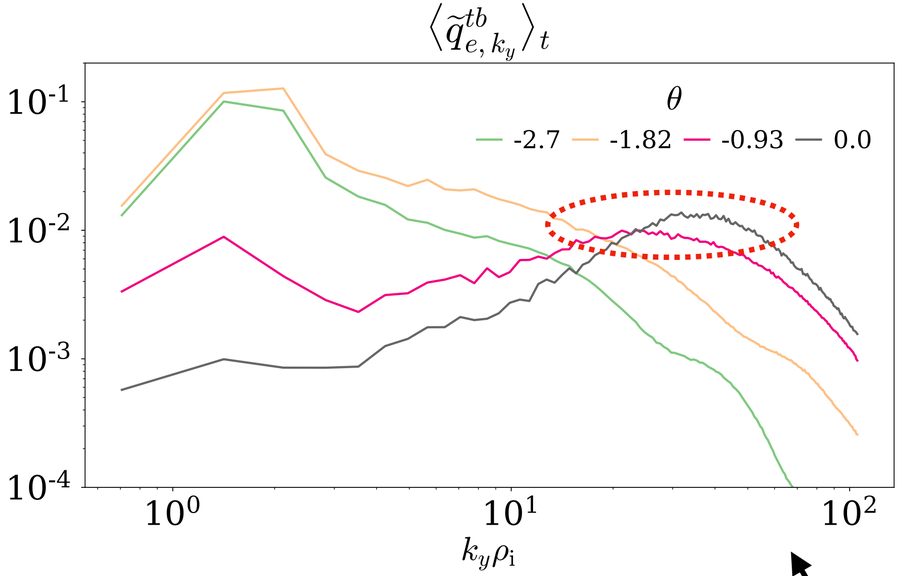

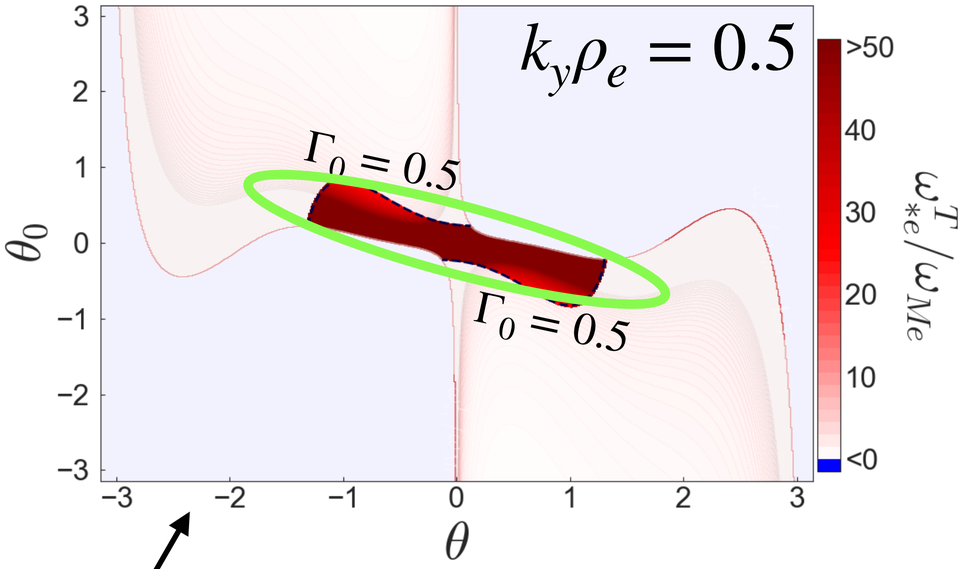

Slab ETG turbulence

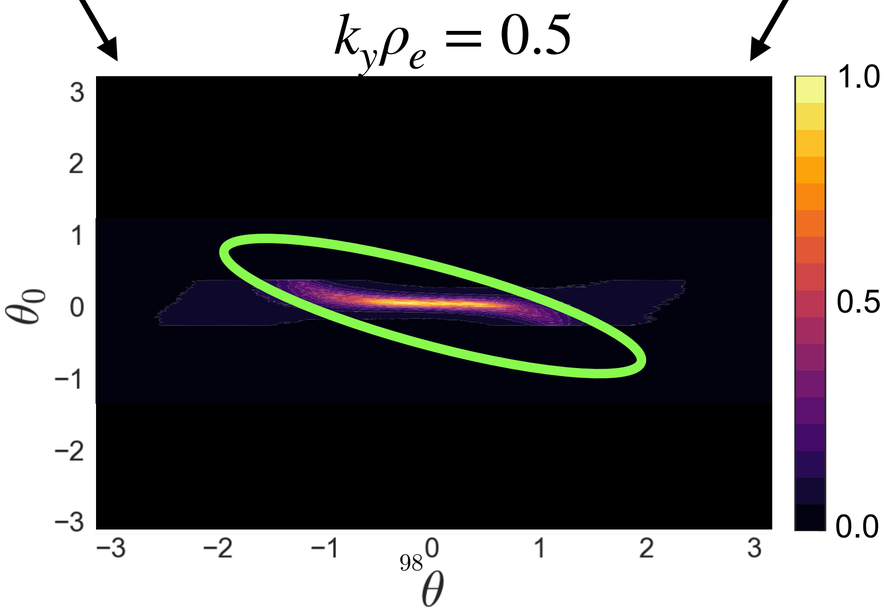

$|\phi^{tb}|^2$
(Arb. units)

Nonlinear results

Heat flux spectrum time evolution

Early

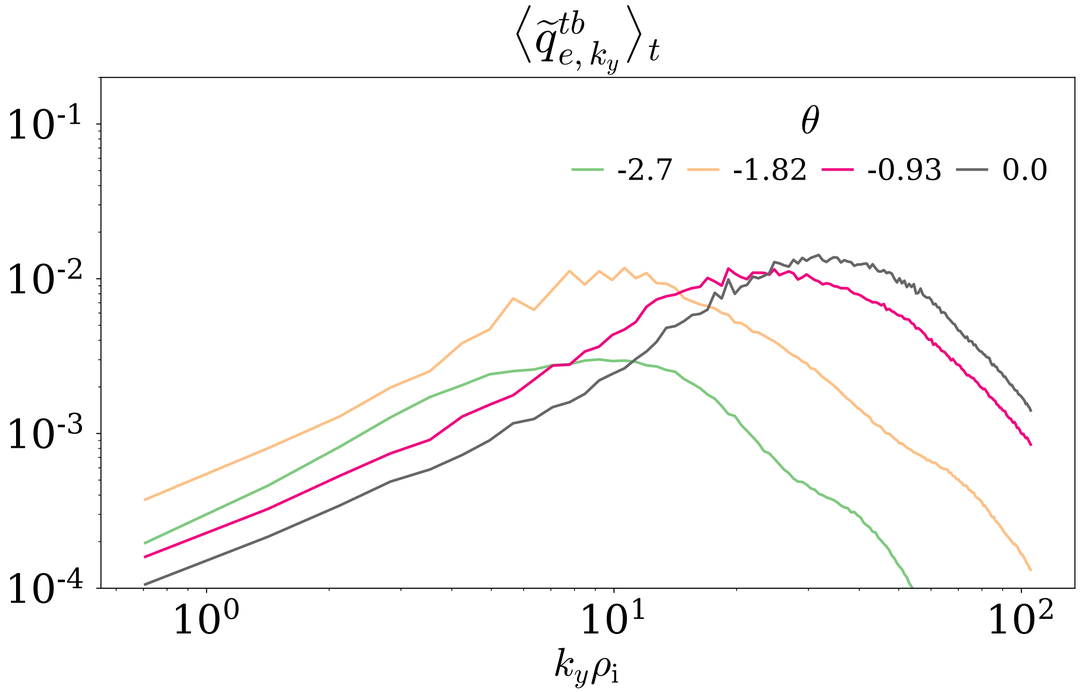

a) electron heat flux at early times.

Late

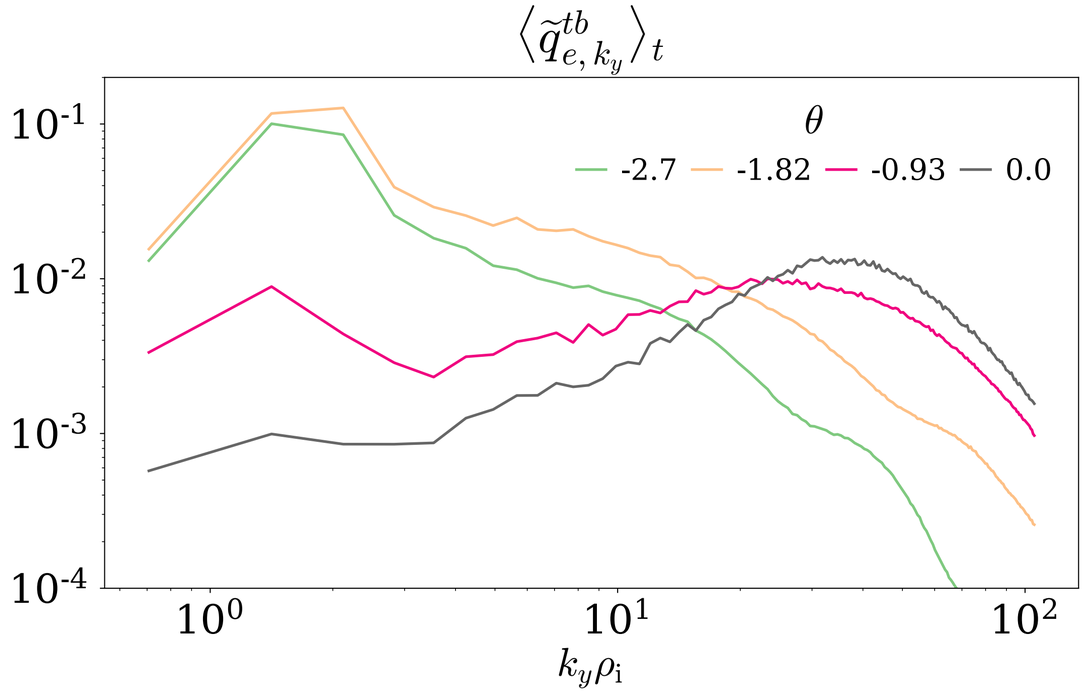

b) electron heat flux at late times.

Nonlinear results Ion-scale ETG regulates electron-scale ETG

- To determine importance of ion-scale ETG, we perform numerical experiment, that shows ion-scale ETG regulates electron-scale ETG.

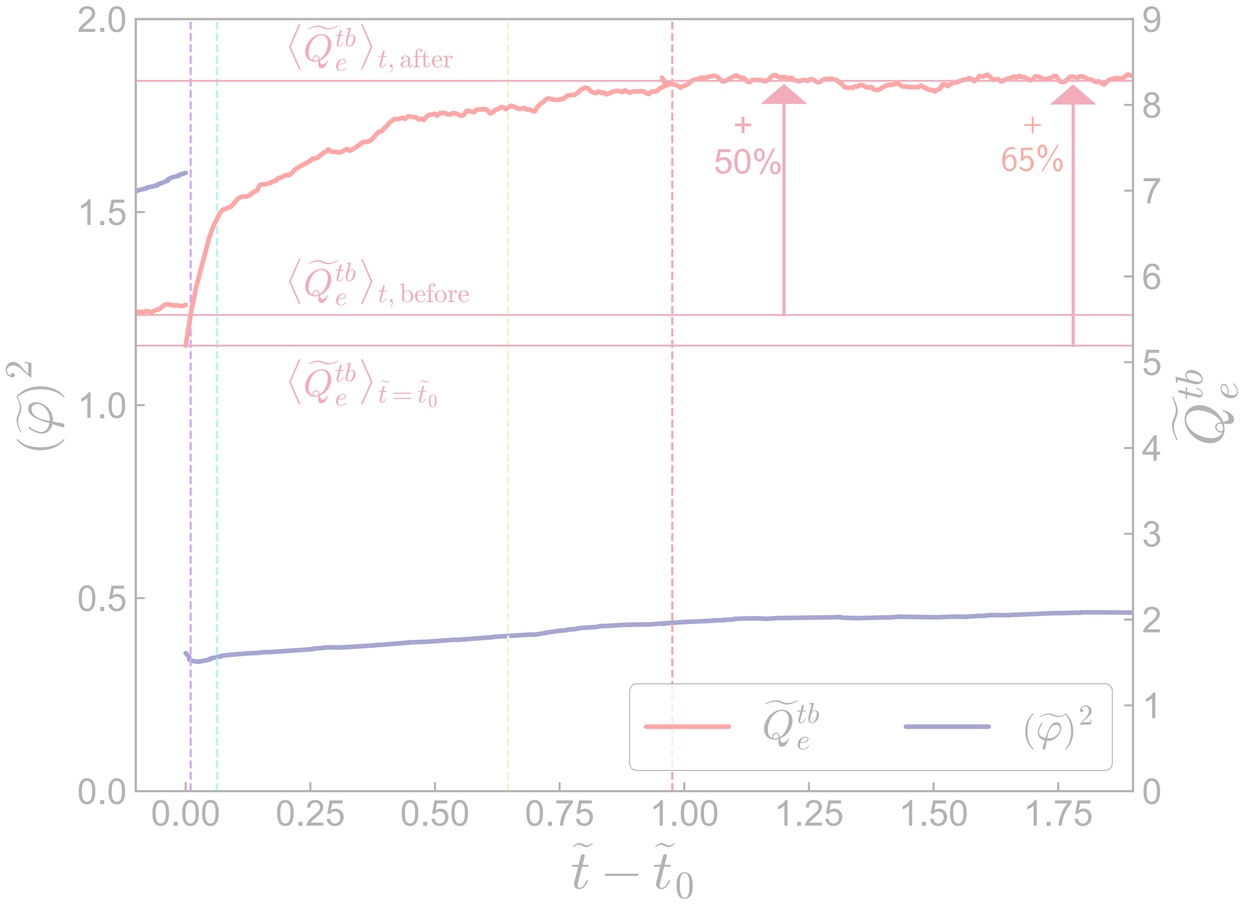

Figure: electron heat flux and potential versus time

Nonlinear results Ion-scale ETG regulates electron-scale ETG

- To determine importance of ion-scale ETG, we perform numerical experiment, that shows ion-scale ETG regulates electron-scale ETG.

- At $\tilde{t}_0 = t_0 v_{ti}/a$, strongly damp $k_y\rho_i \in [0.7 - 4.2]$ modes (recall $k_y\rho_{i,\max} \sim 100$).

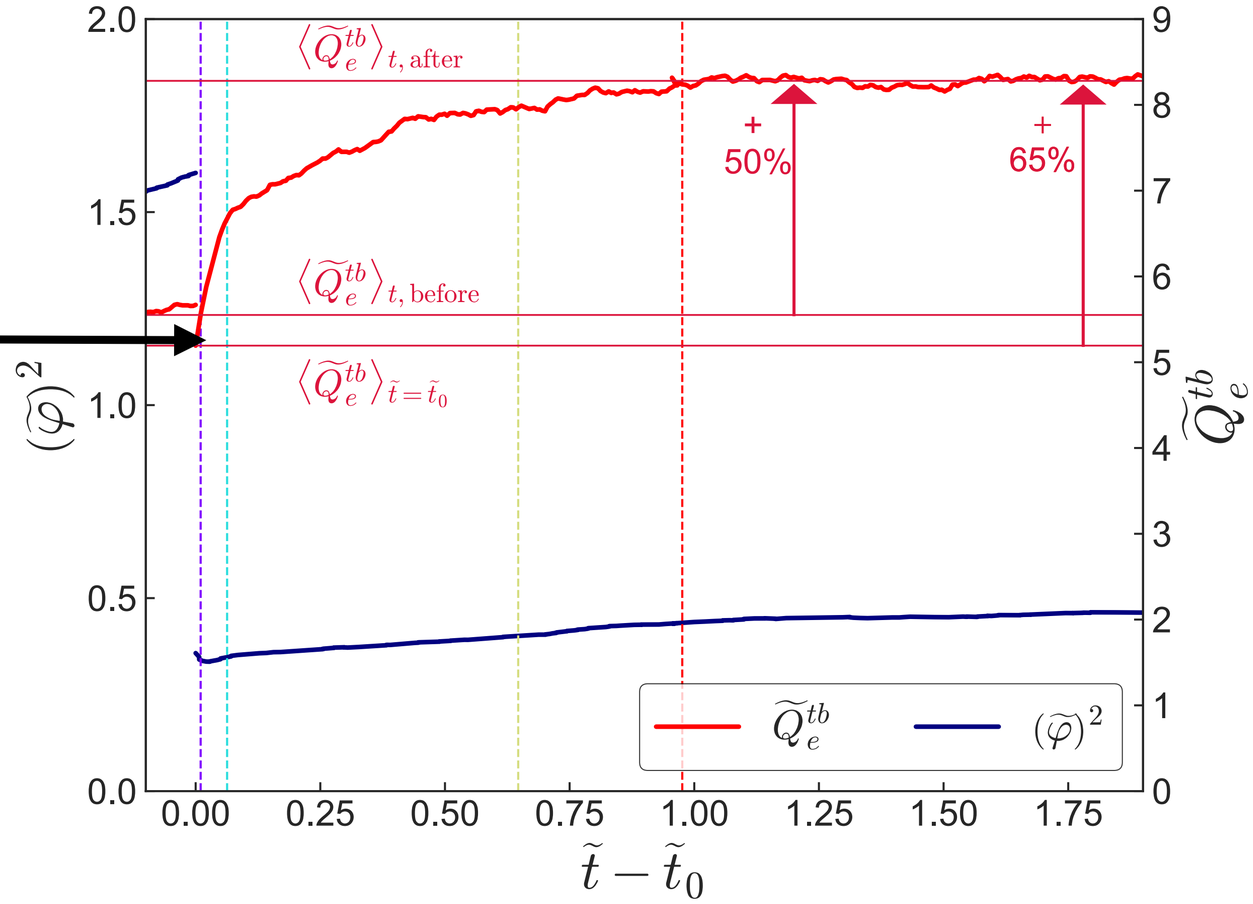

Figure: electron heat flux and potential versus time

Nonlinear results Ion-scale ETG regulates electron-scale ETG

- To determine importance of ion-scale ETG, we perform numerical experiment, that shows ion-scale ETG regulates electron-scale ETG.
- At $\tilde{t}_0 = t_0 v_{ti}/a$, strongly damp $k_y\rho_i \in [0.7 - 4.2]$ modes (recall $k_y\rho_{i,\max} \sim 100$).
- Electron heat flux increases by 65% once ion-scale ETG artificially suppressed.

Electron heat flux increases by 65%.

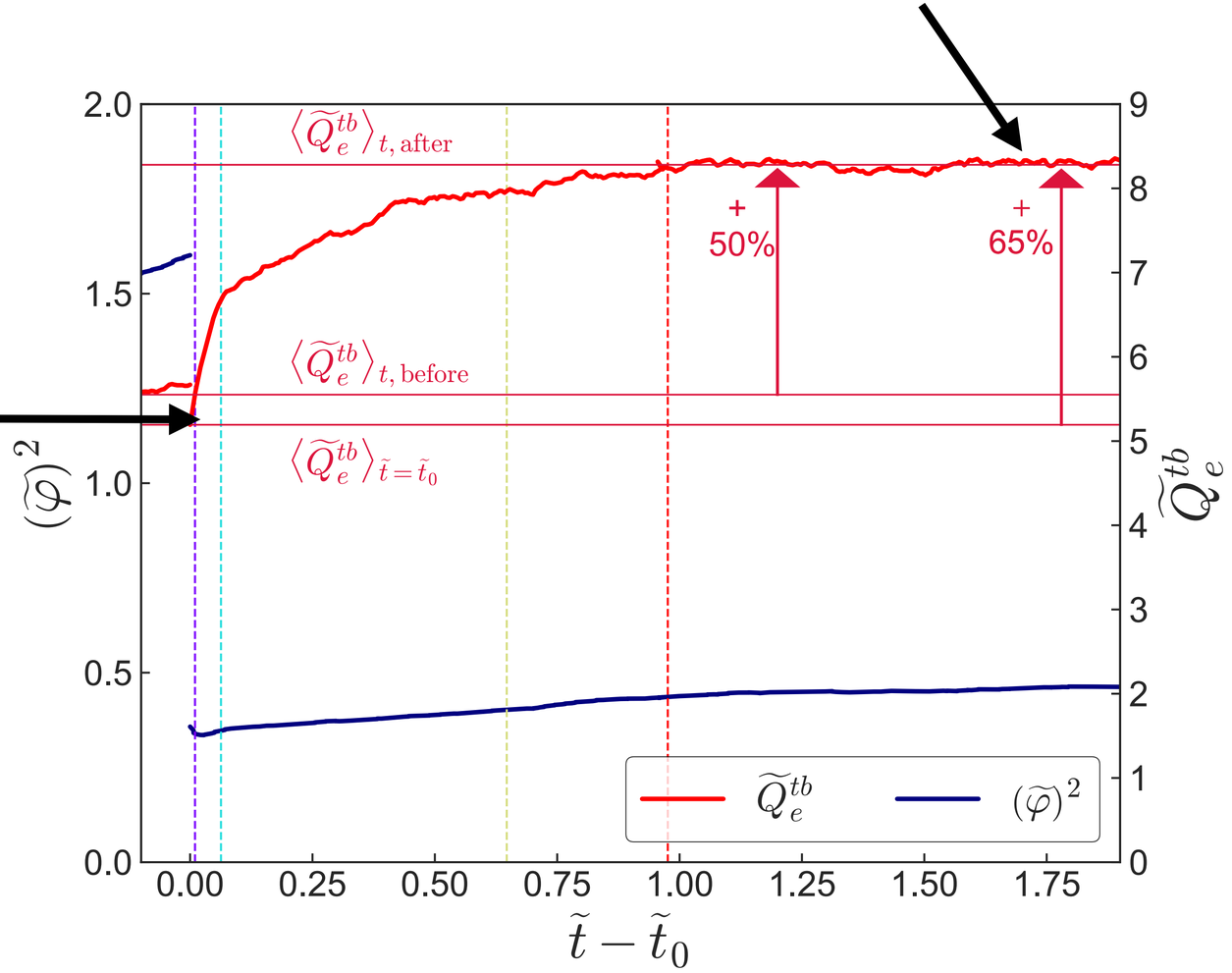

Figure: electron heat flux and potential versus time

Nonlinear results

Ion-scale ETG regulates electron-scale ETG

- To determine importance of ion-scale ETG, we perform numerical experiment, that shows ion-scale ETG regulates electron-scale ETG.
- At $\tilde{t}_0 = t_0 v_{ti}/a$, strongly damp $k_y\rho_i \in [0.7 - 4.2]$ modes (recall $k_y\rho_{i,\max} \sim 100$).
- Electron heat flux increases by 65% once ion-scale ETG artificially suppressed.
- → ion-scale ETG regulates electron-scale ETG transport.

Electron heat flux increases by 65%.

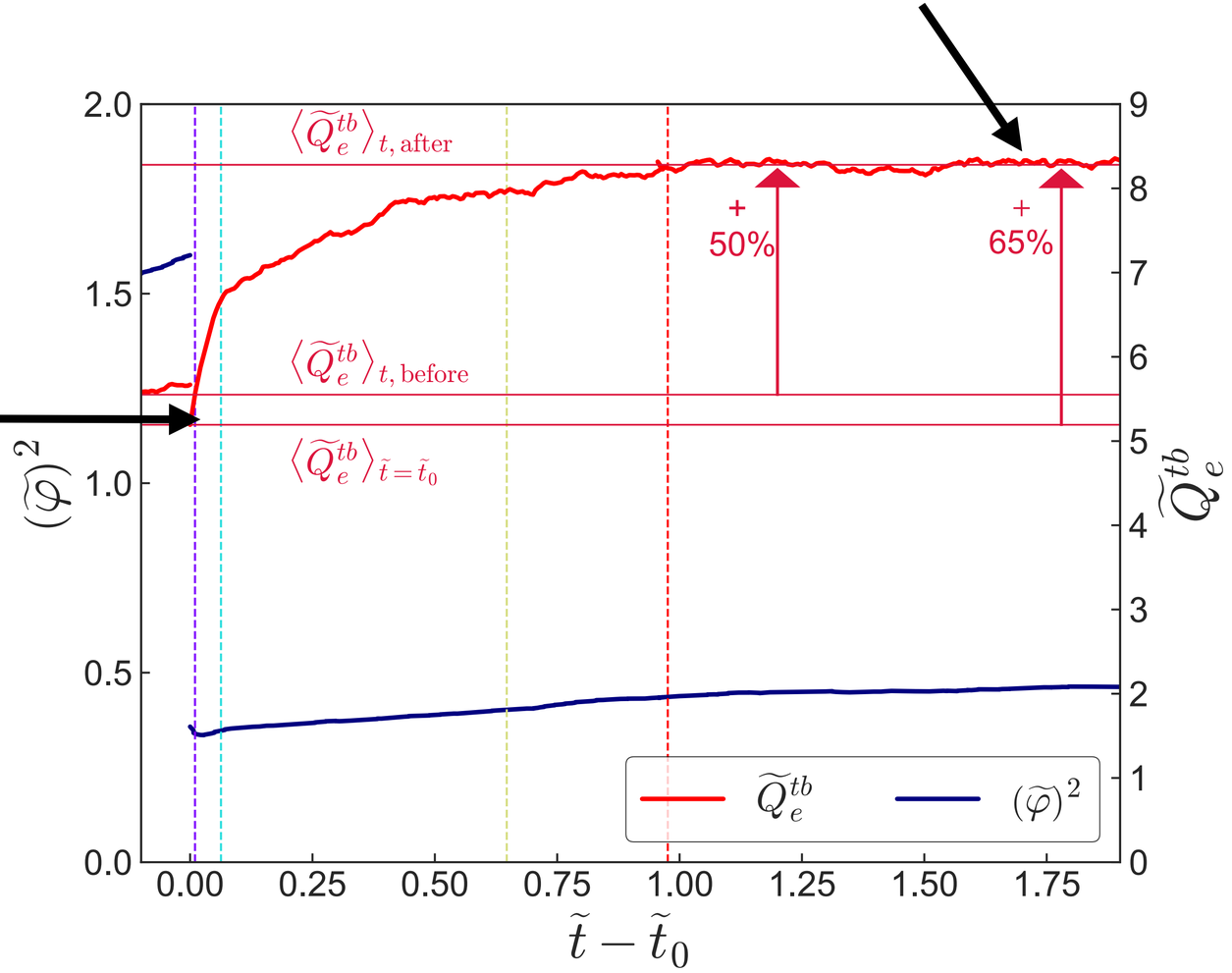

Figure: electron heat flux and potential versus time

Nonlinear results

Ion-scale ETG regulates electron-scale ETG

- To determine importance of ion-scale ETG, we perform numerical experimen that shows ion-scale ETG regulates electron-scale ETG.
- At $\tilde{t}_0 = t_0 v_{ti}/a$, strongly damp $k_y\rho_i \in [0.7 - 4.2]$ modes (recall $k_y\rho_{i,\max} \sim 100$).
- Over time, heat flux increases significantly at higher $k_y\rho_i$ values.

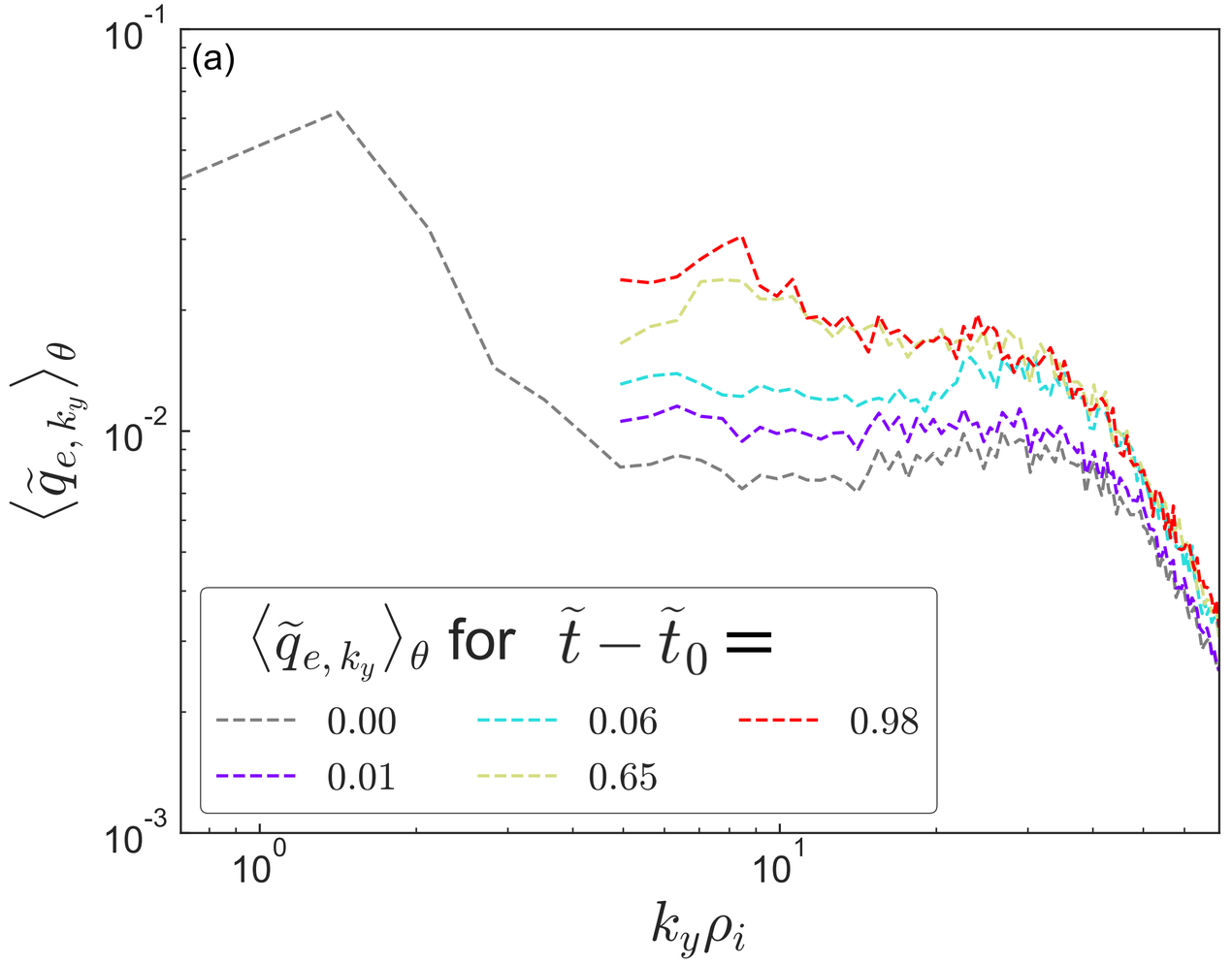

Figure: electron heat flux versus $k_y\rho_i$

Nonlinear results Ion-scale ETG regulates electron-scale ETG

- To determine importance of ion-scale ETG, we perform numerical experiment, that shows ion-scale ETG suppresses electron-scale ETG.
- Not inconsistent with previous multiscale work showing ion-scale modes suppressing electron-scale turbulence [Maeyama, 2015], [Howard, 2016], [Hardman, 2019].

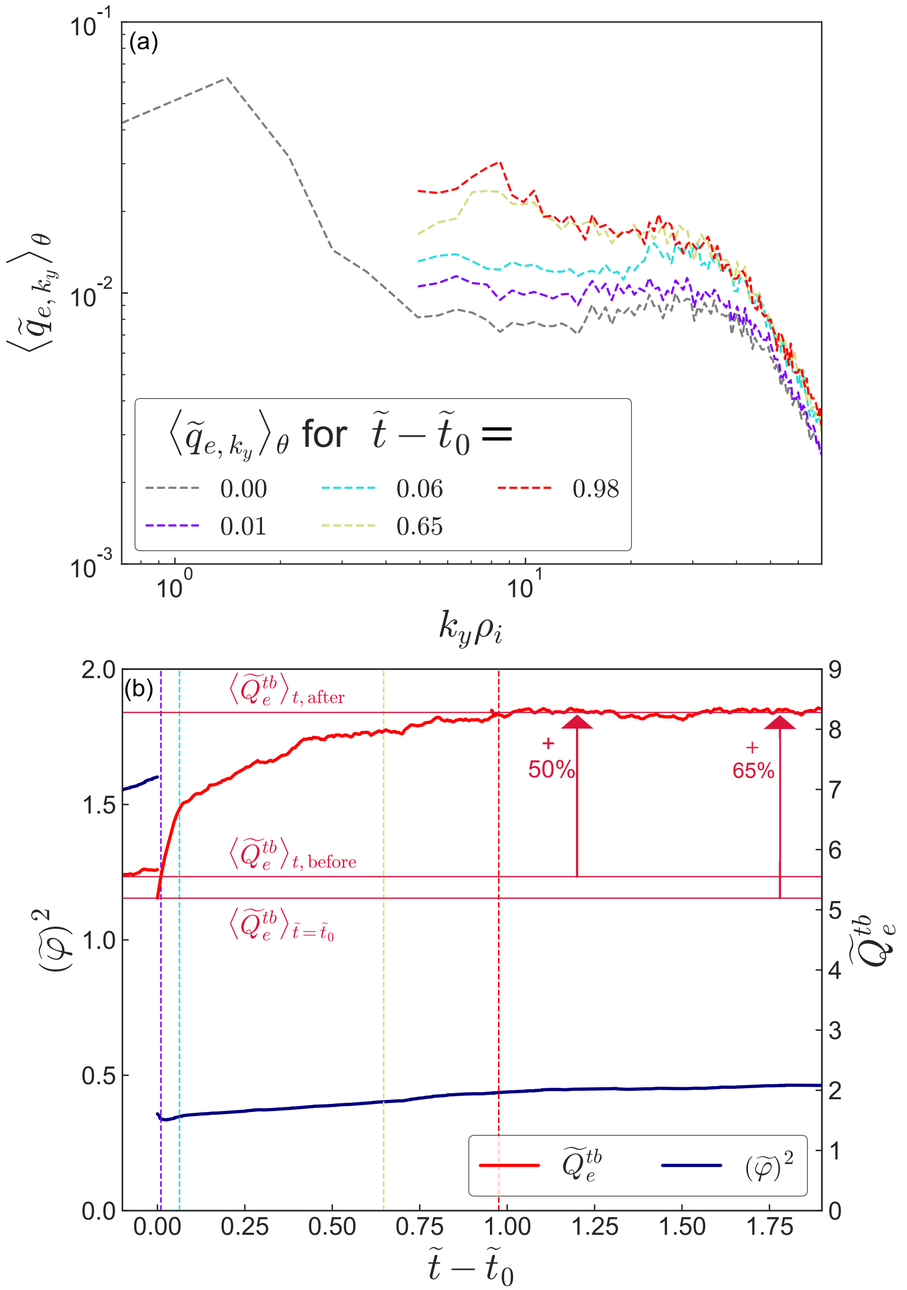

Discussion

Discussion

- ETG turbulence in steep gradient regions of JET-ILW pedestals has complex 3D structure, particularly at ion-scales.
- Ion-scale ETG modes regulate ETG transport at electron-scales through multiscale interactions.
- Measurements of poloidal distribution of electrostatic fluctuations in the pedestal needed to test the predictions from our simulations.
- Prospect of using magnetic shaping to control parallel distribution of 3D ETG turbulence and to regulate transport.
- For more details, see [Parisi, 2022] (in preparation).